UNIVERSITY OF OKLAHOMA

GRADUATE COLLEGE

STUDY ON CHEMICAL ACTIVITY OF PIERRE SHALES AND ITS EFFECT ON NEAR WELLBORE PORE PRESSURE DISTRIBUTION

A THESIS

SUBMITTED TO THE GRADUATE FACULTY

in partial fulfillment of the requirements for the

Degree of

MASTER OF SCIENCE

By

SABARISHA SUBRAMANIYAN
Norman, Oklahoma
2014

STUDY ON CHEMICAL ACTIVITY OF PIERRE SHALES AND ITS EFFECT ON NEAR WELLBORE PORE PRESSURE DISTRIBUTION

A THESIS APPROVED FOR THE
MEWBOURNE SCHOOL OF PETROLEUM AND GEOLOGICAL ENGINEERING

BY

_____
Dr. Ahmad Jamili, Chair

_____
Dr. Deepak Devegowda

_____
Dr. Benjamin (Bor-Jier) Shiau

Dedicated to my parents and my brother

Acknowledgements

I would like to thank god for making all my dreams come true. I would like to thank my brother Suzanth for his valuable guidance in choosing my majors, his friend Sathish Kulathu for inspiring me to become a Petroleum Engineer and also my parents for their constant support and trust they had in me to send me to a different country for pursuing my master's degree.

I would like to express my sincere gratitude to my advisor Dr. Ahmad Jamili for giving me this opportunity to do my research and for the trust he had on me though I came from a different technical background. He has always encouraged me whenever I am distressed about grades and has been a great source of inspiration. I would like to appreciate him for the guidance and valuable suggestions he has given me throughout my research. I would like to thank Dr. Deepak Devegowda for making me understand the rudiments of Reservoir Engineering and also for his constant support throughout my studies at OU. I would like to thank Dr. Ben Shiau wholeheartedly for being so kind and supportive to join the committee and also for taking pains to go through my research at the eleventh hour.

I would like to express my sincere appreciation to Aman Srivastava and K.V Srinivasan for assisting me whenever I had the troubles of understanding the subject.

And now last but not the least I would like to say a big thank you to all my friends Sumeer, Mounraj Aditya Srinivasan, Purnima, Dhivya, Reshma, Krithi and Pavithra for tolerating me whenever I cribbed and for the ensuing valuable advice. A special thanks to my best friends Arun and Kavitha for the awesome home food and for making me to forget that I have a family in India.

Table of Contents

List of Tables

List of Figures

Abstract

The pore pressure distributions and the mechanical response of the poroelastic medium are generally calculated to study the wellbore instability problems that could be encountered during drilling. The mechanical response of the porous medium is generally studied using the Biot's poroelastic model which considers only the fluid flow due to hydraulic pressure gradient. However in case of shales which are chemically active, having a negative colloid diffused on its surface, forms an electrical double layer with the cations of the pore fluid. The double layer influences the movement of the fluid due to the chemical potential and concentration gradients that are generated. Hence shales exhibit the phenomenon of swelling and shrinking when it is separating fluids of different salinities. The fluid movement due to the chemical potential and concentration gradients which are often neglected have to be considered when the near wellbore pore pressure distributions are studied to avoid wellbore instability. This thesis resumes the analytical models developed for a porochemoelectroelastic medium and also the solutions depicting the response of a chemically active porous media when an inclined wellbore is drilled. The model is based on the assumptions that the formation is isotropic, the electrical field developed is static, chemical reactions are uncoupled from ion diffusion and also the advection of ions with pore fluid is negligible. This work presents the pore pressure distributions and also the effective radial and tangential stresses at various distances from the wellbore obtained using the porochemoelastic model by assuming that the electrical potentials are in equilibrium in the porochemoelectroelastic model developed in literature. The results are compared with the results obtained using Biot's model for drilling mud of various salinities. The

significance of the mechanical properties such as porosity, shear and bulk modulus, Poisson's ratio, the hydrological properties such as permeability and surface properties such as Cation Exchange Capacity have been studied and the impact of the properties on pore pressure distributions for a porochemoelastic medium has been quantified. The quantification of the influence of the properties helps in controlling the parameters to overcome the wellbore instability. The coding algorithm has also been presented along with the methods used for validation of the results obtained. An unexpected surge or drop in pore pressures near wellbore occurs when chemical activity of the formations are considered. Using water based mud with an optimum mud activity lower than the pore fluid activity can prevent hydration of shale or shale fractures and wellbore collapse. Formations which are highly porous, less permeable and with low CEC can yield results close to poroelastic medium. However all shale formations have higher percentage of smectite clay which has higher CEC and deviated significantly from properties of poroelastic medium.

Chapter 1: Introduction

1.1: Significance of Shale in Oil and Gas Industry

Shales were left unexplored for a long time because of its low permeability which prevents gas migration. However, the depreciation of the conventional sources of energy, the sufficiency of shale and recent evolution in technology has made shale gas reservoirs an ultimate source of energy for upcoming decades. The recent advancements in horizontal drilling and the stimulation methods have facilitated to explore the shale gas reservoirs and to enhance gas recovery rates. Unlike other unconventional reservoirs, gas production in shale gas reservoirs does not decline once the production has been stabilized - a major cause for the petroleum industries to prefer shale reservoirs over other unconventional resources. This is because shales are more porous and less permeable and needs to be stimulated to allow the flow of natural gas to the wells. Once

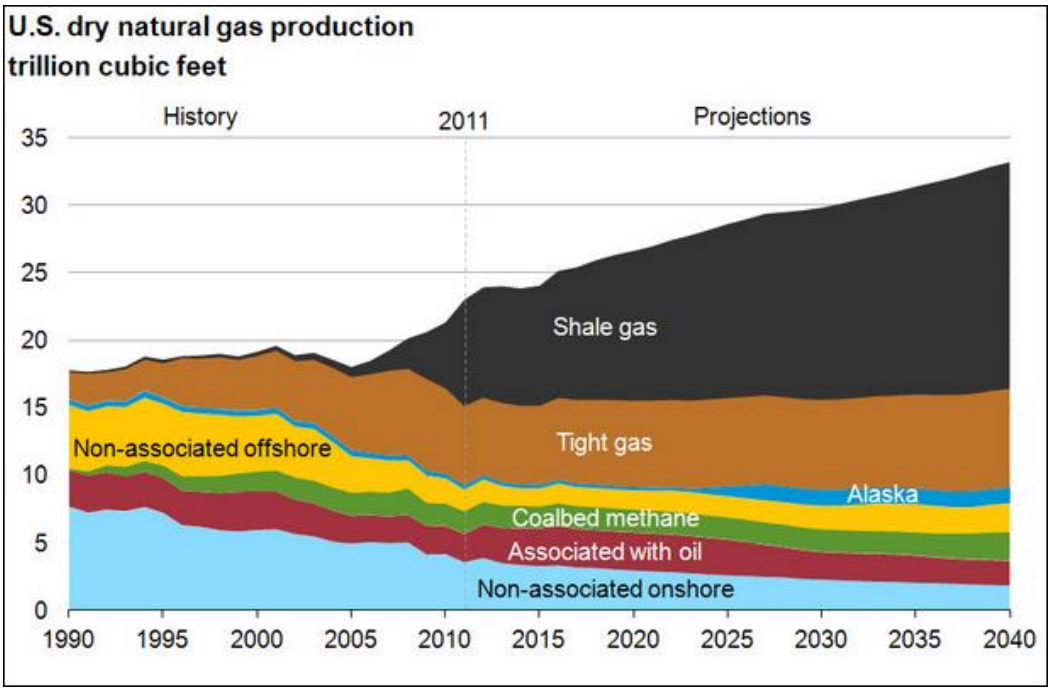

Figure 1: Forecast of natural gas production from different rock sources until 2040 (EIA, Annual Energy Outlook, 2013)

stimulated, shale gas reservoirs are also produced like any other conventional gas wells (CAPP). The U.S Energy Information Administration forecasts that there will be an increase of 44% in natural gas production from 23.0 trillion cubic feet in 2011 to 33.1 trillion cubic feet in 2040 where 88% of the production is from the shale gas industry.

Due to the significant increase in the production of natural gas and the remarkable price difference between the crude oil and the natural gas, the U.S economy has been reshaped by replacing other fuels with natural gas in transportation, electricity and industrial sectors.

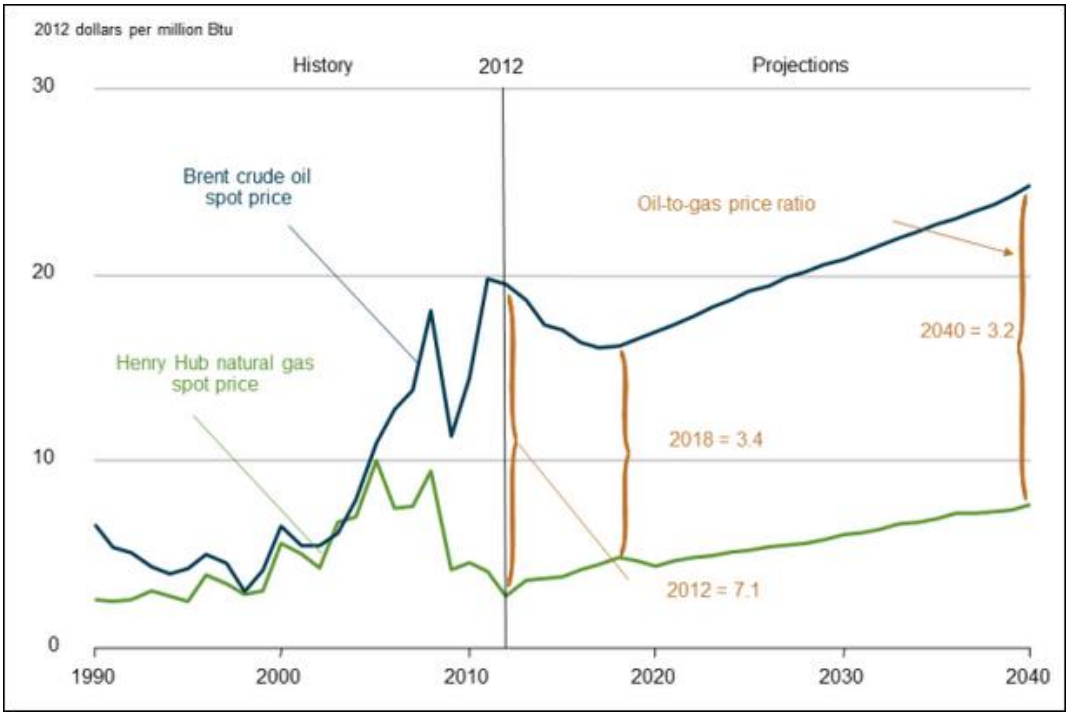

Figure 2: Comparison of prices of Brent crude oil and Henry Hub natural gas from 1990 to 2040 (EIA, Annual Energy Outlook, 2014)

The EIA, Annual Energy Outlook, 2014 has presented the prognosis of oil and gas price ratio of the upcoming years based on which the decision of using Liquefied Natural Gas as a railroad fuel has been made.

1.2: Geological significance and chemical composition of Shale

Shale is a generic term to characterize rocks which are capable of being split or divided into thin sheets in the direction of the grain. Shale is a clastic sedimentary rock comprising clay, quartz and calcite of varying compositions. Shale gas reservoirs are sometimes called as self-sourcing rocks because of the presence of the significant fraction of organic matter called Kerogen. Organic rich shales have 40% of its bulk reservoir occupied by kerogen (Passey et al., 2010). Shale gas reservoirs are one of the major unconventional sources for natural gas. The gas produced is partially from the free gas present in pores of the rock matrix and also from the gas adsorbed to the organic matter. In case of shale gas reservoirs, the gas formed in the source rocks does not migrate because of the low permeability. Hence one of the key parameters controlling the gas flow in shale reservoirs is its effective permeability induced by natural and man-made fractures. Shales are classified based on the thermal maturity attained by heat and pressure producing hydrocarbons. Dry gas shales are highly, thermally mature while shales with wetter gas are less mature and the shales with oil being the least matured.

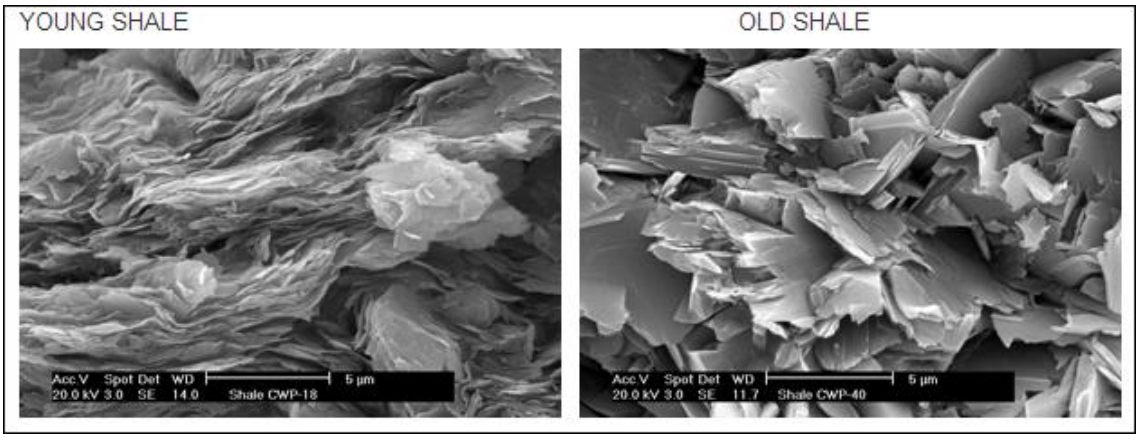

Figure 3: Microstructures of shales based on maturity influencing the brittleness and fracturability (U.S Geoscience News and Information, Geology.com)

Dark colored shales have higher percentage of organic debris thereby making them eligible for oil and gas production. Haynesville Shale, Barnett Shale, Fayetteville Shale are most common gas producing reservoirs while Eagle ford Shale and Bakken Shale produce oil (U.S Geoscience News and Information, Geology.com). Nearly 50-60% of shale is made up of clay, a negative charged colloid, which influences the chemical and physical properties of the rock because of its high ability for water exchange. The degree of influence depends on the types of clays like kaolinite, illite that have minor impact and montmorillonite-smectite which has a higher tendency to change in volume during water exchange poses serious threats during drilling operations.

Table 1: Mineralogical composition of an average shale (Adapted from U.S Geoscience News and Information, Geology.com)

	Shaw and Weaver (1965)	Hillier (2006)
Quartz	30.8	23.9
Feldspar	4.5	3.7 (K-spar) 2.4 (Plag.)
Carbonate	3.6	7.5 (Calcite) 1.3 (Dolomite) 0.5 (Siderite
Fe-oxides	0.5	0.8
Clay minerals	60.9	47.7 (Di-clay) 7.5 (Tri-clay)
Other minerals	2	0.5 (Pyrite)
Organic matter	1	Not determined

1.3: Wellbore Instability in shale

Wellbore instability is an unfavorable condition during which the diameter of the borehole is remarkably different from the estimated shape and size and loses its structural wholeness. The wellbore instability leads to the following problems:

a. Enlargement of the borehole

b. Hole shrinkage

c. Hole fracture

d. Hole collapse

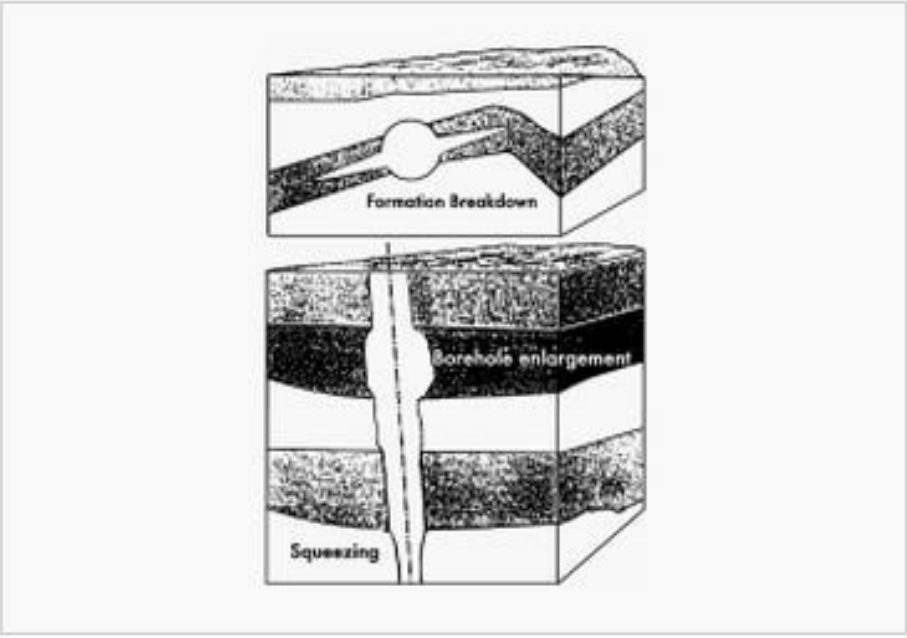

Figure 4: Types of wellbore instability problems (Petrowiki.spe.org)

1.3.1: Principle of borehole stability

Borehole stability is based on the principle of equilibrium between the rock strength and the in-situ stresses existing before the drilling operations. However when a wellbore is drilled, the equilibrium is disturbed. The disturbance is amplified due to chemical interactions between the injected fluids and the formation fluid. The doubtfulness in some of the input data has made many borehole stability simulation models unsuccessful. One of the important parameters being the pore pressure is affected due to rock dilation and contraction which is commonly found in shales.

1.3.2: Causes for wellbore instability

Reasons attributing to the wellbore instability are:

1. Mechanical instability due to disturbance of stress equilibrium
2. Chemical instability due to rock-chemical interaction

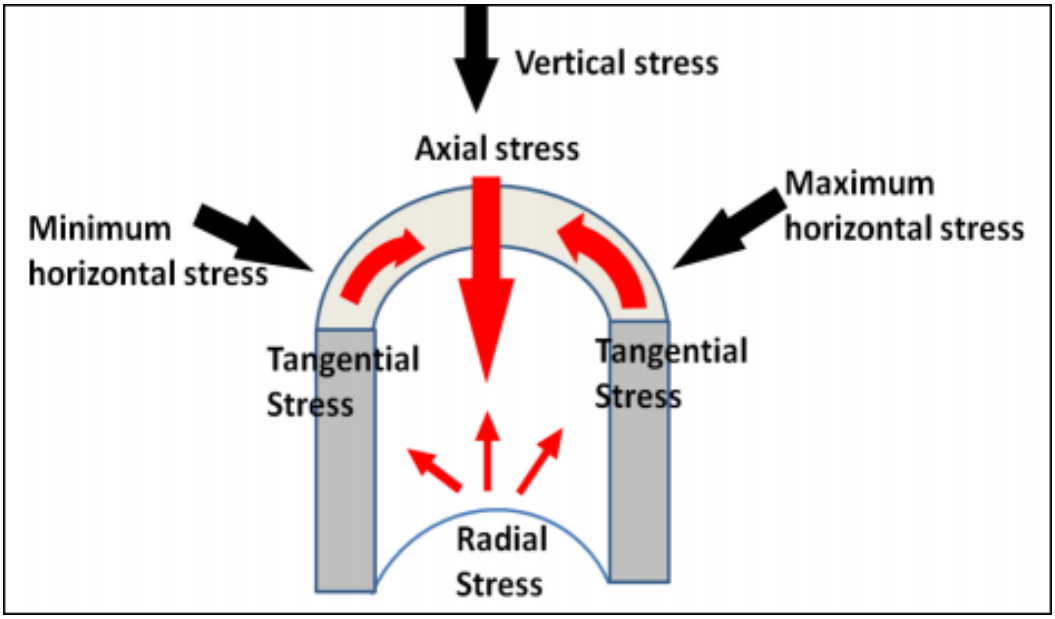

Figure 5: Wellbore stresses after drilling (McLean, 1990)

1.3.3: Classification of chemical instability mechanisms

The chemical instability mechanisms of the wellbore drilled can be classified as follows (petrowiki.spe.org/borehole-instability):

1. Osmotic pressure
2. Capillary pressure
3. Near wellbore pressure diffusion
4. Mud invasion into the formation due to overbalanced drilling

1.4: Pierre Shale formation

1.4.1: Stratigraphic positioning of Pierre Shale

Pierre shale rocks were deposited in a north south oriented trough approximately 1000 miles extending from Canadian arctic to south of New Mexico and sometimes plunges into Gulf of Mexico. The Pierre shale rocks form a sedimentary wedge thinning from thousands of feet in west to 1000 ft. in the east. All the sediments derived were from the west and most of the sediments in the Far East are finely grained shale (Schultz et al., 1980). Normal and reverse faults exist in Pierre shale formation in central South Dakota with dips ranging from 40° to 90° and vertical displacements range from less than 1 m to 37 m (Nichols et al., 1994).

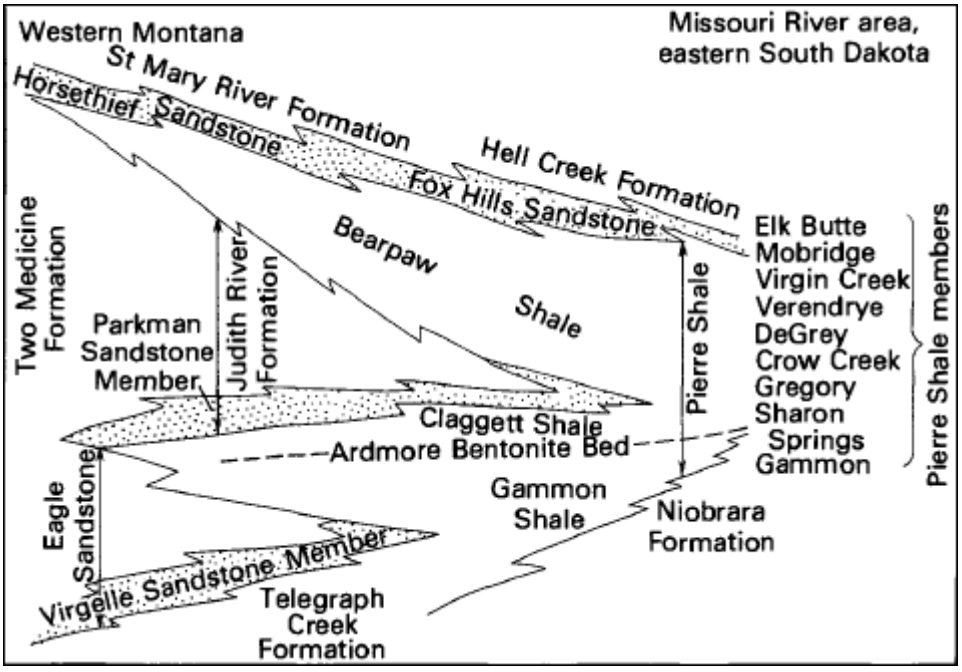

Figure 6: Cross section of Pierre Shale in northern Great Plains region (adapted from Schultz et al., 1980)

1.4.2: Mineralogical composition of Pierre Shale

Major proportion of the Pierre Shale formation consists of clay stone that has little fissile and have few proportions of fissile, fine grained, clayey rock (Schultz et al., 1980). The presence of Kaolinite and Chlorite is generally minor and constitute to 10% of clay minerals, illite makes up to 15-20 % of clay minerals and more than half of the total clay (about 30-60%) is made up of mixed-layer clays. Quartz makes up more than a few percent of most of the bentonite, and plagioclase and biotite may be abundant especially at the bottom of the bed (Schultz 1978). The Pierre shale contains more than 59% of smectite, which is calcium saturated montmorillonite. Pierre shale is expected to have high cation-exchange capacity and swelling potential compared to other shales (Richard et al., 1991).

Table 2: Mineralogical composition of Pierre Shale formation (adapted from Aminul Islam et al., 2013)

Quartz	k-fsp	Plag	Chl	Ka	Mi/Ill	ML	Sm	Calc	Sid	Dol/Ank	Pyr
20.1	0.7	15.7	2.2	6.8	16.6	0.3	31.5	1.8	0.7	1.8	2.0

Chl chlorite, *Ka* kaolinite, *Mi/Ill* mica and illite, *ML* mixed layer, *Sm* smectite, *Sid* siderite, *Dol* dolomite, *Ank* ankerite, *Pyr* pyrite

1.5: Essentiality of the research

Wellbore instability is a frequent problem that occurs while drilling shale formations. Consequences of the wellbore instability can lead to many hole problems which could result in expensive drilling operations. In a field, the instability is contributed by both the mechanical and chemical effects. However only the mechanical effect has been quantified in the earlier research ignoring the time dependent effects due to pore fluid migration (McLean et al., 1990). When the wells are in exploratory stage many cores and logs are obtained in order to understand the mechanical and hydrological properties. However these mechanical and hydrological properties are completely altered when a

shale formation is drilled because shale has a very rich content of clay which holds complicated water molecules and also has complex interactions between the ions of the pore fluid and drilling fluid. Moreover the swelling pressures are modified based on the mud chemistry (Abass et al., 2006). Osmotic effects are common in shale which can act as a semi permeable membrane separating fluids of different salinities and electro chemical potentials affecting the pore pressure distribution and the effective stress of the rock. In order to avoid cost overruns and non- productive time, a model predicting the pressure and stress distributions, and also helpful in determining optimum chemical properties for drilling fluid by including both chemical and mechanical instability mechanisms is essential.

The clay on the surface of shale has negative charges which forms a diffuse layer and results in electro-kinetic phenomena when influenced by external electrochemical potential gradients of the ions of drilling and pore fluids. The macroscopic transport equations for the electro-kinetic phenomena are formulated based on the non-equilibrium thermodynamics for irreversible process (Yeung et al., 1993).

Hence a mathematical model predicting the pore pressure distributions, effective radial and tangential stresses including the electro-kinetic phenomena to the existing Biot's theory of poromechanics was first developed by Nguyen Vinh and Abousleiman (2008). Nguyen et al., (2008) have developed the model to study the mechanical response of a chemically active and charged formation through a comprehensive research on transport mechanisms of the ions developed based on non-equilibrium thermodynamics by Yeung et al.,(1993).

Main objectives of the research:

1. To give a comprehensive idea on how the presence of clay has been an attribute to many of the unknown characteristics of shale
2. To elucidate the coupled transport of ions, fluid and chemical species that happens inside shale due to the existence of different driving forces.
3. To summarize the transport equations those are used for such coupled flows through a semi permeable membrane.
4. To enumerate the flaws in original theory of poromechanics by Biot which helps to comprehend the current consolidation theory including the effects of electrokinetics as developed by Nguyen Vinh and Abousleiman (2008).
5. To understand the relationship between various properties of shale such as Cation Exchange Capacity, water activity, porosity, permeability and conductivity.
6. To identify the key parameters those influence the pore pressure distributions significantly and can be controlled to prevent the wellbore instability.

1.6: Précis of the thesis

Chapter 1 gives an insight of the work carried out in this literature. Chapter 2 gives a brief description of the petro-physical properties of shale affecting the wellbore stability that needs to be considered and also the observations from previous research papers. Chapter 3 lists out transport formulations for irreversible processes happening in shale and also expressions for the coupling and conductivity coefficients in terms of field parameters. Chapter 4 presents the mathematical model developed by Nguyen et al., (2008) based on the formulations of chapter 3 to simulate the pressure and stress

distributions. Chapter 5 describes the mechanical and hydrological properties of Pierre shale (formation of consideration) and also enumerates the boundary conditions used by Nguyen et al., (2008) to obtain the analytical solutions for the mathematical model framed. Chapter 6 lists the superposed solutions of the model which is decomposed into 3 sub models of different loading conditions. Chapter 7 presents the plots obtained using the mathematical model developed in MATLAB based on assumption of equilibrium of electrical potentials to simplify the porochemoelectroelastic model to porochemoelastic model followed by the results and discussion. Algorithm of the code used for simulation has been presented along with the methods used for validating the results. Chapter 8 resumes the conclusions based on the observations from the plots, the limitations of the model and also the recommendations for improving the wellbore stability based on the conclusions.

Chapter 2: Literature Review

2.1: Clay colloidal chemistry

Clays are charged due to isomorphic substitution of metal atoms inside the crystalline structure and chemical reactions between the reactive silanol and aluminol groups present on surfaces of shale and pore water (Revil et al., 2001). Fine pores and the negative charge of clay on shale surface causes shale to behave like a semi permeable membrane (Fritz et al., 1994).

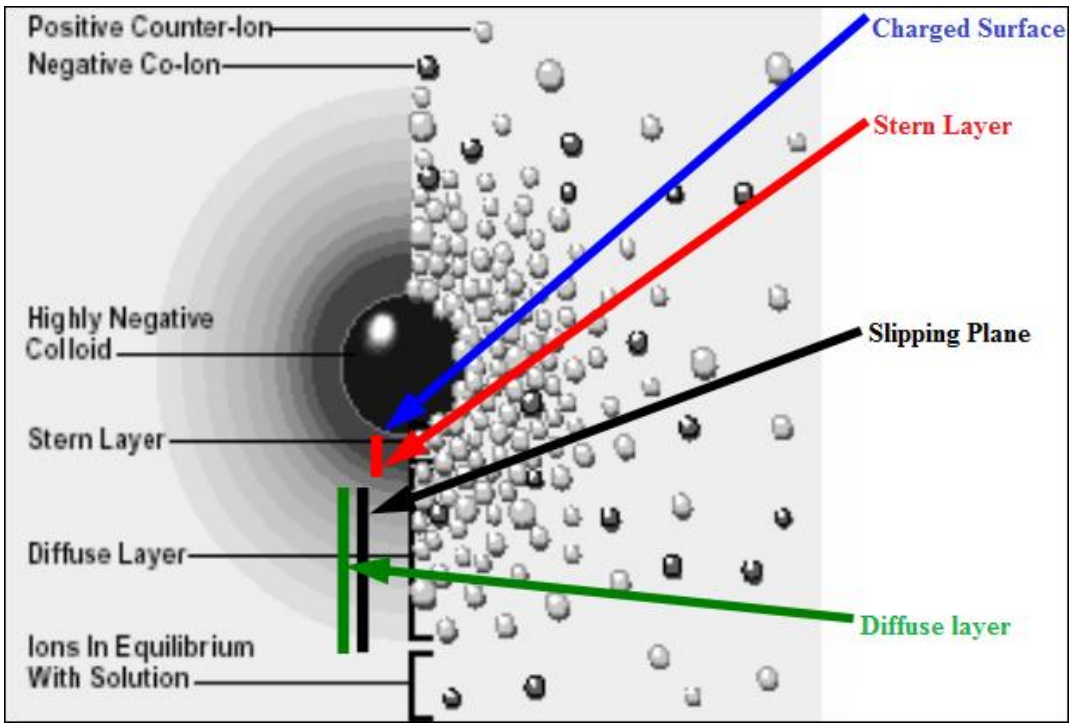

Figure 7: Surface charge characteristics-Diffuse double layer diagram (Colloid chemistry department, University of Szeged)

The basic mechanism in electro-kinetic phenomena which occurs in soil due to presence of clay is explained by the electrical double layer theory for charged surfaces immersed in aqueous solutions. This colloidal chemistry of clay particles has to be considered as it has negative surface charge which influences the motion of the particles. The aqueous

solution in formation is the pore fluid which behaves like an electrolyte and dissociates into ions in presence of the negatively charged shale surface. The ions of pore fluid redistribute to neutralize the charges on the shale surface. The quantity of the exchangeable cations needed to neutralize the charge deficiency of clay is described as Cation Exchange Capacity (CEC) and is often expressed in milli-equivalents for 100 g of dry clay (Akram et al., 2000). The cations of the pore fluid move towards the negative surface charge. The cations are adsorbed and held tightly to form a thick layer called the Stern layer. The stern layer is surrounded by diffuse layer where the ions are in thermal motion. The stern layer and the diffuse layers are separated by a slipping plane and the voltage possessed by the slipping plane is called the zeta potential (Van Olphen, 1963).

The electrical potential decreases as the distance from the surface increases. The zeta potential influences the velocity of particle motion in the electrical field. The zeta potential depends on the Cation Exchange Capacity of the shale medium. Higher the CEC more negative zeta potential is developed and the velocity is greater within the electrical field (Van Olphen 1963). The semi permeability exhibited by shale due to presence of clay when it is separating two fluids of different salinities establishes Donnan equilibrium. This is because shale is impermeable to some solutes of bigger size as a result of which ions redistribute between shale to be in chemical equilibrium. However the ions on either side of shale are not in equilibrium electrically (Overbeek 1956). The important aspects of Donnan equilibrium are:

1. unequal distribution of ions
2. osmotic pressure

3. potential differences between the phases

2.2: Cation Exchange Capacity (CEC) of Shale

CEC is considered as an index of the dispersibility of the shale formation which affects the properties of the drilling fluids and the wellbore stability (Gray and Darley, 1980). CEC is expressed as milliequivalents per 100 g of clay. The cation exchange capacity is a measurement of the exchangeable cations present in the clays of a shale sample. The exchangeable cations are positive ions which neutralize the negative charges on the shale surface. Most common cations are sodium, calcium, magnesium, iron, potassium and most common exchangeable ions in shale are from bentonite, montomorilloite clays (Stephens et al., 2009).

Several analytical methods to determine the CEC were proposed. Some of them are calorimetric technique based on the cobalt hexamine trichloride depletion (Bardon et al., 1983), ammonium acetate saturation method (Sumner et al., 1996) and the copper complexes method (Meier et al., 1999), barium exchange methods (Hendershot and Duquette 1986). The methylene blue test (MBT) recommended by the API is the most commonly used method to determine CEC which requires 1 gram of fine, dry shale powder dispersed in water with dispersant, sulfuric acid, hydrogen peroxide and boiled for few minutes followed by cooling to room temperature and titration with methylene blue solution. The end point is observed when the sample suspension droplet on the filter paper becomes a blue halo surrounding the dyed solids (API recommended practices 13 I, 2004).

The higher the value of CEC, higher the reactivity of shale. Sandstone and limestone are non-reactive and have CEC less than 1 meq/ 100 g. Average reactive shale has CEC of

10 – 20 meq/ 100 g, and highly reactive shale has CEC more than 20 meq/ 100 g. The shale gets its CEC value based on the percentage of the composition of the different clays and sand with the following individual CEC (Stephens et al., 2009):

Table 3: Cation Exchange capacities of different clays and sand present in Shale (adapted from Stephens et al., 2009)

Types of clay / sand	CEC in meq/ 100 g
Smectite	80-120
Illite	10-40
Kaolinite	3-15
Chlorite	10-40
Sand	< 0.5

Since the clays exhibit surface conductivity effect, the clays with larger surface area has larger CEC values

2.3: Membrane Efficiency of Shales

The osmotic pressure generated in the shale formations is proportional to the shale membrane efficiency which is estimated using the wireline measurements. The flow of water and ions through the shale is controlled by the membrane efficiency. The membrane efficiency of shale is influenced by the porosity and the permeability. When variation of membrane efficiency with porosity and permeability was studied by Collins et al., (2008), it was found that membrane efficiency is negatively related to the shale porosity until porosity of 7.5% (figure 8) and is related to permeability of order of 0.1 nD (figure 7) while there are no significant changes beyond the threshold values of porosity and permeability.

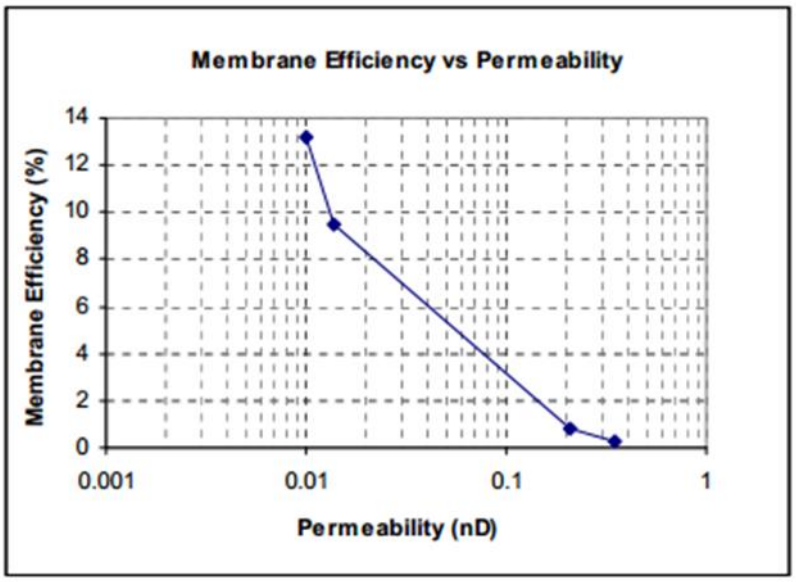

Figure 8: Membrane efficiency Vs Permeability when shale is contacting NaCl solution (Collins et al., 2008).

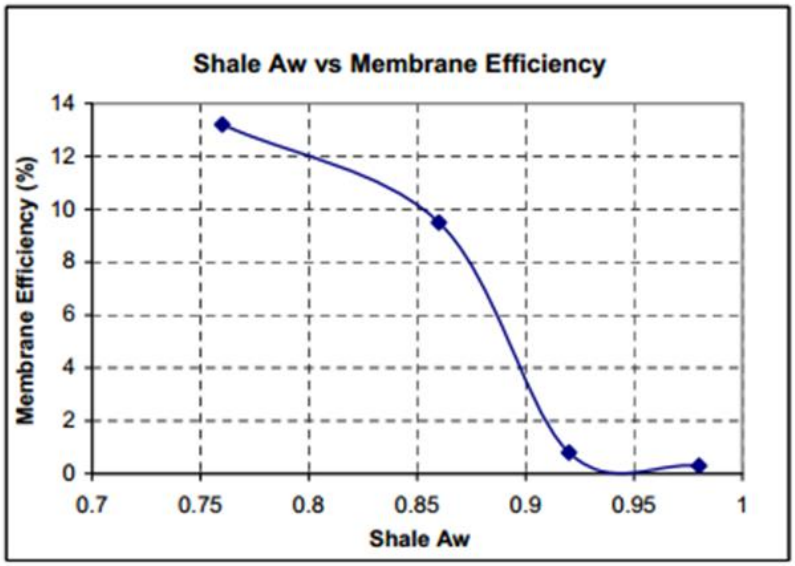

Figure 9: Membrane efficiency Vs Water activity when shale is contacting NaCl solution (Collins et al., 2008)

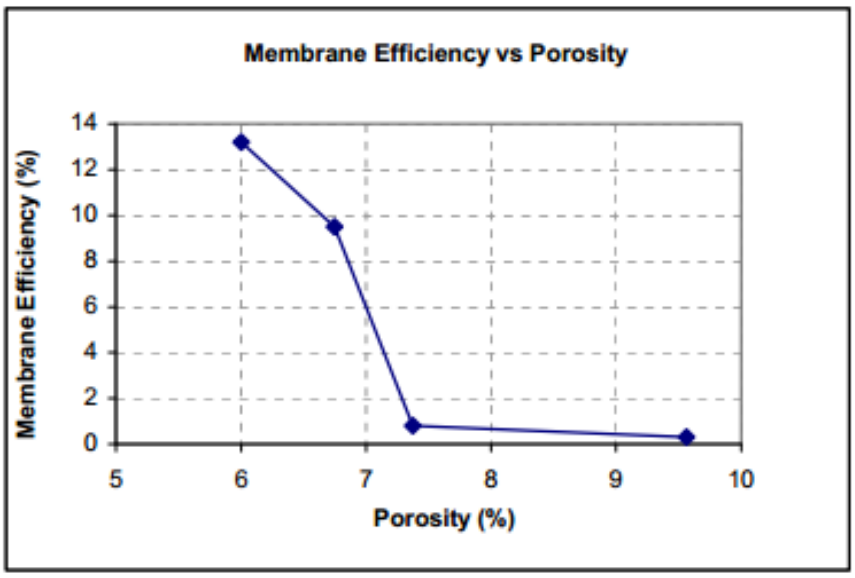

Figure 10: Membrane efficiency Vs porosity when NaCl mud is used (Collins et al., 2008)

The above plots show that the rate of the solute transport is influenced by the porosity and permeability until it reaches its threshold values. The membrane efficiency values of shale to brine solutions range from 0-10% (Van Oort et al., 1996 and Collins et al., 2008).

The membrane efficiency of shale increases with the increase in Cation Exchange Capacity and is also proportional to ratio of (CEC/k) where 'k' is permeability. The membrane efficiency is directly proportional to the hydrated diameters of the ions in the drilling fluid (Al Bazali Talal. M et al., 2006).

Keijzer et al., (2001) represented membrane efficiency of shale as a function of porosity for various clay types (as shown in figure 11) based on the empirical relation developed by Fritz et al., (1986).

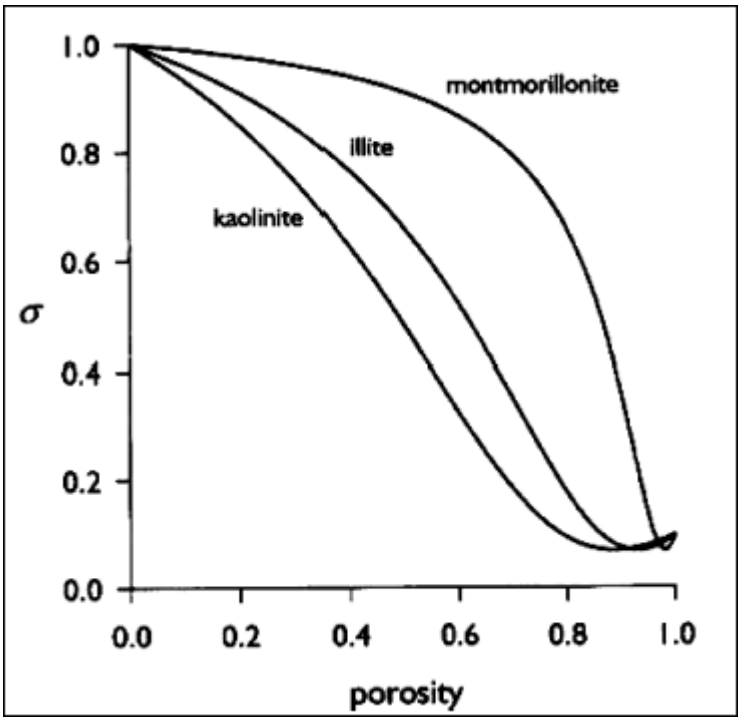

Figure 11: Variation of membrane efficiency with porosity for different clay types (adapted from Keijzer et al., 2001)

Figure 11 shows that the membrane efficiency increases with decrease in the porosity. This is true because when the porosity decreases the clay membrane compacts and the diffuse double layer overlap and the net negative potential developed excludes the anions from the surface making the ion exclusion behavior of the membrane more ideal. Similarly when the net negative charges on the clay surface increases the ion exclusion behavior is more predominant in shale.

2.4: Water activity of shale

Water activity of the shale formation is an indicator of the state of hydration of the shale, and its potentiality to absorb or lose water. The water activity is affected by factors such as pressure, temperature, mineralogy, platelets spacing and pore fluid compositions. The water activity is usually measured in a laboratory by using a

hygrometer which measures the relative humidity of an enclosed space containing the cuttings (Winston et al., 1960). The percentage of relative humidity divided by 100 gives an approximate value of water activity. A recent technology of using chilled mirror to find water activity was developed (Jarrett et al., 2004). The most common method to find the water activity of shale is by using adsorption isotherm method (Chenevert 1970) which uses the desiccators with saturated salt solutions that maintain the vapor pressure of water. The degree of adsorption depends on the amount of moisture adsorbed onto the shale surface. This relationship is conveniently represented in an adsorption isotherm which plots moisture adsorbed onto shale surface as a function of relative vapor pressure at constant temperature. Though the adsorption isotherm is distinct for different shales, there is a common observation of increase in the number of adsorbed molecules with increasing pressure.

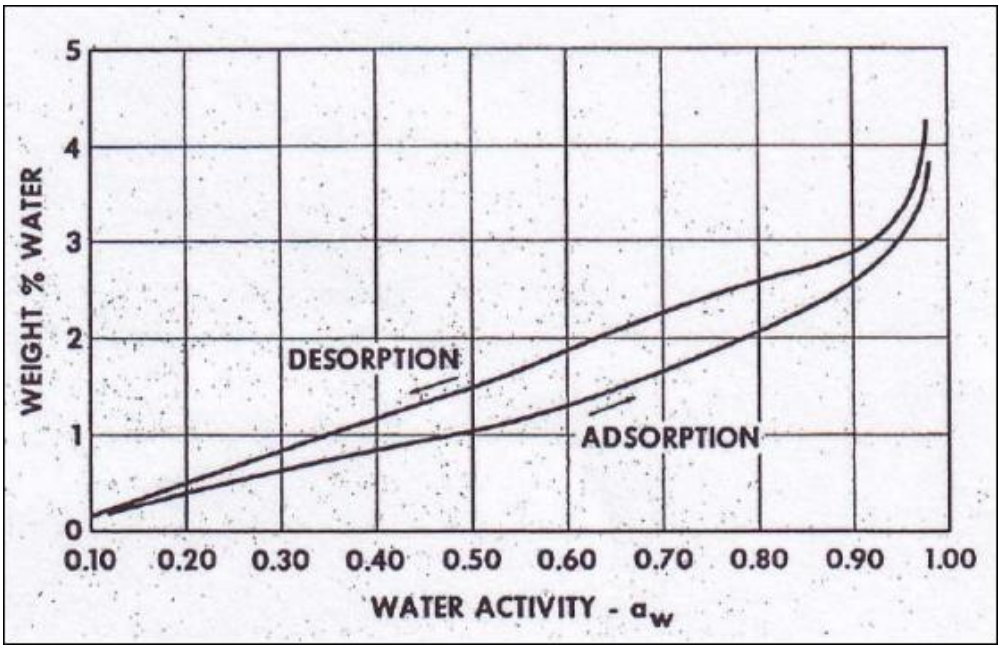

Figure 12: Adsorption isotherm of shale (adapted from Chenevert 1970)

The figures 13 and 14 show that the water activity of shale increases with increase in confining pressure and temperature.

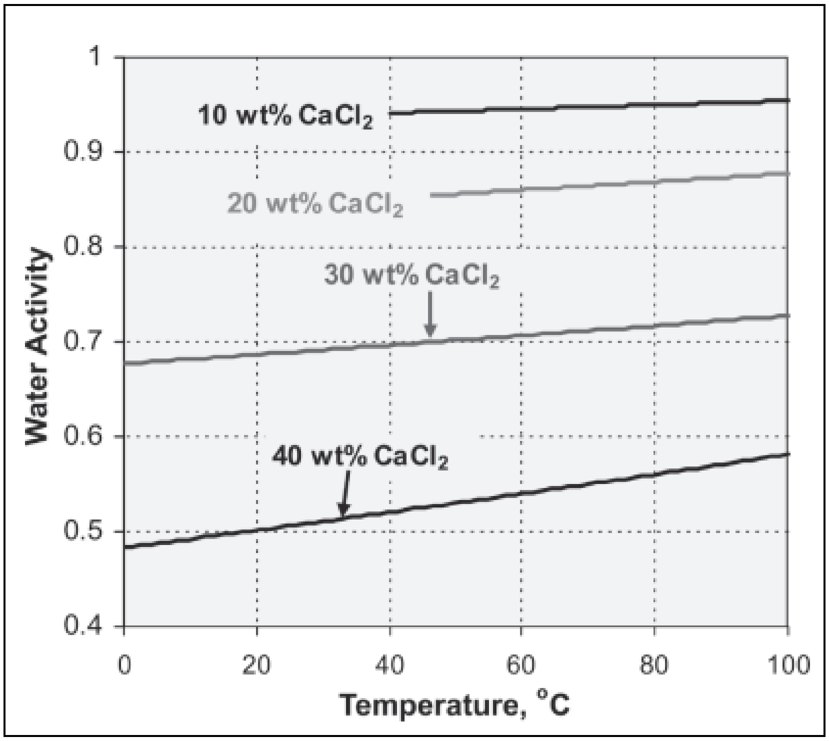

Figure 13: Effect of temperature on water activity of shale (adapted from Chenevert and Strassner 1975)

The water activity of the drilling fluid is also calculated based on the correlation

$$a_{w,mud} = C_1 exp C_2 T \ldots\ldots\ldots\ldots\ldots\ldots\ldots\ldots\ldots\ldots\ldots\ldots\ldots\ldots\ldots\ldots. (1)$$

Where C1 and C2 are constants depending on concentration of the salt in the solution (Chenevert and Strassner 1975).

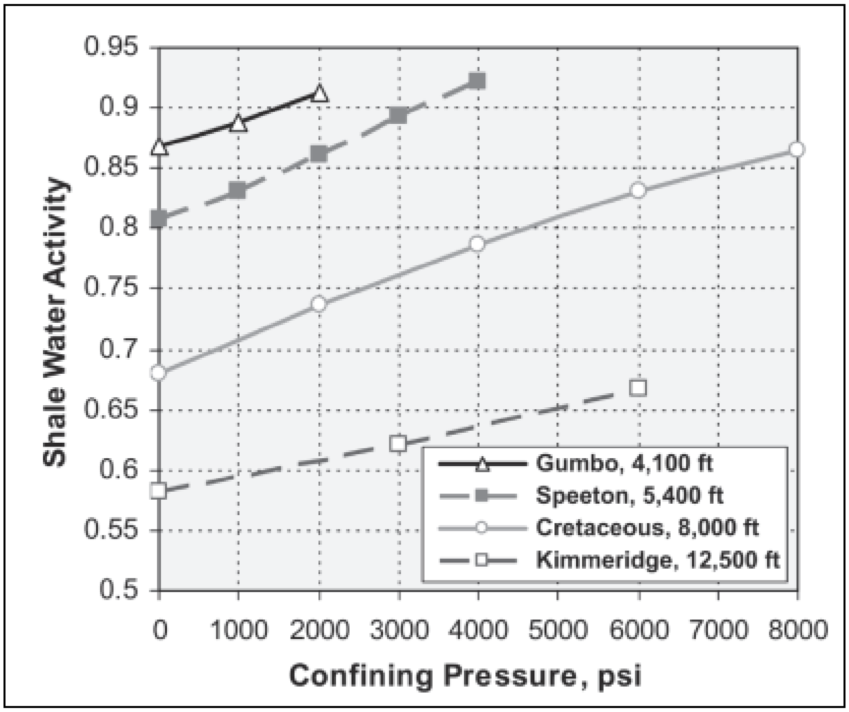

Figure 14: Effect of confining pressure on water activity of shale (adapted from Fonseca and Chenevert 1996)

The osmotic pressure is calculated from the activity of the shale and the drilling fluid as shown in the equation 2. The osmotic potential of an ideal membrane is greater than the osmotic potential of a non- ideal membrane. Equation 2 is adapted from Fritz et al 1981.

$$P_w = \sigma_m \frac{RT}{V_w} \ln\left(\frac{a_{w,mud}}{a_{w,shale}}\right) \ldots\ldots\ldots\ldots\ldots\ldots\ldots\ldots\ldots\ldots\ldots\ldots (2)$$

Where

$P_w = osmotic\ pressure$

$\sigma_m = membrane\ efficiency$

$V_w = molar\ volume\ of\ water\ (0.018\ l/\ mol)$

2.5: Transport Mechanisms in Shale

When the water based muds come in contact with the shale formations the ions and the water flow into the shale due to different driving forces. The driving forces in shale are:

Hydraulic pressure difference, electrical potential difference, chemical potential difference of water between mud and pore fluid and the concentration gradients between the solutes of the mud and the pore fluid (Simpson et al., 2000).

2.5.1: Osmotic flow

The osmotic pressure developed in shale influences the transfer of solutes and the associated water between the drilling mud and the pore fluid, through clay which acts as a semi permeable membrane.

The osmotic pressure developed due to difference in the water activity of the drilling mud and the pore fluid causes the flow of water from region of high water activity (low salt concentration) to region of low water activity (high salt concentration) and the process is termed as capillary osmosis. It is a reverse process for diffusion osmosis discussed in section 2.5.2. Similarly osmotic pressure built due to electrical potential gradient of the components in the two fluids causes ions to move from fluid of high electrical potential to fluid of low electrical potential. The process is called electrophoresis and is accompanied with associated water movement termed as electro-osmosis. Hydration of shales makes it weaker thus aggravating the problems of wellbore instability (Abass et al., 2006).

In 1947 Sitter figured that the changes in the salinity of subsurface water with depth is due to the semi-permeable nature of shale. In 1965 Allen Young and Philip Low demonstrated the osmotic flow of water through shale samples which causes the subsurface pressure anomalies. Though Young et al., (1965) were able to justify the osmotic phenomena in shales, the quantification of osmotic pressure was less compared to the theoretical pressures associated with water flux. The reasons attributed for such

discrepancy are micro-cracks in the core samples, inability of the large weakly charged pores to restrict the solute movement.

In 2000 Neuzil conducted tests on Pierre shale to study the influence of osmotic pressure developed on fluid movement and also the longevity of the effect. The fluid flow in shale can be expressed as (Bresler 1973)

$$q = -\frac{k}{\mu}\frac{\partial p}{\partial r} + \sigma\frac{k}{\mu}\frac{\partial \pi}{\partial r} \dots\dots\dots\dots (3)$$

The 1st term in the equation is Darcy's law generated due to pore pressure gradient and the 2nd term is for osmotic pressure gradient. The fluid flux stops when the osmotic equilibrium is attained (q=0). The osmotic pressure built can be found at equilibrium by integrating equation 3 (Neuzil 2000)

$$\Delta p = \int_{cmax}^{cmin} \sigma(c)\frac{d\pi}{dc}dc \dots\dots\dots\dots (4)$$

Π (measure of decrease in chemical potential of water due to solute presence) and σ (osmotic efficiency) are functions of c (solute concentration).

Π is related to 'c' through water activity. However the relation between 'c' and σ is complex and the relationship is established between σ and b$\sqrt{c}$ by Bresler (1973), where 'b' is half distance between the platelets proving the dependency of osmotic efficiency of shale on shale compaction and the solute concentration. The osmotic pressure decreases only when the TDS differences that created it dissipate by diffusion and the longevity is influenced by the membrane effective ionic diffusion coefficient $\widehat{D_d}$.

$$\widehat{D_d}\left[\frac{\partial^2 c}{\partial r^2} + \frac{1}{r}\frac{\partial c}{\partial r}\right] = \frac{\partial c}{\partial t} \dots\dots\dots\dots (5)$$

The time taken for TDS difference to reduce to half its value for shale of thickness 'L' and diffusion coefficient $\widehat{D_d}$ is given by Crank. J (1957)

$$t = 0.1 * \frac{L^2}{\widehat{D_d}} \quad \ldots \ldots (6)$$

The non -osmotic pressure decays 1000 times faster than osmotic pressure (Neuzil, 2000).

2.5.2: Diffusional Flow

Diffusional flow is opposite to capillary osmotic flow. By principle of Fick's law of diffusion, the solutes flow from the solution with high salt concentration (with low chemical potential of water) to solution with low salt concentration (high chemical potential of water) while water passes from solution with high chemical potential of water to solution which has lower water chemical potential. The diffusional flow is effective when the shale membrane efficiency is less and has high permeability to allow the solutes to pass through them. The diffusional flow is significant in fractured or high permeable formations affecting the shale stability compared to formations which are less permeable. For example when the shale is in contact with the brine, the clay structure is altered and destabilized due to the cation exchange reactions (Abass et al., 2006). If the diffusional force is greater than the chemical osmotic force, invasion of ions and water increases the pore pressure and water content of shale near the wellbore region. Water and solutes can be transferred from mud to shale by diffusion osmosis even when the hydraulic pressure difference and chemical osmotic pressure difference does not exist. Addition of salt to a water based mud to reduce the water activity causes an increase in the diffusional osmotic force affecting the desired increase in the chemical osmotic force (Simpson et al., 2000). The concentration gradient in soil causes

a drag of bulk pore fluid by diffusional flow of species from concentrated to dilute solutions. Though diffusional osmosis and chemical osmosis happen simultaneously, chemical osmosis is significant in densely compacted formation with high cation exchange capacity while diffusion osmosis is significant in less compacted formation with less cation exchange capacity (Olsen et al., 1990). By Curie Prigogine principle, there is no coupling between the scalar and vector quantities in isotropic medium. Hence diffusion and chemical reaction are not coupled.

2.5.3: Hydraulic flow

The fluid flow in the subsurface is always considered to be an effect of pressure differences between the drilling mud and the shale pore fluid which is governed by Darcy's law. The flow is usually directed from the mud to the shale formation during an overbalanced drilling. Increase in mud weight of the drilling fluid increases the confining pressure which stabilizes the shale formation. However it also increases the shale hydration. The water based muds are at a disadvantage compared to oil based muds which has threshold capillary pressure and prevents shale hydration. Water based muds dissipate pressure because of the miscibility with shale pore water while oil based muds don't and have high radial stress (Abass et al., 2006). Hydraulic conductivity of shale increases with the fractures created and is found to be thrice the magnitude of the unfractured shale (McKay et al., 1993).

2.6: Shale consolidation theories

2.6.1: Terzaghi and Biot's poroelastic consolidation

The phenomena of soil consolidation when load is applied was first proposed by Terzaghi (1925). He assumed the soil to be a porous medium possessing elastic

properties and the pores are filled with water analogous to a rubber sponge. He propounded that the rate at which the soil consolidates or settles depends on the rate at which the water is squeezed out of the pores when a load is applied. He also formulated equations representing the soil consolidation phenomena mathematically. However Terzaghi's formulations were limited to one dimensional consolidation for a fixed load. Biot (1941) overcame these limitations by extending the equations to three dimensions and also validated them for any load varying with time. He assumed the soil to have the following properties:

a. Isotropy of soil
b. Reversibility of stress-strain relations under equilibrium conditions
c. Linearity of stress strain relationship
d. Smaller strains
e. Incompressible pore water
f. Water may contain air bubbles
g. Water flows through pores in accordance to Darcy's law

2.6.2: Porochemoelectroelastic consolidation

Though the first theoretical investigation on electro-osmosis was started by Reuss (1908) based on his observations on thin clay diaphragm it was not practically taken into consideration for modelling transport equations for shale as it was considered to be a poroelastic medium and the knowledge of colloidal chemistry of shale was insufficient. Casagrande (1949) investigated on the electro osmotic transport of water in soil and found the process to be constant irrespective of the soil types. Later when the behavior of clay rich porous formations were studied it was found that shale behaves

like a semi permeable membrane restricting the transport of solute of some species in pore fluid (Young and low 1965, Olsen 1969, Neuzil 2000). Esrig (1968) studied the electro-kinetic consolidation of shale and predicted that the positive and negative pore pressures develop because of the application of electrical field. The magnitude of the pore pressures developed depends on the electric field applied and also on the geometry of the electrodes. He also studied that the rate of consolidation due to electric potential applied is very slow as the soil consolidation depends mainly on soil compressibility and permeability. He developed a one dimensional solution for consolidation problem but ignored ion transportation. Since shale has a higher percentage of clay which acts like a semi permeable membrane and allows fluid flow due to non-hydraulic driving forces, shale also exhibited swelling and shrinking phenomena termed osmosis when it was brought in contact with aqueous solutions. The concept of osmosis has invoked to explain the anomalous pressure behavior in subsurface aquifers (Neuzil 2000). The low permeability and the negative charges on the surface of shale membrane are the reasons for shale to have high membrane efficiency. The fluid components separated by shale with different chemical potentials cause movement of chemical species along with water which is termed as chemical-osmosis. Similarly when shale with pore fluid which acts like an electrolyte with its ions is subjected to an electrical potential gradient, it causes movement of ions along with water from fluid with high to low electrical potentials. This is similar to the coupled flows that take place in soil with simultaneous flows of water, ions and chemical species. Since then shale is considered as a porochemoelectroelastic medium and the electrochemical interactions between the fluids separated by shale and also with shale media which affects the pore pressure

distribution and effective stress has to be quantified for predicting the overall mechanical response of shale. The transport formulations for the coupled irreversible processes in soil derived based on non- equilibrium thermodynamics (Katchalsky and Curran 1967, Yeung and Mitchell 1993) was adopted for explaining the transport mechanisms in shale. The original poromechanics theory by Biot (1941) was reformulated for porous medium to include the electrochemical interactions based on non-equilibrium thermodynamics (Sachs et al., 1989, Corapcioglu 1991). The analytical solutions explaining the mechanical response of the porochemoelectroelastic medium were presented by Lui et al., 1999 and Van Meerveld et al., 2003. However the solutions were restricted to one dimensional consolidation problem.

2.7: Recent research on consolidation theory to study wellbore stability

For many years significant efforts have been made to understand the rock mechanics causing the wellbore instabilities. Before the advent of electrokinetic phenomena happening in shale, it was considered that the swelling and shrinking of clays happened only due to adsorption of water molecules onto shale surface. Later the analytical solutions explaining the mechanical response of many semi permeable membranes were incorporated to shale to understand its wellbore stability. However many analytical solution developed were one dimensional and could not completely predict the mechanical response. Ekbote and Abousleiman (2006) developed generalized a coupled formulation for chemically active formation in which an inclined wellbore has been drilled and is subjected to in-situ stresses. However this formulation ignored the electrical coupling. Nguyen Vinh et al., (2008) developed the analytical solution for the coupled porochemoelectroelastic processes when an inclined wellbore is drilled into an

isotropic formation. Nguyen Vinh et al., (2009) developed a finite element model to study the responses for a naturally fractured porous medium using dual porosity dual permeability method. Ghassemi et al., (2009) analyzed the pore pressure and stress distribution around the wellbore based on a coupled thermo elastic model of chemically active rock showing the interactions between temperature, stress and chemistry. Roshan and Rahman (2010) have developed a finite element based chemo-thermo-poroplastic model to study the stress and pore pressure distribution in naturally fractured shale formations. Tran et al., (2013) have formulated the analytical solution for anisotropic porochemoelectroelastic medium with a cylindrical wellbore drilled into the formation and subjected to various loading conditions.

Table 4: Hierarchy of observations in developing model describing the flow in soil

YEAR	AUTHOR	FORMULATION	LIMITATIONS
1908	Von Reuss	Initiated the investigation on electro-osmosis in soil	Did not model transport equations due to lack of knowledge about colloidal chemistry of soil
1925	Terzaghi	Soil is a porous medium with elastic properties filled with water. The rate of consolidation depends on rate of liquid drop out when load is applied	Limited to 1-D consolidation for fixed load
1941	Biot	Extended the existing Terzaghi's equations to 3 dimensions and validated for any load varying with time	Later reformulated to include the electrochemical interactions
1949	Casagrande	Investigated on electro osmotic transport of water in soil and found that the porocess is constant in all soils	
1965,1969, 2000	Young and low, Olsen, Neuzil	Confirmed shale behaves like a semi permeable membrane restricting transport of solute of some species	

1967, 1993	Katchalsky & Curran, Yeung & Mitchell	Developed formulations for coupled irreversible transport processes based on non equilibrium thermodynamics	
1968	Esrig	Studied electro-kinetic consolidation and suggested that negative pore pressure are due to electrical field application. Magnitude of pore pressure depends on electrical field and also on geometry of the electrodes.	Developed a 1 D solution for consolidation but ignored ion transport
1989, 1991	Sachs et al., Corapcioglu	Reformulated Biot's theory including electrochemical interactions based on non equilibrium thermodynamics	
1999, 2003	Lui et al., Van Meerveld et al.,	Developed analytical solutions explaining mechanical response of porochemoelectroelastic medium	But restricted to 1 dimensional consolidation
2000	Neuzil	Found anamalous pressure behavior is due to osmosis and also framed equations to calculate the presure developed and also time to calculate the longevity of the developed pressure	
2006	Ekbote and Abousleiman	Developed a generalized coupled formulations for chemically active formations with inclined wellbore and subjected to in-situ stress	Ignored electrical coupling and simplified isotropic medium
2008	Nguyen and Abousleiman	Developed analytical solutions for coupled porochemoelectroelastic medium with inclined wellbore	Ignored thermal effects and simplified isotropic medium
2009	Nguyen and Abousleiman	Studied the responses of the naturally fractured coupled flow porous medium using dual porosity dual permeability method	Ignored thermal effects and simplified isotropic medium

2009	Ghassemi	Analyzed pore presure and stress distribution near wellbore for a coupled thermo elastic chemically active porous medium explaining the relationship between the tempertaure, stress and chemistry.	Ignored electrical coupling and simplified isotropic medium
2010	Roshan and Rahman	Developed chemothermoporoplastic model to study stress and pore pressure distributions in naturaly fractured shale formations	Ignored electrical coupling and simplified isotropic medium
2013	Tran et al	Developed analytical solutions for anisotropic porochemoelectroelastic medium with cylindrical wellbore	Ignored thermal effects

Chapter 3: Coupled flow formulations for Shale

3.1: Extension of classical thermodynamics for irreversible processes

The coupled fluid, electrical and chemical flows in soil have been analyzed by Yeung and Mitchell (1993) based on the concept of non-equilibrium thermodynamics to comprehend the transport processes involved.

The coupled flow is understood as the linear relationship existing between the flow and the corresponding driving forces or gradients based on the previous formulations such as Darcy law relating the fluid flow and the pressure gradient, Fick's law relating the flow of individual species in solution and its concentration gradient, Fourier's law relating the heat flow and the temperature gradient.

The linear relationship existing between the coupled flows is given by the following equation where the total flow of a particular type 'i' is related to the summation of the contribution from all existing flows due to the corresponding gradients (Yeung and Mitchell 1993).

$$\vec{J_i} = \sum_{j=1}^{n} L_{ij}\vec{X}_j \quad \ldots\ldots (7)$$

Where L_{ij} is the coupling coefficient relating the flow of type 'i' with gradients 'j'. The magnitude of the coupling coefficient L_{ij} greatly influences the coupled flows and has to be quantified for practical use of equation 7. The coupled flows in the shale system is out of equilibrium and the formulations are framed based on non-equilibrium thermodynamics. The transport coefficients can be expressed in terms of field measurable parameters based on the concept of irreversible or non-equilibrium thermodynamics (Gray 1966).

Non equilibrium thermodynamics differs from the classical thermodynamics by defining state of the system at all times during the path of an irreversible process.

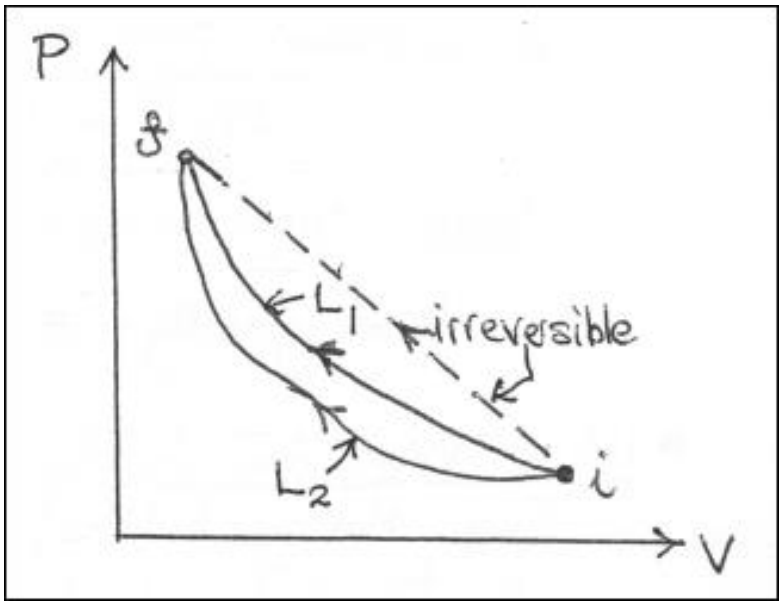

Figure 15: Representation of reversible and irreversible processes in classical thermodynamics (Department of Physics, University of Manchester)

The classical thermodynamics can be extended to define the irreversible processes by including few postulates such as (Yeung and Mitchell 1993)

1. Local equilibrium
2. Linear phenomenological equations
3. Validity of the Onsager reciprocal relations

3.1.1: Local equilibrium

The system under consideration can be divided into smaller segments where in each of the segments the state functions exist and the segments are assumed to be in local equilibrium as the state functions are continuous with space and time (infinitesimal changes). Since process in each segment is in equilibrium state and can be considered

reversible, classical thermodynamics is applied in each segment (Yeung and Mitchell 1993).

3.1.2: Linear phenomenological equations

The linear equation relating the flow of one type with the effective driving forces in the system as shown in equation 7. The transport coefficients L_{ij} are also called as phenomenological coefficients and are independent of the driving forces. If i = j then L_{ii} is the conductivity coefficient of the flows and if i $\neq$ j then L_{ij} are the coupling coefficients relating flows of different types producing cross effects (Mitchell 1976).

3.1.3: Validity of Onsager reciprocal relations

Onsager (1931) put forward his theory of reciprocal relations based on the assumption of local equilibrium and reversibility of the processes in small segments which states that the phenomenological coefficients are symmetrical if they are not influenced by the external magnetic field or Coriolis forces (Fitts 1962). This postulate helps to reduce the number of coefficients from n^2 to ((n+1)*n)/2.

$$L_{ij} = L_{ji} \quad \ldots \ldots \ldots (8)$$

3.2: Formulations of the irreversible processes

The fluxes and the driving forces exist only when the state parameters deviate from the equilibrium values. The driving forces and the fluxes are selected only if it is in accordance with 2nd law of thermodynamics (Yeung 1990).

$$\overrightarrow{X_i} = \frac{\partial \Delta s}{\partial \alpha_i} \quad \ldots \ldots \ldots (9)$$

Where

$\overrightarrow{X_i} = driving\ forces$

$\partial \Delta s = changes\ in\ entropy\ per\ unit\ volume\ from\ equilibrium\ values$

$\partial\alpha_i = deviation\ in\ state\ parameters\ from\ equilibrium\ values$

$$\vec{J_i} = \frac{\partial \alpha_i}{\partial t} \dots\dots\dots\dots\dots\dots\dots\dots\dots\dots\dots\dots \quad (10)$$

From equation 9 and 10 the entropy produced per unit volume per unit time during the irreversible process can be calculated as

$$\frac{ds}{dt} = \sigma = \sum_{i=1}^{n} \vec{J_i}.\vec{X_i} \dots\dots\dots\dots\dots\dots\dots\dots\dots\dots \quad (11)$$

Based on equation 11 and the Gibbs equation relating the intensive properties of a system in equilibrium undergoing reversible changes Katchalsky and Curran 1965 derived an expression similar to equation 11 to determine the local dissipation energy per unit volume per unit time (Φ = σ *T).

$$\Phi = \sum_{i=1}^{n} \vec{J_i}.\vec{X_i} \dots\dots\dots\dots\dots\dots\dots\dots\dots\dots \quad (12)$$

Equation 12 is different from equation 11 by a factor of 'T'. Hence under isothermal conditions it is convenient to use Φ than σ (as Φ is related to Gibbs free energy while σ is related to entropy as seen in s = q/ T).

The formulations are framed by a) estimating the dissipation function b) forming linear phenomenological equations relating the predefined fluxes and driving forces c) applying the Onsager's reciprocal theory and d) expressions for phenomenological coefficients in field parameters.

3.2.1: Dissipation function for shale media

Based on the coupled flows and the driving forces present in the soil, dissipation function for the above irreversible processes was framed by Yeung and Mitchell 1993 as following:

$$\Phi = \sum_{i=1}^{n} \vec{J_i} . \nabla(-\tilde{\mu}_i) \ldots \ldots \ldots \ldots \ldots \ldots \ldots \ldots \ldots \ldots \ldots \ldots \ldots \ldots \ldots \ldots .. (13)$$

Where

$\tilde{\mu}_i$ *is the electrochemical potential of species i*

$$\tilde{\mu}_i = \mu_i + z_i FE \ldots \ldots \ldots \ldots \ldots \ldots \ldots \ldots \ldots \ldots \ldots \ldots \ldots \ldots \ldots \ldots . (14)$$

Where

$\mu_i = chemical\ potential\ of\ species\ i$

$z_i = charges\ of\ species\ i$

$F = Faraday's\ constant$

$E = electrical\ potential\ of\ species\ i$

The chemical potential of species ‘i’ has concentration dependent, temperature dependent and pore pressure dependent components.

$$\mu_i = \mu_i^o(T) + \tilde{V}_i P + \mu_i^c \ldots \ldots \ldots \ldots \ldots \ldots \ldots \ldots \ldots \ldots \ldots \ldots \ldots \ldots \ldots . (15)$$

Substitute equations 14 and 15 in 13 for isothermal conditions to get

$$\phi = \left(\sum_{i=1}^{n} \vec{J}_i \vec{V}_i \right) . \nabla (-P) + \sum_{i=1}^{n} \vec{J}_i . \nabla (-\mu_i^c - z_i FE) \ldots \ldots \ldots \ldots \ldots \ldots \ldots .. (16)$$

In equation 16 $\left(\sum_{i=1}^{n} \vec{J}_i \vec{V}_i \right) = \vec{J}_v$ (rate of volume of fluid flowing per unit area of an element) and for isothermal conditions $\sum_{i=1}^{n} c_i \nabla (\mu_i^c + z_i FE) = 0$ by Gibbs-Duhem relation. By incorporating the above conditions and replacing the absolute diffusional flow ($\vec{J}_i$) by relative diffusional flow ($\vec{J}_d$) in equation 16 gives

$$\phi = \vec{J}_v . \nabla (-P) + \vec{I} . \nabla (-E) + \vec{J}_C^d \nabla (-\mu_c^c) + \vec{J}_a^d \nabla (-\mu_a^c) \ldots \ldots \ldots \ldots \ldots \ldots \ldots . (17)$$

Where $\vec{I} = \sum_{i=1}^{n-1} (\vec{J}_i^d z_i F)$ is the electric current density passing through clay rich shale (Fitts 1962).

3.2.2: Transport equations for shale media

Based on equation 17 and theory of linear phenomenological equations the flows and the driving forces in shale are related as

$$\vec{J}_v = L_{11}\nabla(-P) + L_{12}\nabla(-E) + L_{13}\nabla(-\mu_c^c) + L_{14}\nabla(-\mu_a^c) \dots\dots\dots\dots\dots\dots\dots\dots\dots\dots (18)$$

$$\vec{I} = L_{21}\nabla(-P) + L_{22}\nabla(-E) + L_{23}\nabla(-\mu_c^c) + L_{24}\nabla(-\mu_a^c) \dots\dots\dots\dots\dots\dots\dots\dots\dots\dots (19)$$

$$\vec{J}_c^d = L_{31}\nabla(-P) + L_{32}\nabla(-E) + L_{33}\nabla(-\mu_c^c) + L_{34}\nabla(-\mu_a^c) \dots\dots\dots\dots\dots\dots\dots\dots\dots\dots (20)$$

$$\vec{J}_a^d = L_{41}\nabla(-P) + L_{42}\nabla(-E) + L_{43}\nabla(-\mu_c^c) + L_{44}\nabla(-\mu_a^c) \dots\dots\dots\dots\dots\dots\dots\dots\dots\dots (21)$$

3.3: Phenomenological coefficients in terms of field parameters

Based on Onsager's reciprocal theory as shown in equation 8, the phenomenological coefficients are reduced from 16 to 10. Expressions of the coefficients in field parameters are found from experiments by maintaining conditions such that 1 or 2 gradients disappear. The conductivity parameter of any flow type 'i' is defined as the ratio of the flow of type 'i' per unit area to its corresponding gradient applied.

3.3.1: Conductivity coefficients

Hydraulic conductivity coefficient

$$L_{11} = \frac{k_h}{\gamma_t n} + \frac{L_{12}L_{21}}{L_{22}} \dots\dots\dots\dots\dots\dots\dots\dots\dots\dots\dots\dots\dots\dots\dots\dots\dots\dots\dots\dots\dots\dots\dots\dots\dots\dots (22)$$

Where

$k_h = hydraulic\ conductivity\ \ of\ porous\ media$

$\gamma_t = unit\ weight\ of\ pore\ fluid$

$n = porosity\ of\ shale$

k_h varies from $1x10^{-13}$ to 1 m/s (Freeze et al., 1979).

Electrical conductivity coefficient is given by

$$L_{22} = \frac{\kappa}{n} \dots \dots \dots \dots \dots \dots \dots \dots \dots \dots \dots \dots \dots \dots \dots \dots \dots \dots \dots \dots \dots \dots \dots \dots \dots \dots \dots \dots \dots \dots \dots . (23)$$

Where

$\kappa = electrical\ conductivity\ of\ shale\ media$

κ generally varies from 0.01 to 0.1 S/m (Yeung and Mitchell 1993).

Chemical conductivity coefficient is given by

$$L_{33} = \frac{D_c^* C_c}{RT} \dots \dots \dots \dots \dots \dots \dots \dots \dots \dots \dots \dots \dots \dots \dots \dots \dots \dots \dots \dots \dots \dots \dots \dots \dots \dots \dots \dots \dots \dots (24)$$

$$L_{44} = \frac{D_a^* C_a}{RT} \dots \dots \dots \dots \dots \dots \dots \dots \dots \dots \dots \dots \dots \dots \dots \dots \dots \dots \dots \dots \dots \dots \dots \dots \dots \dots \dots \dots \dots \dots (25)$$

Where

$C_i = concentration\ of\ the\ chemical\ species\ i$

$R\ and\ T = universal\ gas\ constant\ , temperature\ respectively$

$D_i^* = effective\ diffusion\ coefficient\ of\ chemical\ species\ i$

The effective diffusion coefficient of chemical species in shale is generally greater than its value in aqueous solutions due to tortuosity (τ longer flow path in soil) which generally varies from 1.2 to 2.8 (Gillham et al., 1982). The relation between effective diffusion coefficient in soil and its diffusivity in solution is given by $D_i^* = D_i n^{\tau}$ (Gillham et al., 1984). The diffusivity of ions in extremely dilute solutions at room temperature ranges from 5 x 10^{-10} to 20 x 10^{-10} (Dean 1973).

3.3.2: Coupling coefficients

Coefficients of fluid flow due to applied electric field and vice versa

$$L_{12} = L_{21} = \frac{k_e}{n} \dots \dots \dots \dots \dots \dots \dots \dots \dots \dots \dots \dots \dots \dots \dots \dots \dots \dots \dots \dots \dots \dots \dots \dots \dots \dots \dots \dots \dots (26)$$

Where

$k_e = electro - osmotic\ permeability$

k_e is the ratio of volumetric flow rate of fluid per unit area to applied electrical gradient and ranges from 1 x 10^{-9} to 10 x 10^{-9} m^2/ V.s (Casagrande 1983).

Interionic-diffusional coefficients

The pore fluid in shale is highly saturated and can be considered as a dilute solution. The interactions between ions in dilute solution is very weak such that the flow of ions of one type is not influenced by the concentration gradient of other type of ions.

$$L_{34} = L_{43} = 0 \quad \ldots\ldots (27)$$

Coefficients of ionic migration due to applied electrical field and vice versa

The effective ionic mobility in soil (the velocity of ionic migration in soil when electric field is applied) is less compared to ionic mobility in free aqueous solutions due to tortuosity (Mitchell and Yeung 1990). The similarity between effective diffusion coefficient and effective ionic mobility was observed by Koryta (1982) and he propounded the validity of Nernst equation for the chemical species in pore fluids of shale to relate the effective diffusion coefficient and ionic mobility as $u_i^* = D_i^*|z_i|F/RT$. Based on these conceptions

$$L_{23} = L_{32} = \frac{D_c^*|z_c|FC_c}{RT} \quad \ldots\ldots (28)$$

$$L_{24} = L_{42} = \frac{D_a^*|z_a|FC_a}{RT} \quad \ldots\ldots (29)$$

Coefficients of ionic migration due to applied hydraulic gradient and vice versa

The coefficients depend on ω (membrane efficiency or reflection coefficient or osmotic selectivity coefficient) which has been discussed in section 2.3.

$$L_{13} = -\frac{\omega C_c (L_{11}L_{22} - L_{12}L_{21}) - L_{12}L_{23}}{L_{22}} \dots\dots\dots\dots\dots\dots\dots\dots\dots\dots\dots\dots\dots\dots\dots\dots (30)$$

$$L_{14} = -\frac{\omega C_a (L_{11}L_{22} - L_{12}L_{21}) - L_{12}L_{24}}{L_{22}} \dots\dots\dots\dots\dots\dots\dots\dots\dots\dots\dots\dots\dots\dots\dots\dots (31)$$

3.4: Concentration of the ions, net charges and pH of the pore fluid in shale

Based on the principle of conservation of mass for steady state flow, an equation to determine the concentration of chemical species 'i' in the pore fluid as function of space and time has been formulated by Yeung and Datla (1994).

$$\frac{\partial c_i}{\partial t} = -\nabla . J_i - \frac{\rho_{dry}}{n}\frac{\partial S_i}{\partial t} - G_i \dots\dots\dots\dots\dots\dots\dots\dots\dots\dots\dots\dots\dots\dots\dots\dots\dots\dots\dots\dots\dots\dots (32)$$

Where

$\rho_{dry} = dry\ density\ of\ matrix$

$S_i = mass\ of\ chemical\ species\ adsorbed\ on\ shale\ surface\ per\ unit\ shale\ mass$

$G_i = source/sink\ indicating\ rate\ of\ removal\ species\ per\ unit\ volume$

In addition to electro-kinetic flows that happen when electric current is applied in presence of the diffuse double layer some electro chemical reactions also take place generating pH gradient across the shale. Changes in the pH gradient affect the adsorption and desorption phenomena that particles undergo.

The pore fluid is acidic in the region of high cationic concentration and more alkaline in the region of high anionic concentration. The entire system of shale along with pore fluid is electrically neutral (Snoeyink and Jenkins 1980). The electrical neutrality of the shale media which is disturbed by applying an electric field can be restored by formation of hydrogen and hydroxyl ions (Yeung and Datla 1994).

The equation relating the net positive and negative charges is

$$C_T + [H^+] = A_T + [OH^-] \dots\dots\dots\dots\dots\dots\dots\dots\dots\dots\dots\dots\dots\dots\dots\dots\dots\dots\dots\dots\dots\dots\dots (33)$$

Where

$C_T, A_T = total\ positive\ and\ negative\ charges\ per\ unit\ volume\ respectively$

$[H^+], [OH^-] = concentration\ of\ hydrogen\ and\ hydroxyl\ ions\ respectively$

The total positive and negative charges in shale are given by the following equations based on the assumption that the activity coefficients of chemical species are 1.

$$C_T = \sum_{i=1}^{n} z_{c,i} c_{c,i} \dots \dots \dots \dots \dots \dots \dots \dots \dots \dots \dots \dots \dots \dots \dots \dots \dots \dots \dots \dots \dots \dots \dots \dots \dots \dots \dots \dots \dots \dots \dots (34)$$

$$A_T = \sum_{j=1}^{n} z_{a,j} c_{a,j} \dots \dots \dots \dots \dots \dots \dots \dots \dots \dots \dots \dots \dots \dots \dots \dots \dots \dots \dots \dots \dots \dots \dots \dots \dots \dots \dots \dots . \dots \dots (35)$$

Equation 32 is evaluated for every time step and is used to calculate the net charges from equation 34 and 35. Equations 33 and 36 are solved simultaneously to determine the concentration of hydrogen ions as a function of space and time.

$$[H^+] + [OH^-] = K_w \dots \dots \dots \dots \dots \dots \dots \dots \dots \dots \dots \dots \dots \dots \dots \dots \dots \dots \dots \dots \dots \dots \dots \dots \dots \dots \dots . (36)$$

The values of pH generated can be found as a function of time and space using the following equation

$$pH = -\log_{10}[H^+] \dots \dots \dots \dots \dots \dots \dots \dots \dots \dots \dots \dots \dots \dots \dots \dots \dots \dots \dots \dots \dots \dots \dots \dots \dots \dots \dots . . (37)$$

3.5: Alternative formulation of Electro-Chemico-Osmotic processes in Shale

Corapcioglu (1991) developed a set of one dimensional governing equations for the explaining the simultaneous flows of water, chemical species and electric current in a porous medium based on the macroscopic conservation of mass equations and principle of continuum, an alternative to the previous approach based on the irreversible coupled flows. Some of the important equations from his literature are

Mass balance equation for the entire water phase

$$\frac{k}{\mu_f}\frac{\partial^2 p}{\partial x^2} + k_{hc}\frac{\partial^2 C_s}{\partial x^2} + k_e\frac{\partial^2 \varphi}{\partial x^2} + \frac{D}{\rho_f}\frac{\partial^2 \rho_f}{\partial x^2} = (\alpha + n\beta)\frac{\partial p}{\partial t} \ldots\ldots\ldots\ldots\ldots\ldots\ldots\ldots\ldots\ldots\ldots\ldots (38)$$

Mass balance equation for the chemical species in water phase with an assumption of zero net mass transfer rate due to reactions

$$\frac{\rho_f C_s k}{\mu_f}\frac{\partial^2 p}{\partial x^2} + \rho_f C_s k_{hc}\frac{\partial^2 C_s}{\partial x^2} + \rho_f C_s k_e\frac{\partial^2 \varphi}{\partial x^2} + D\frac{\partial^2 \rho_f C_s}{\partial x^2} = \rho_f C_s \alpha\frac{\partial p}{\partial t} + n\frac{\partial \rho_f C_s}{\partial t} \ldots\ldots (39)$$

One dimensional model for current flow

$$\frac{\sigma_h}{g\rho_f}\frac{\partial^2 p}{\partial x^2} + \sigma_e\frac{\partial^2 \varphi}{\partial x^2}k_{ec}\frac{\partial^2 C_s}{\partial x^2} = 0 \ldots\ldots\ldots\ldots\ldots\ldots\ldots\ldots\ldots\ldots\ldots\ldots\ldots\ldots\ldots\ldots\ldots\ldots\ldots\ldots\ldots (40)$$

Equation of state

$$\rho_f = \rho_{f0} exp\left[\beta_p(p - p_0) + \sum_{i=w,s} v_i(m_i - m_{i0})\right] \ldots\ldots\ldots\ldots\ldots\ldots\ldots\ldots\ldots\ldots\ldots\ldots\ldots\ldots (41)$$

Pore fluid viscosity

$$\mu_f = 1.002 * 10^{-3}\left(1 + 0.4819C_s + 0.2774{C_s}^2 + 0.7814{C_s}^3\right) \ldots\ldots\ldots\ldots\ldots\ldots\ldots\ldots (42)$$

Where

$C_s = mass\ fraction\ of\ chemical\ component\ in\ water\ phase$

$\varphi = electrical\ potential$

$\mu_f\ , \rho_f = viscosity\ and\ density\ of\ water\ phase\ respectively$

$D = mechanical\ dispersion\ coefficient$

$k = permeability\ of\ porous\ medium$

$k_e = coeficient\ of\ electro\ osmotic\ permeability$

$k_{ec} = migration\ potential\ coefficient$

$k_{hc} = chemico\ osmotic\ coefficient$

$\sigma_h, \sigma_e = streaming\ current\ conductivity, electrical\ conductivity\ respectively$

$p, g = pore\ pressure\ and\ gravitational\ acceleration\ respectively$

$\alpha = matrix\ compressibility\ coefficient$

$n, \beta = porosity\ and\ water\ phase\ compressibility$

However the formulations framed for clay rich soil by Corapcioglu cannot be used efficiently as the transport coefficient cannot be determined readily (Yeung and Datla 1995).

Chapter 4: Governing equations for modeling Shale consolidation

4.1: Transport Equations

Since the time Fourier formulated a linear relationship between the heat flow and the temperature gradient, many researchers have tried to relate the flows and the driving forces. However some researchers like Rouss, tried to relate the flows not only with the driving forces but also with other gradients present in the system after observing the flow of volume along with charges when electric field was applied and also same happened with application of hydrostatic pressure. Similar phenomena was observed even in Seebeck effect and Peltier effect, thus proving that in a slow process any flow is related directly and linearly to both conjugated and non-conjugated forces. After Lord Rayleigh formulated an equation relating the mechanical flows with all the mechanical forces available in the system, Onsager extended this equation to accommodate the thermodynamic forces and flows and named them as phenomenological equations as discussed in chapter 3. The equations 18, 19, 20 and 21 formulated by Yeung and Mitchell (1993) are the transport equations and are repeated below.

$$q_i = L_{11}\frac{\partial(-p)}{\partial x_i} + L_{12}\frac{\partial(-\psi)}{\partial x_i} + L_{13}\frac{RT}{m_o^a}\frac{\partial(-m^a)}{\partial x_i} + L_{14}\frac{RT}{m_o^c}\frac{\partial(-m^c)}{\partial x_i} \dots\dots\dots\dots\dots\dots (43)$$

$$I_i = L_{21}\frac{\partial(-p)}{\partial x_i} + L_{22}\frac{\partial(-\psi)}{\partial x_i} + L_{23}\frac{RT}{m_o^a}\frac{\partial(-m^a)}{\partial x_i} + L_{24}\frac{RT}{m_o^c}\frac{\partial(-m^c)}{\partial x_i} \dots\dots\dots\dots\dots\dots (44)$$

$$J_i^{a,d} = L_{31}\frac{\partial(-p)}{\partial x_i} + L_{32}\frac{\partial(-\psi)}{\partial x_i} + L_{33}\frac{RT}{m_o^a}\frac{\partial(-m^a)}{\partial x_i} + L_{34}\frac{RT}{m_o^c}\frac{\partial(-m^c)}{\partial x_i} \dots\dots\dots\dots\dots (45)$$

$$J_i^{c,d} = L_{41}\frac{\partial(-p)}{\partial x_i} + L_{42}\frac{\partial(-\psi)}{\partial x_i} + L_{43}\frac{RT}{m_o^a}\frac{\partial(-m^a)}{\partial x_i} + L_{44}\frac{RT}{m_o^c}\frac{\partial(-m^c)}{\partial x_i} \dots\dots\dots\dots\dots (46)$$

4.2: Driving force equation

Model is developed based on the following assumptions:

1. The pore fluid (NaCl solution) behaves like an electrolyte with a solvent and one type of cations and anions.
2. The porous medium might be charged or neutral but the entire system is electrically neutral.

The electrochemical potential of each ionic species in shale which is controlled by the electrostatic potential field in addition to the existing chemical potential is given by Katchalsky and Curran (1965).

$$\widetilde{\mu^r} = V^r p + RTln[a^r] + z^r F\psi = V^r p + RTln[\varsigma^r m^r] + z^r F\psi \dots\dots\dots\dots\dots\dots\dots\dots (47)$$

$\widetilde{\mu^r} = the\ electro\ chemical\ potential\ of\ the\ fluid\ components\ 'r'$

$V^r = partial\ molar\ volume$

$p = hydrostatic\ pressure$

$R\ and\ T = universal\ gas\ constant\ and\ temperature\ respectively$

$a^r = chemical\ activity, a\ product\ of\ activity\ coeficient\ \varsigma^r\ \&\ mole\ fraction\ m^r$

$F\ and\ \psi = Faraday\ constant\ and\ electric\ potential\ respectively$

$z^r = valence\ of\ the\ ionic\ species$

4.3: Equations related to physical structure of shale

As mentioned in section 2.6.1, earlier equations developed to define the mechanics in physical structure of soil based on Biot's theory ignores the electrical and chemical potentials developed in soil. However these equations can facilitate only poroelastic medium unlike soil where electrochemical potentials play a significant role in fluid and

ion fluxes. Hence Biot's poroelastic equations have to be extended to be compatible to soil.

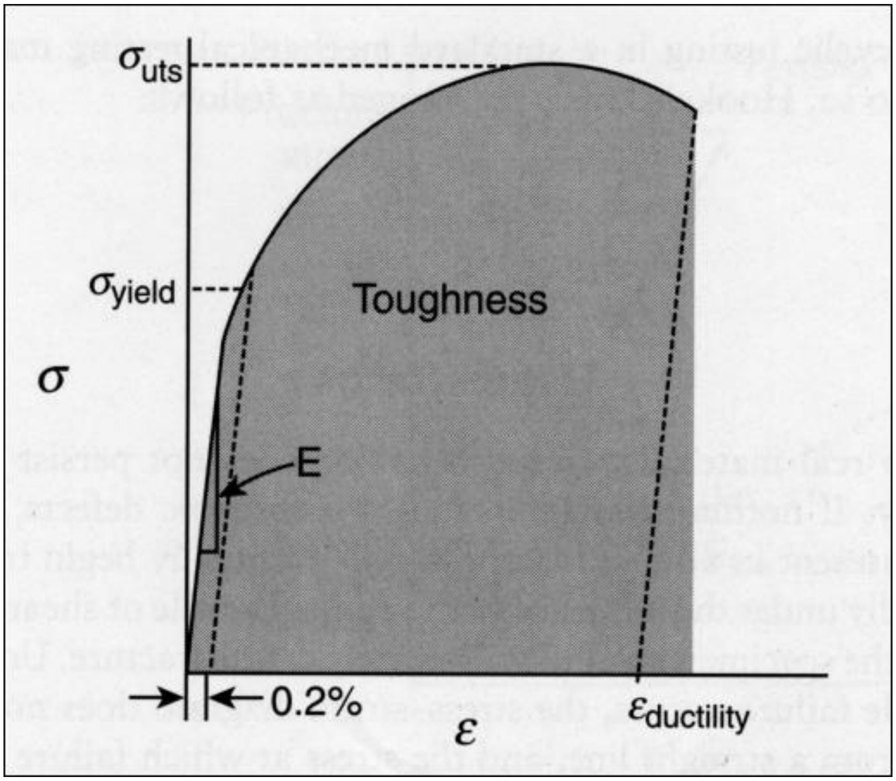

Figure 16: Stress Vs strain curve for ductile material (Ratner et al., 2004)

The area under the curve gives the amount of work or energy required per volume to deform the specimen until it fails. The area under the curve is a product of stress and strain which is in units of work. The movement of ions and charges of the electrolyte solution inside the porous medium absorbs some potential energy and weakens the porous medium. Coussy (2004) derived an expression for the change in free energy density of soil which is porous and saturated with salt solution under isothermal conditions and negligible deformation.

$$dW = \sigma_{ij} d\varepsilon_{ij} - \sum_{r=a,c,f} M^r d\widetilde{\mu^r} \ldots\ldots\ldots\ldots\ldots\ldots\ldots\ldots\ldots\ldots\ldots\ldots\ldots\ldots\ldots\ldots\ldots\ldots\ldots\ldots\ldots\ldots\ldots\ldots\ldots\ldots. (48)$$

Where

$\sigma_{ij} \& \varepsilon_{ij} = stress\ tensor\ \&\ strain\ tensor\ respectively$

$M^r = mass\ of\ fluid\ species\ in\ moles\ per\ unit\ volume\ of\ the\ rock$

The gradients of all the electrochemical potentials of the components in the pore fluid are related to each other through Gibbs-Duhem equation (Katchalsky and Curran 1965).

$$-\phi dp + \sum_{r=a,c,f} M^r d\widetilde{\mu^r} = 0 \ldots\ldots\ldots\ldots\ldots\ldots\ldots\ldots\ldots (49)$$

Assuming the pore space is completely saturated with the fluid and hence the porosity is given by the following equation (Nguyen Vinh et al., 2010).

$$\phi = V^{sol} = \sum_{r=a,c,f} V^r M^r \ldots\ldots\ldots\ldots\ldots\ldots\ldots\ldots\ldots (50)$$

Substituting equation 48 in 49 gives

$$dW = \sigma_{ij} d\varepsilon_{ij} - \phi dp \ldots\ldots\ldots\ldots\ldots\ldots\ldots\ldots\ldots (51)$$

Equation 51 is compared with the constitutive equations developed by Coussy (2004) developed for an isotropic medium

$$d\sigma_{ij} = 2G d\varepsilon_{ij} + \frac{2G\nu}{1-2\nu} d\varepsilon_{kk}\delta_{ij} + \alpha dp\delta_{ij} \ldots\ldots\ldots\ldots\ldots\ldots (52)$$

$$d\phi = -\alpha d\varepsilon_{kk} + \frac{1}{K_\phi} dp \ldots\ldots\ldots\ldots\ldots\ldots\ldots\ldots\ldots (53)$$

Where

$\alpha = biot's\ coefficient\ or\ pore\ pressure\ coefficient$

$\varepsilon_{kk} = volumetric\ strain = sum\ of\ linear\ strain$

$G \& \nu = shear\ modulus\ and\ poisson\ ratio\ respectively$

$K_\phi = pore\ compressibility$

$\delta_{ij} = kronecker\ delta, function\ of\ variables, 1\ if\ variables\ are\ equal\ else\ 0$

Based on the statement in equation 50, the changes in porosity in equation 53 is replaced by the total fluid content in the rock matrix which is given by

$$d\zeta = \frac{dM^{sol}}{\rho_o^{sol}} = \frac{d(\phi\rho^{sol})}{\rho_o^{sol}} = d\phi + \phi_o \frac{d\rho^{sol}}{\rho_o^{sol}} \dots\dots\dots\dots\dots\dots\dots\dots\dots\dots\dots\dots\dots\dots\dots\dots (54)$$

Where

$$M^{sol} = total\ mass\ of\ fluid\ in\ pores\ in\ moles = \sum_{r=a,c,f} M^r$$

$$\rho_o^{sol} = initial\ density\ of\ the\ fluid\ in\ pores\ in\ moles/m^3$$

$$\frac{d\rho^{sol}}{\rho_o^{sol}} = \frac{1}{K_f} dp \dots\dots\dots\dots\dots\dots\dots\dots\dots\dots\dots\dots\dots\dots\dots\dots\dots\dots\dots\dots\dots\dots\dots\dots\dots\dots\dots\dots (55)$$

By substituting equation 55 and 53 in 54 we get

$$d\zeta = -\alpha d\varepsilon_{kk} + \frac{1}{K_\phi} dp + \phi_o \frac{1}{K_f} dp \dots\dots\dots\dots\dots\dots\dots\dots\dots\dots\dots\dots\dots\dots\dots\dots\dots\dots\dots\dots\dots\dots\dots\dots\dots\dots\dots\dots (56)$$

The coefficients of dp are grouped together under ground water storage coefficient M as

$$M = \frac{1}{K_\phi} + \phi_o \frac{1}{K_f} \dots\dots\dots\dots\dots\dots\dots\dots\dots\dots\dots\dots\dots\dots\dots\dots\dots\dots\dots\dots\dots\dots\dots\dots\dots\dots\dots\dots\dots (57)$$

Like equation 54 the fluid content changes in each species of the fluid is given by

$$d\zeta^r = \frac{dM^r}{\rho_o^{sol}} = \frac{d(m^r M^{sol})}{\rho_o^{sol}} = m_o^r d\zeta + \phi_o dm^r \dots\dots\dots\dots\dots\dots\dots\dots\dots\dots\dots\dots\dots\dots\dots\dots\dots\dots\dots\dots\dots\dots\dots\dots\dots\dots\dots\dots (58)$$

Where

$$m^r = mole\ fraction\ of\ fluid\ species$$

Substituting equations 56 and 57 in 58 gives

$$d\zeta^r = m_o^r \left(-\alpha d\varepsilon_{kk} + \frac{1}{M} dp\right) + \phi_o dm^r \dots\dots\dots\dots\dots\dots\dots\dots\dots\dots\dots\dots\dots\dots\dots\dots\dots\dots\dots\dots\dots\dots\dots\dots\dots\dots\dots\dots (59)$$

Equation 59 can be rewritten for anionic and cationic species as

$$d\zeta^a = m_o^a\left(-\alpha d\varepsilon_{kk} + \frac{1}{M}dp\right) + \phi_o dm^a \dots\dots\dots\dots\dots\dots\dots\dots\dots\dots\dots\dots\dots\dots\dots\dots\dots\dots. (60)$$

$$d\zeta^c = m_o^c\left(-\alpha d\varepsilon_{kk} + \frac{1}{M}dp\right) + \phi_o dm^c \dots\dots\dots\dots\dots\dots\dots\dots\dots\dots\dots\dots\dots\dots\dots\dots\dots\dots. (61)$$

Equations 52, 56, 60 and 61 are the important equations pertaining to the physical structure of the porous medium. It is evident from equations 52 and 56 that the changes in stress and fluid content of the porous medium are due to pore pressure changes and are uninfluenced by the electrochemical potentials.

4.4: Governing equations of the porous medium

4.4.1: Strain displacement equation:

$$\varepsilon_{ij} = 0.5 * \left(\frac{\partial u_i}{\partial x_j} + \frac{\partial u_j}{\partial x_i}\right) \dots\dots\dots\dots\dots\dots\dots\dots\dots\dots\dots\dots\dots\dots\dots\dots\dots\dots\dots\dots\dots\dots\dots\dots. (62)$$

Where

u_i & u_j $= displacemnt\ vectors\ in\ unit\ directions\ i, j\ respectively$

4.4.2: Semi-static stress equilibrium equation:

$$\frac{\partial \sigma_{ij}}{\partial x_i} = 0 \dots\dots\dots\dots\dots\dots\dots\dots\dots\dots\dots\dots\dots\dots\dots\dots\dots\dots\dots\dots\dots\dots\dots\dots\dots\dots\dots\dots\dots\dots\dots\dots (63)$$

4.4.3: Mass conservation equations:

$$\frac{\partial \zeta}{\partial t} = -\frac{\partial q_i}{\partial x_i} \dots\dots\dots\dots\dots\dots\dots\dots\dots\dots\dots\dots\dots\dots\dots\dots\dots\dots\dots\dots\dots\dots\dots\dots\dots\dots\dots\dots\dots\dots.. (64)$$

For ionic species the volumetric flux is a product of molar volume and absolute flux

$$q_i^r = V_o^f J_i^r \dots\dots\dots\dots\dots\dots\dots\dots\dots\dots\dots\dots\dots\dots\dots\dots\dots\dots\dots\dots\dots\dots\dots\dots\dots\dots\dots\dots\dots\dots\dots. (65)$$

Equation 64 is modified for ionic species by incorporating equation 65 and including the advectional transport of ions (movement of ions along with horizontal movement of fluid) when relative diffusional fluxes are considered is as following

$$d\zeta^a = -V_o^f \frac{\partial J_i^a}{\partial x_i} = -\frac{\partial}{\partial x_i}\left(V_o^f J_i^{a,d} + m^a q_i\right) \ldots\ldots\ldots\ldots\ldots\ldots\ldots\ldots\ldots\ldots\ldots\ldots\ldots\ldots\ldots\ldots\ldots\ldots (66)$$

$$d\zeta^c = -V_o^f \frac{\partial J_i^c}{\partial x_i} = -\frac{\partial}{\partial x_i}\left(V_o^f J_i^{c,d} + m^c q_i\right) \ldots\ldots\ldots\ldots\ldots\ldots\ldots\ldots\ldots\ldots\ldots\ldots\ldots\ldots\ldots\ldots\ldots\ldots (67)$$

4.4.4: Conservation of charges

Since the entire matrix with the pore fluid is electrically neutral without any charge development, the field generated is assumed to be electro static such that the total charge density is constant and does not vary with time (Corapcioglu 1991). Hence the charge conservation equation is given by

$$\frac{\partial \rho_e}{\partial t} = -\frac{\partial I_i}{\partial x_i} \ldots\ldots\ldots\ldots\ldots\ldots\ldots\ldots\ldots\ldots\ldots\ldots\ldots\ldots\ldots\ldots\ldots\ldots\ldots\ldots\ldots\ldots\ldots\ldots\ldots\ldots\ldots\ldots\ldots\ldots (68)$$

The electrostatic condition and equation 68 makes 1st derivative of equation 44 equal to 0.

$$L_{21}\nabla^2 p + L_{22}\nabla^2\psi + L_{23}\frac{RT}{m_o^a}\nabla^2 m^a + L_{24}\frac{RT}{m_o^c}\nabla^2 m^c = 0 \ldots\ldots\ldots\ldots\ldots\ldots\ldots\ldots\ldots\ldots\ldots\ldots (69)$$

The above equations are the governing equation of the porous medium saturated with electrolytic solution including its electro chemical potentials.

The phenomenological coefficients/ transport coefficients depend on 5 field parameters in case of poroelastic medium unlike porochemoelectroelastic medium which depends on 10 field parameters.

4.5: Equations applied for field purposes

Combining equations 52 and 63, and Kronecker delta =1 as i = j we get

$$2G\frac{\partial \varepsilon_{ij}}{\partial x_i} + \frac{2G\nu}{1-2\nu}\frac{\partial \varepsilon_{kk}}{\partial x_j} + \alpha\frac{\partial p}{\partial x_j} = 0 \ldots\ldots\ldots\ldots\ldots\ldots\ldots\ldots\ldots\ldots\ldots\ldots\ldots\ldots\ldots\ldots\ldots\ldots\ldots\ldots\ldots\ldots\ldots\ldots\ldots\ldots\ldots\ldots\ldots\ldots (70)$$

Differentiating equation 70 with respect to x_j

$$2G\frac{\partial^2\varepsilon_{ij}}{\partial x_j\partial x_i}+\frac{2G\nu}{1-2\nu}\frac{\partial^2\varepsilon_{kk}}{\partial x_j\partial x_j}+\alpha\frac{\partial^2 p}{\partial x_j\partial x_j}=0\ldots\ldots\ldots\ldots\ldots\ldots\ldots\ldots\ldots\ldots\ldots\ldots\ldots\ldots\ldots\ldots\ldots (71)$$

Differentiating equation 62 with respect to x_i & x_j

$$\frac{\partial^2\varepsilon_{ij}}{\partial x_j\partial x_i}=\frac{1}{2}\frac{\partial^2}{\partial x_j\partial x_i}\left(\frac{\partial u_i}{\partial x_j}+\frac{\partial u_j}{\partial x_i}\right)=\frac{\partial^2}{\partial x_j\partial x_j}\left(\frac{\partial u_i}{\partial x_i}\right)=\frac{\partial^2\varepsilon_{kk}}{\partial x_j\partial x_j}=\nabla^2\varepsilon_{kk}\ldots\ldots\ldots\ldots\ldots (72)$$

The above strain equation can be further simplified by simultaneously solving equations 71 and 72 as following

$$\nabla^2\left(\varepsilon_{kk}+\frac{\eta}{G}p\right)=0\ldots\ldots\ldots\ldots\ldots\ldots\ldots\ldots\ldots\ldots\ldots\ldots\ldots\ldots\ldots\ldots\ldots\ldots\ldots\ldots\ldots\ldots\ldots\ldots\ldots\ldots\ldots\ldots. (73)$$

Nguyen Vinh et al., 2010 derived the diffusion equations that can be used for practical purposes by using equations 56, 60 61 & 43-46 in 64, 66, and 67.

$$-\alpha\frac{\partial\varepsilon_{kk}}{\partial t}+\frac{1}{M}\frac{\partial p}{\partial t}=L_{11}\nabla^2 p+L_{12}\nabla^2\psi+\ L_{13}\frac{RT}{m_o^a}\nabla^2 m^a+\ L_{14}\frac{RT}{m_o^c}\nabla^2 m^c\ldots\ldots\ldots\ldots (74)$$

$$m_o^a\left(-\alpha\frac{\partial\varepsilon_{kk}}{\partial t}+\frac{1}{M}\frac{\partial p}{\partial t}\right)+\phi_o\frac{\partial m^a}{\partial t}$$
$$=V_o^f\left(L_{31}\nabla^2 p+L_{32}\nabla^2\psi+\ L_{33}\frac{RT}{m_o^a}\nabla^2 m^a+\ L_{34}\frac{RT}{m_o^c}\nabla^2 m^c\right)+m_o^a\frac{\partial q_i}{\partial x_i}$$
$$+q_i\frac{\partial m^a}{\partial x_i}\ldots\ldots\ldots\ldots\ldots\ldots\ldots\ldots\ldots\ldots\ldots\ldots\ldots\ldots\ldots\ldots\ldots\ldots\ldots\ldots\ldots\ldots\ldots\ldots\ldots. (75)$$

$$m_o^c\left(-\alpha\frac{\partial\varepsilon_{kk}}{\partial t}+\frac{1}{M}\frac{\partial p}{\partial t}\right)+\phi_o\frac{\partial m^c}{\partial t}$$
$$=V_o^f\left(L_{41}\nabla^2 p+L_{42}\nabla^2\psi+\ L_{43}\frac{RT}{m_o^a}\nabla^2 m^a+\ L_{44}\frac{RT}{m_o^c}\nabla^2 m^c\right)+m_o^c\frac{\partial q_i}{\partial x_i}$$
$$+q_i\frac{\partial m^c}{\partial x_i}\ldots\ldots\ldots\ldots\ldots\ldots\ldots\ldots\ldots\ldots\ldots\ldots\ldots\ldots\ldots\ldots\ldots\ldots\ldots\ldots\ldots\ldots\ldots\ldots\ldots. (76)$$

However based on the conclusions of Yeung and Datla (1994) that the hydraulic diffusion is small compared to the ionic diffusion, the advective transport terms (last 2

terms in equations 75 and 76) are ignored and the electrostatic potential field is also disregarded based on equation 69 to obtain equations with non -symmetric coefficients to form a matrix.

$$-\alpha\frac{\partial\varepsilon_{kk}}{\partial t}+\frac{1}{M}\frac{\partial p}{\partial t}=D_{11}\nabla^2 p+D_{12}\nabla^2 p^a+\ D_{13}\nabla^2 p^c \ldots\ldots\ldots\ldots\ldots\ldots\ldots\ldots\ldots\ldots\ldots\ldots\ldots\ldots(77)$$

$$m_o^a\left(-\alpha\frac{\partial\varepsilon_{kk}}{\partial t}+\frac{1}{M}\frac{\partial p}{\partial t}\right)+\frac{\phi_o V_o^f}{RT}\frac{\partial p^a}{\partial t}=D_{21}\nabla^2 p+D_{22}\nabla^2 p^a+\ D_{23}\nabla^2 p^c \ldots\ldots\ldots\ldots\ldots(78)$$

$$m_o^c\left(-\alpha\frac{\partial\varepsilon_{kk}}{\partial t}+\frac{1}{M}\frac{\partial p}{\partial t}\right)+\frac{\phi_o V_o^f}{RT}\frac{\partial p^c}{\partial t}=D_{31}\nabla^2 p+D_{32}\nabla^2 p^a+\ D_{33}\nabla^2 p^c \ldots\ldots\ldots\ldots\ldots(79)$$

Where

$$p=\frac{RT}{V}m$$

From the above equations it is evident that the electrical transport coefficients are considered only if there is a streaming flux due to the formation of diffuse double layer.

$$\begin{bmatrix} D_{11} & D_{12} & D_{13} \\ D_{21} & D_{22} & D_{23} \\ D_{31} & D_{32} & D_{33} \end{bmatrix}$$

$$=\begin{bmatrix} \kappa & -\chi\kappa & -\chi\kappa \\ m_o^a(1-\chi)\kappa & D_{eff}^a\left(\frac{V_o^f}{RT}\right)-m_o^a(1-\chi)\chi\kappa & -m_o^a(1-\chi)\chi\kappa \\ m_o^c(1-\chi)\kappa & -m_o^c(1-\chi)\chi\kappa & D_{eff}^c\left(\frac{V_o^f}{RT}\right)-m_o^c(1-\chi)\chi\kappa \end{bmatrix}\ldots\ldots(80)$$

The equations developed so far in this chapter have been used to develop a mathematical model for drilling an inclined wellbore in chemically active porous medium.

Chapter 5: Mathematical model

5.1: Initial wellbore conditions and stress transformations

An inclined wellbore is drilled such that the axis of the wellbore is inclined to the in-situ stresses. The Cartesian coordinate axes x', y', z' overlap the principle axes of the far field stresses Sx', Sy', Sz' as shown in figure 17.

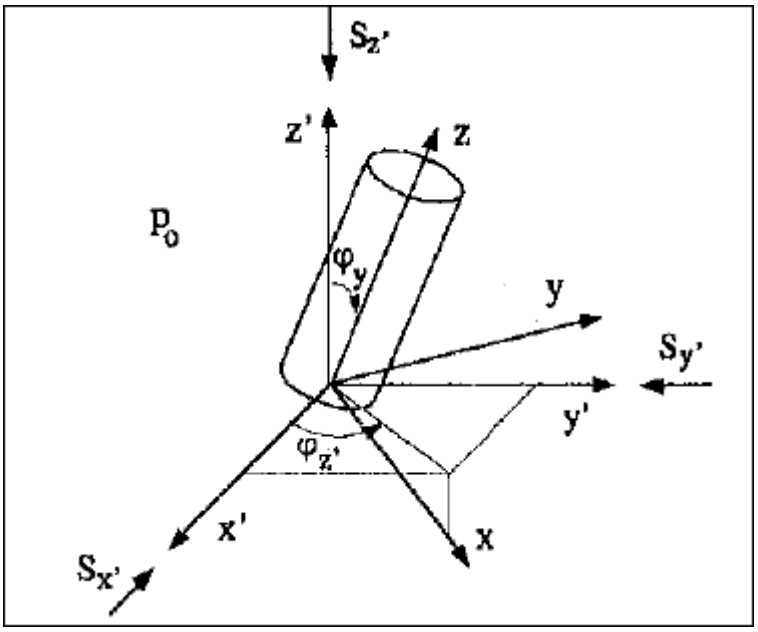

Figure 17: Inclined wellbore with axes inclined to in-situ stresses (Adapted from Cui et al., 1997)

The deviation of the wellbore from the vertical axis is called as inclination angle φ_y and the angle the wellbore makes with the axis along maximum horizontal in-situ stress is called as azimuth angle φ_z.

The local coordinates are considered such that the axis of the wellbore is parallel to the vertical axis z of the coordinate system xyz as shown in figure 18.

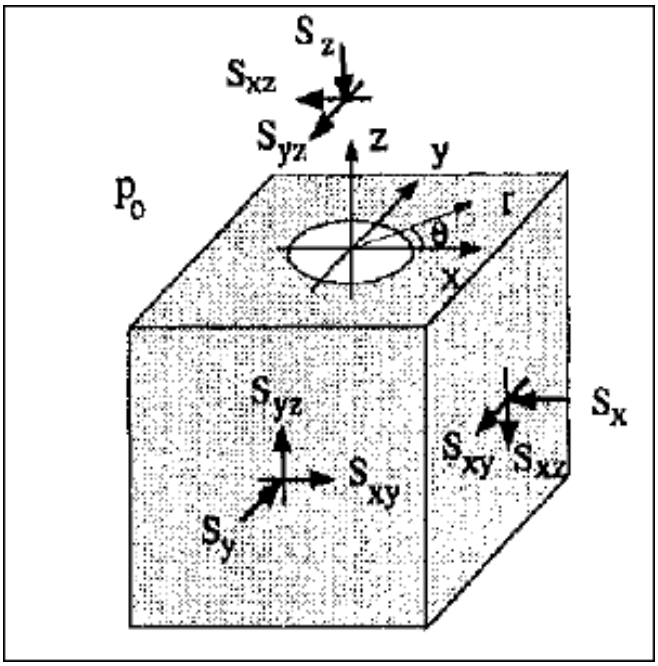

Figure 18: Physical model of inclined wellbore in local coordinate system (adapted from Cui et al., 1997)

The in-situ stresses can be transformed from the Cartesian coordinates to local coordinates. The transformation is described mathematically by direction cosines as following (Fjaer et al 2008).

$$\begin{Bmatrix} S_x \\ S_y \\ S_z \\ S_{xy} \\ S_{yz} \\ S_{xz} \end{Bmatrix} = \begin{bmatrix} l_{xx'}^2 & l_{xy'}^2 & l_{xz'}^2 \\ l_{yx'}^2 & l_{yy'}^2 & l_{yz'}^2 \\ l_{zx'}^2 & l_{zy'}^2 & l_{zz'}^2 \\ l_{xx'}l_{yx'} & l_{xy'}l_{yy'} & l_{xz'}l_{zz'} \\ l_{yx'}l_{zx'} & l_{yy'}l_{zy'} & l_{yz'}l_{zz'} \\ l_{zx'}l_{xx'} & l_{zy'}l_{xy'} & l_{zz'}l_{xz'} \end{bmatrix} \begin{bmatrix} S_{x'} \\ S_{y'} \\ S_{z'} \end{bmatrix} \dots\dots\dots\dots\dots\dots\dots\dots\dots\dots\dots\dots\dots\dots\dots\dots (81)$$

Where $l_{ij'}$ is the cosine of the angle between the axes 'i' and 'j' and is given as

$$\begin{bmatrix} l_{xx'} & l_{xy'} & l_{xz'} \\ l_{yx'} & l_{yy'} & l_{yz'} \\ l_{zx'} & l_{zy'} & l_{zz'} \end{bmatrix} = \begin{bmatrix} cos\varphi_z cos\varphi_y & sin\varphi_z cos\,\varphi_y & -sin\varphi_y \\ -sin\varphi_z & cos\varphi_z & 0 \\ cos\varphi_z sin\varphi_y & sin\varphi_z sin\varphi_y & cos\varphi_y \end{bmatrix} \dots\dots\dots\dots\dots\dots\dots\dots (82)$$

5.2: Initial conditions of the formation before drilling

As mentioned in earlier chapters, the shale formation is negatively charged and when the matrix is considered along with the pore fluid, the entire medium is electrically neutral such that it satisfies the following condition

$$z^c m_o^c + z^a m_o^a + z^{fc} m_o^{fc} = 0 \quad (83)$$

Where z^c is valence of cations and is positive and z^a, z^{fc} are valences of the anions and fixed charges of formation respectively which are negative values.

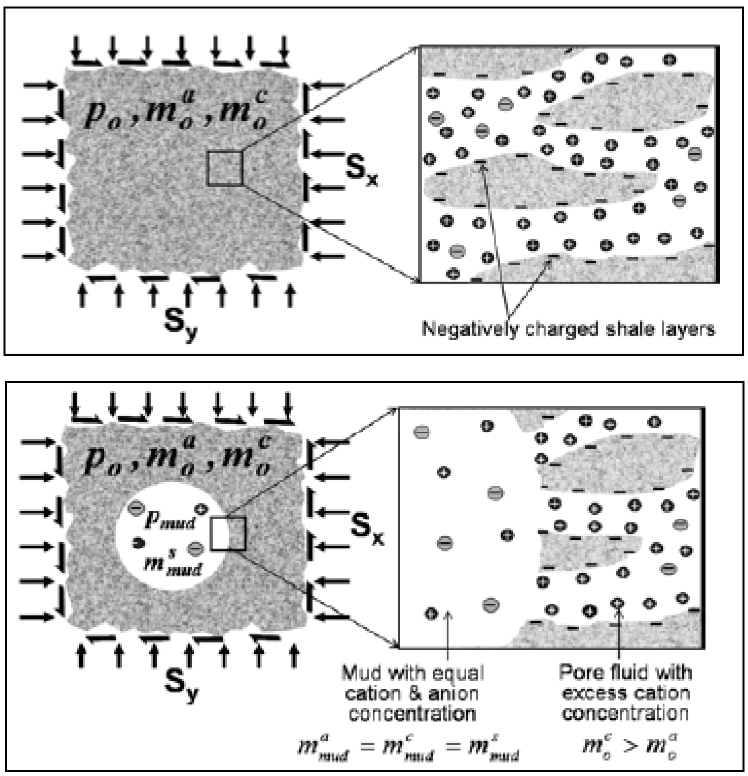

Figure 19: Initial and after drilling conditions of shale (adapted from Nguyen et al 2010)

The mole fractions of cations, anions and the fixed charges on the formation cannot be determined easily. It demands a complete knowledge of the cation exchange capacity and pore fluid water activity which is equal to the water activity of the fluid in

equilibrium with it on other side of the porous medium (Overbeek 1956). The electrochemical potentials of the initial ionic species in pore fluid are given as

$$\tilde{\mu}_{eq}^{f} = \tilde{\mu}_{o}^{f} \qquad \tilde{\mu}_{eq}^{c} = \tilde{\mu}_{o}^{c} \qquad \tilde{\mu}_{eq}^{f} = \tilde{\mu}_{o}^{f} \ldots\ldots\ldots\ldots\ldots\ldots\ldots\ldots\ldots\ldots (84)$$

Equation 84 can be extended for a mud shale interface which avoids infinite ionic fluxes by maintaining a continuous electrochemical potential for all fluid species.

$$\tilde{\mu}_{mud}^{f} = \tilde{\mu}_{shale}^{f} \qquad \tilde{\mu}_{mud}^{c} = \tilde{\mu}_{shale}^{c} \qquad \tilde{\mu}_{mud}^{f} = \tilde{\mu}_{shale}^{f} \ldots\ldots\ldots\ldots\ldots\ldots\ldots\ldots (85)$$

Simultaneously solving equations 47 and 84, using the electrical neutrality of the outer fluid which is in equilibrium and also by ignoring the electrical potential terms we get expressions to determine the initial mole fractions of the cations and anions for a monovalent salt which is further simplified by ignoring the negligible pressure exponential term (Nguyen et al., 2010).

$$m_{o}^{c} m_{o}^{a} = (m_{eq}^{s})^{2} \ldots\ldots\ldots\ldots\ldots\ldots\ldots\ldots\ldots\ldots\ldots\ldots\ldots\ldots\ldots\ldots\ldots (86)$$

Where

$m_{eq}^{s} = mole\ fraction\ of\ solute\ in\ fluid\ in\ equilibrium\ with\ pore\ fluid$

The mole fractions of the cations and the anions in the shale formation are given by the following equations

$$m_{shale}^{a} = 0.5\left(-m^{fc} + \sqrt{(m^{fc})^{2} + 4(m_{mud}^{s})^{2}}\right) \ldots\ldots\ldots\ldots\ldots\ldots\ldots\ldots\ldots (87)$$

$$m_{shale}^{c} = 0.5\left(m^{fc} + \sqrt{(m^{fc})^{2} + 4(m_{mud}^{s})^{2}}\right) \ldots\ldots\ldots\ldots\ldots\ldots\ldots\ldots\ldots (88)$$

Where

$m_{mud}^{s} = mole\ fraction\ of\ salt/solute\ in\ drilling\ mud$

The above equations 87 and 88 are framed such that it satisfies the condition in equation 85.

For a monovalent salt in mud the mole fraction of cations and anions are same such that

$$m^s_{mud} = m^a_{mud} = m^c_{mud} \dots\dots\dots\dots\dots\dots\dots\dots\dots\dots\dots\dots\dots\dots\dots\dots\dots\dots\dots\dots\dots\dots\dots\dots\dots\dots (89)$$

The initial mole fraction of the ionic species can be calculated only if the mole fraction of the fixed charges on the porous media is known.

$$m^{fc} = 10^{-2} * \frac{CEC(1-\phi_o)\rho_s V^f_o}{\phi_o} \dots\dots\dots\dots\dots\dots\dots\dots\dots\dots\dots\dots\dots\dots\dots\dots\dots\dots\dots\dots\dots (90)$$

Where

$\rho_s = grain\ density\ in\ g/cc$

$V^f_o = molar\ volume\ of\ water\ in\ shale\ in\ litre/mol$

CEC has to be calculated before calculating mole fraction of the fixed charges. The significance of CEC and different methods adopted to measure have been discussed in detail in chapter 2.

Initially when the solution dissociates into its corresponding cations and anions, the water activity is measured (water content of the fluid inside shale). Using this water activity, the mole fraction of the salt in the fluid present outside the porous medium which is in equilibrium with the pore fluid can be calculated as following

$$a^f_o = 1 - (x+y)m^s_{eq} \dots\dots\dots\dots\dots\dots\dots\dots\dots\dots\dots\dots\dots\dots\dots\dots\dots\dots\dots\dots\dots\dots\dots\dots\dots\dots\dots. (91)$$

Replacing m^{fc} and m^s_{mud} in equation 87 with equations 90 and 91 we get

$$m^a_{shale} = 0.5\left(-10^{-2} * \frac{CEC(1-\phi_o)\rho_s V^f_o}{\phi_o} + \sqrt{(10^{-2} * \frac{CEC(1-\phi_o)\rho_s V^f_o}{\phi_o})^2 + (1-a^f_o)^2}\right) \dots\dots\dots\dots\dots\dots\dots\dots (92)$$

Some of the observations from equation 92 are

1. Geological membranes have pore sizes big enough to allow the passage of largest hydrated radii of ions found in ground water. However the salt exclusion behavior of clay is mainly due to the electrical restrictions operating within the clay membrane structure. Hence the efficiency of the salt exclusion behavior for clay is high when the clay has higher Cation Exchange Capacity. Ex: Smectite membranes are inherently more ideal than kaolinite membranes (Marine & Fritz 1981).
2. If the porosity of the formation is very small approaching zero, the mole fraction of anions decreases. This is because as the porous medium undergoes consolidation/compaction the membrane efficiency increases excluding the ions and allowing only the passage of fluids separated.
3. When the water activity a_o^f approaches unity, the mole fraction of anions in fluid is approaching zero. This is because if $a_o^f = 1$ then the pore fluid is just water.

5.3: Boundary conditions and Problem definition

5.3.1: Interfacial and far field stresses of the porous medium and drilling fluid

The total mole fraction of the ions in the formation is greater than the mole fraction of the ions in the mud at the interface between the shale and drilling fluid. Hence a pressure differential is generated which causes flow of water from one fluid to another. The reason for this phenomenon is explained under section 2.1 in chapter 2 as a consequence of Donnan equilibrium effect.

The pressure difference generated at the mud shale interface is

$$p_{shale} - p_{mud} = \frac{RT}{V_o^f} * (m_{shale}^a + m_{shale}^c - 2m_{mud}^s) \quad (93)$$

$$\Delta p_{mud-shale} = \frac{RT}{V_o^f} * \left(\sqrt{(m^{fc})^2 + 4(m_{mud}^s)^2} - 2m_{mud}^s \right) \quad (94)$$

Pore pressure, normal and shear stresses in local coordinates at the far field conditions when $r \to \infty$ are

$$\sigma_{xx} = S_x \quad (95.1)$$

$$\sigma_{yy} = S_y \quad (95.2)$$

$$\sigma_{zz} = S_z \quad (95.3)$$

$$\tau_{xy} = S_{xy} \quad (95.4)$$

$$\tau_{yz} = S_{yz} \quad (95.5)$$

$$\tau_{xz} = S_{xz} \quad (95.6)$$

$$p = p_o \quad (95.7)$$

$$p^c = \frac{RT}{V_o^f} m_o^c \quad (95.8)$$

$$p^a = \frac{RT}{V_o^f} m_o^a \quad (95.9)$$

Pore pressure, normal and shear stresses in cylindrical coordinates at the interface when $r = r_w$ (wellbore radius) are

$$\sigma_{rr} = (\sigma_m + \sigma_d \cos\left(2(\theta - \theta_r)\right) H(-t) + p_{mud} H(t) \quad (96.1)$$

$$\tau_{r\theta} = -\sigma_d \sin\left(2(\theta - \theta_r)\right) H(-t) \quad (96.2)$$

$$\tau_{rz} = (S_{xz} \cos(\theta) + S_{yx} \sin(\theta)) H(-t) \quad (96.3)$$

$$p = p_o H(-t) + (p_{mud} + \Delta p_{mud-shale}) H(t) \quad (96.4)$$

$$p^a = \frac{RT}{V_o^f}(m_o^a H(-t) + (m_{mud}^s + \Delta m_{mud-shale}^a) H(t) \ldots \ldots \ldots \ldots \ldots \ldots \ldots \ldots \ldots \ldots \ldots \ldots (96.5)$$

$$p^c = \frac{RT}{V_o^f}(m_o^c H(-t) + (m_{mud}^s + \Delta m_{mud-shale}^c) H(t) \ldots \ldots \ldots \ldots \ldots \ldots \ldots \ldots \ldots \ldots \ldots \ldots (96.6)$$

Where H is Heaviside step function or unit step function which is discontinuous and is used to represent a piecewise constant function such as

H (- t) = 1 if t < 0

H (- t) = 0 if t > 0

H is a function of time and the graph of unit step function is shown in the following figure

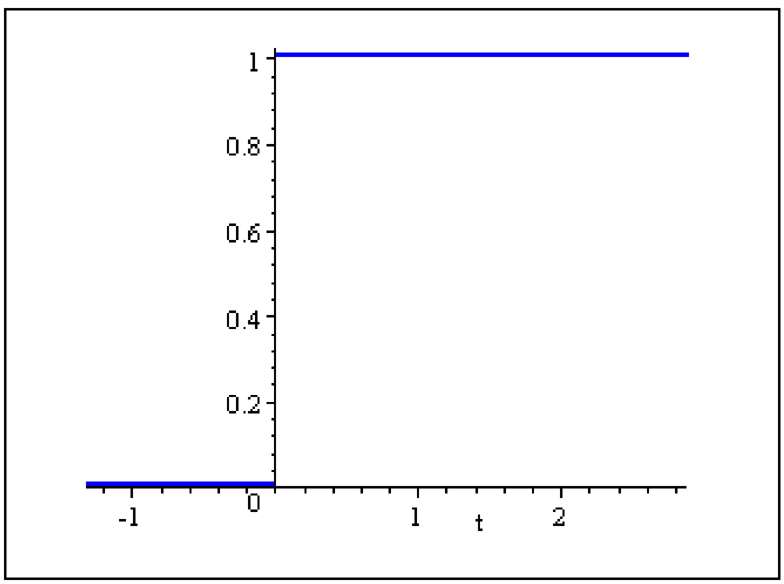

Figure 20: Heaviside step function (www.intmath.com\laplace)

In equations 96,

$$\sigma_m = \frac{S_x + S_y}{2} \ldots \ldots \ldots \ldots \ldots \ldots \ldots \ldots \ldots \ldots \ldots \ldots \ldots \ldots \ldots \ldots \ldots \ldots \ldots \ldots \ldots \ldots \ldots \ldots \ldots \ldots \ldots \ldots \ldots \ldots (97)$$

$$\sigma_d = 0.5\sqrt{(S_x - S_y)^2 + 4S_{xy}^2} \ldots \ldots \ldots \ldots \ldots \ldots \ldots \ldots \ldots \ldots \ldots \ldots \ldots \ldots \ldots \ldots \ldots \ldots \ldots \ldots \ldots \ldots \ldots (98)$$

$$\theta_r = 0.5tan^{-1}\left(\frac{2S_{xy}}{S_x - S_y}\right) \ldots \ldots \ldots \ldots \ldots \ldots \ldots \ldots \ldots \ldots \ldots \ldots \ldots \ldots \ldots \ldots \ldots \ldots \ldots \ldots \ldots \ldots \ldots \ldots . (99)$$

Where

$\sigma_m, \sigma_d, = mean\ compressive\ \&\ deviatoric\ stresses\ respectively$

$\theta_r = principle\ angle\ in\ polar\ coordinates\ (Cui\ et\ al., 1997).$

The concentration differential generated at the shale mud interface is given by the following equations

$$\Delta m^a_{mud-shale} = m^a_{shale} - m^s_{mud} \ldots \ldots \ldots \ldots \ldots \ldots \ldots \ldots \ldots \ldots \ldots \ldots \ldots \ldots \ldots \ldots \ldots \ldots \ldots \ldots \ldots (100)$$

$$\Delta m^c_{mud-shale} = m^c_{shale} - m^s_{mud} \ldots \ldots \ldots \ldots \ldots \ldots \ldots \ldots \ldots \ldots \ldots \ldots \ldots \ldots \ldots \ldots \ldots \ldots \ldots \ldots \ldots (101)$$

5.3.2: Loading decomposition of the porous medium

Due to the linearity of the governing equations of the chemically active porous medium the boundary conditions can be split into 3 different problems, such that the solutions of which can be superposed to obtain the final pore pressure and the effective radial and tangential stresses (Cui et al., 1997). The mechanical loading of the porous medium is decomposed into the following 3 problems:

1. **Poroelastic plane strain problem**

   It is a state of strain when the normal strain to x-y plane and the shear strains are zero (Plane strain module UCSB College of Engineering).

2. **Elastic Uniaxial stress problem**

   It is the condition when the porous medium is subjected to tension by opposite forces of magnitude acting along its axes.

3. **Elastic anti-plane shear problem**

   It is a state of strain in the medium when all the stresses except the normal stress and the shear stress to x-y plane are zero (Plane strain module UCSB College of Engineering).

The decomposition of the loading problem can be shown diagrammatically as

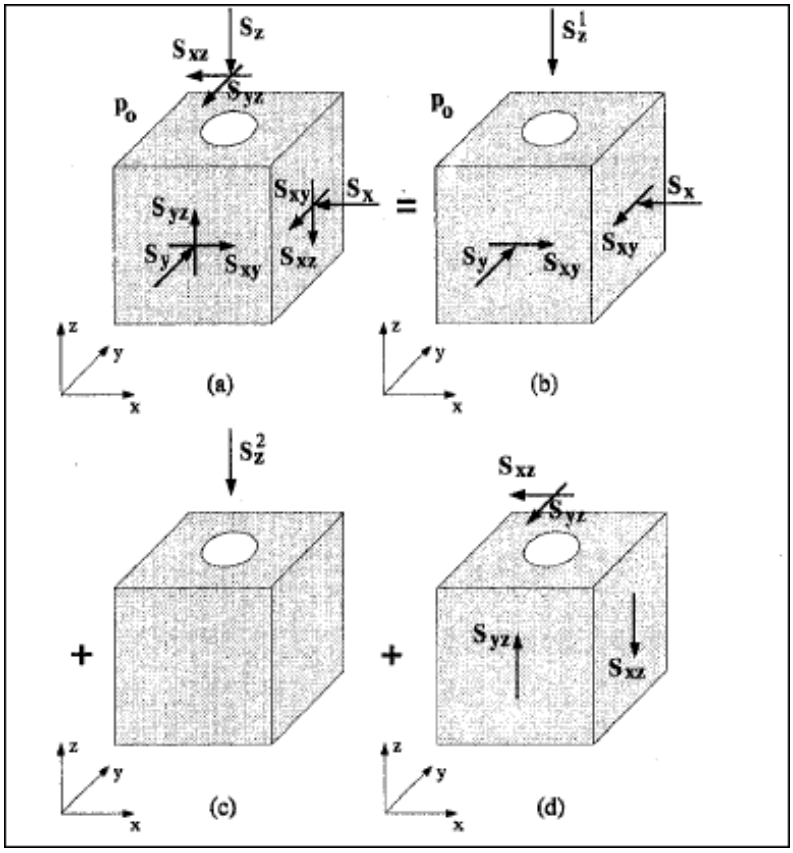

Figure 21: Loading decomposition of an inclined wellbore (adapted from Cui et al., 1997)

Chapter 6: Superposed Solutions of the chemically active porous medium

6.1: Poroelastic plane strain problem

As mentioned in section 5.3.2 of chapter 5, the plane strain problem remains in a state of strain during which the shear strains to x-y plane are zero such that the corresponding shear stresses are also zero. In a plane strain problem, the far field conditions having $\sigma_{zz}, \tau_{yz}, \tau_{xz}$ and interfacial stress $\tau_{r\theta}$ become superfluous (Cui et al., 1997). The analytical solution to the plane strain problem has been adapted from Detourney et al., (1988). The analytical solution was derived in Laplace space transform, based on the assumption of plane strain conditions in the plane normal to the axis of the wellbore. The solution can be used only if the coordinates are rotated about z axis such that x axis is along the direction of minimum horizontal principal stress and y along the maximum stress.

6.1.1: Far field conditions

$$\sigma_{xx} = S_x \quad (102.1)$$

$$\sigma_{yy} = S_y \quad (102.2)$$

$$\sigma_{zz} = 2\nu\sigma_m + \alpha(1-2\nu)p_o \quad (102.3)$$

$$\tau_{xy} = S_{xy} \quad (102.4)$$

$$\tau_{yz} = 0 \quad (102.5)$$

$$\tau_{xz} = 0 \quad (102.6)$$

$$p = p_o \quad (102.7)$$

$$p^c = \frac{RT}{V_o^f} m_o^c \quad (102.8)$$

$$p^a = \frac{RT}{V_o^f} m_o^a \ldots \ldots \ldots \quad (102.9)$$

6.1.2: Near wellbore conditions

At the wellbore wall, the problem is analyzed based on the assumption that the drilling operation is instantaneous only if the time required for drilling a distance which is 5 times the radius of the wellbore is smaller than the characteristic time given by

$$t_c = \frac{wellbore\ radius}{generalized\ consolidation\ coefficient} \ldots \ldots \ldots \quad (103)$$

The physical version of the problem is facilitated by decomposing the problem further into 3 modal conditions (Detournay et al., 1998) such as

1. Far field isotropic stress (axisymmetric)
2. Virgin pore pressure (axisymmetric)
3. Far field stress deviator (asymmetric)

For a poroelastic plane strain problem, the solution for the near wellbore conditions includes the superposed solution of the 3 individual modal solutions.

$$\sigma_{rr} = \sigma_m + \sigma_d \cos\big(2(\theta - \theta_r)\big) + \sigma_{rr}^1 + \sigma_{rr}^2 + \sigma_{rr}^3 \ldots \ldots \ldots \quad (104.1)$$

$$\tau_{r\theta} = -\sigma_d \sin\big(2(\theta - \theta_r)\big) + \tau_{r\theta}^3 \ldots \ldots \ldots \quad (104.2)$$

$$p = p_o + p^2 + p^3 \ldots \ldots \ldots \quad (104.3)$$

$$p^a = \frac{RT}{V_o^f} m_o^a + p^{a(2)} + p^{a(3)} \ldots \ldots \ldots \quad (104.4)$$

$$p^c = \frac{RT}{V_o^f} m_o^c + p^{c(2)} + p^{c(3)} \ldots \ldots \ldots \quad (104.5)$$

The Laplace solution of the volumetric strain which is in polar coordinates depending only on time and radial distance is given by Carter et al., (1982) as following

$$\tilde{E}_{kk} = -\left(\frac{\eta}{G}\right)\tilde{P} + C_o r^{-n} \quad (105)$$

Where

$$\eta = lumped\ poroelastic\ coefficient = \frac{\alpha(1-2\nu)}{2(1-\nu)} \quad (106)$$

$C_o = C_o[s] = constant\ determined\ from\ boundary\ conditions$

Equation 105 is substituted in diffusion equations 77-79 to replace the volumetric strain yielding a set of differential equations giving a coefficient matrix of

$$[Z] = [Y]^{-1}[D] \quad (107)$$

Where

$[D] = nonsymmetric\ lumped\ coefficient\ matrix\ given\ by\ equation$ 80

$$[Y] = \begin{bmatrix} \frac{1}{M} + \frac{\alpha\eta}{G} & 0 & 0 \\ m_o^a(\frac{1}{M} + \frac{\alpha\eta}{G}) & \frac{\phi_O V_o^f}{RT} & 0 \\ m_o^c(\frac{1}{M} + \frac{\alpha\eta}{G}) & 0 & \frac{\phi_O V_o^f}{RT} \end{bmatrix} \quad (108)$$

The $[Z]$ in equation 107 yields real values only if the matrix is positive definite. However if the determinant and the elements along the leading diagonal are positive then the matrix is positive definite (Johnson 1970).

6.1.3: Mode 1-Elastic radial loading / far field isotropic stress

For elastic radial loading the near wellbore conditions are given as

$$\sigma_{rr} = -\sigma_m + p_{mud} \quad (109.1)$$

$$\sigma_{r\theta} = 0 \quad (109.2)$$

$$p = p^a = p^c = 0 \quad (109.3)$$

The diffusional equation in pressure terms (equation 109.4) yields a classical Lamé solution which is purely elastic (Detournay et al., 1988).

$$\frac{\partial^2 p}{\partial r^2} + \frac{1}{r}\frac{\partial p}{\partial r} = \frac{1}{c}\frac{\partial p}{\partial t} \quad \ldots\ldots (109.4)$$

$$\sigma_{rr}^1 = -(\sigma_m - p_{mud})\left(\frac{R_w^2}{r^2}\right) \quad \ldots\ldots (109.5)$$

$$\sigma_{\theta\theta}^1 = (\sigma_m - p_{mud})\left(\frac{R_w^2}{r^2}\right) \quad \ldots\ldots (109.6)$$

In this mode of loading, rock deformation happens only due to deviatoric strain and the pore pressure is not generated.

6.1.4: Mode 2- Virgin pore pressure/ diffusional loading

Mode 2 loading reduces to an uncoupled diffusional problem for pore pressure. In this mode of loading the radial stresses are zero at the wellbore (Detournay et al., 1988).

$$\sigma_{rr} = \sigma_{r\theta} = 0 \quad \ldots\ldots (110.1)$$

Other boundary conditions at the wellbore are

$$p = \Delta p \quad \ldots\ldots (110.2)$$

$$p^a = \Delta p^a \quad \ldots\ldots (110.3)$$

$$p^c = \Delta p^c \quad \ldots\ldots (110.4)$$

The unsteady state solutions in Laplace domain are listed below

$$s\tilde{p}^{(2)} = m_{11}\Delta_1\Phi[\xi_1] + m_{12}\Delta_2\Phi[\xi_2] + m_{13}\Delta_3\Phi[\xi_3] \quad \ldots\ldots (110.5)$$

$$s\tilde{p}^{a(2)} = m_{21}\Delta_1\Phi[\xi_1] + m_{22}\Delta_2\Phi[\xi_2] + m_{23}\Delta_3\Phi[\xi_3] \quad \ldots\ldots (110.6)$$

$$s\tilde{p}^{c(2)} = m_{31}\Delta_1\Phi[\xi_1] + m_{32}\Delta_2\Phi[\xi_2] + m_{33}\Delta_3\Phi[\xi_3] \quad \ldots\ldots (110.7)$$

$$s\widetilde{\sigma_{rr}}^{(2)} = -2\eta\{m_{11}\Delta_1\Xi[\xi_1] + m_{12}\Delta_2\Xi[\xi_2] + m_{13}\Delta_3\Xi[\xi_3] \quad \ldots\ldots (110.8)$$

$$s\widetilde{\sigma_{\theta\theta}}^{(2)} = 2\eta\{m_{11}\Delta_1(\Xi[\xi_1] + \Phi[\xi_1]) + m_{12}\Delta_2(\Xi[\xi_2] + \Phi[\xi_1]) + m_{13}\Delta_3(\Xi[\xi_3] + \Phi[\xi_1])\} \ldots\ldots\ldots\ldots\ldots\ldots\ldots\ldots\ldots\ldots\ldots\ldots\ldots\ldots\ldots\ldots (110.9)$$

The above solution in Laplace domain can be inverted to time domain using the Stehfast Algorithm described in Appendix A.

In the above solutions

$\xi_i = \sqrt{s/\lambda_i}\ where\ \lambda_i\ is\ eigen\ value\ of\ [Z]$

$\{m_{1i}, m_{2i}, m_{3i}\} = corresponding\ eigen\ vector\ of\ [Z] where\ i = 1,2,3$

The functions Δ_i, Φ, Ξ are defined as following

$$\Delta_1 = [(m_{22}m_{33} - m_{23}m_{32})\Delta p + (m_{13}m_{32} - m_{12}m_{33})\Delta p^a + (m_{12}m_{23} - m_{13}m_{22})\Delta p^c]/m \ldots\ldots\ldots\ldots\ldots\ldots\ldots\ldots\ldots\ldots\ldots\ldots (110.10)$$

$$\Delta_2 = [(m_{23}m_{31} - m_{21}m_{33})\Delta p + (m_{11}m_{33} - m_{13}m_{31})\Delta p^a + (m_{13}m_{21} - m_{11}m_{23})\Delta p^c]/m \ldots\ldots\ldots\ldots\ldots\ldots\ldots\ldots\ldots\ldots\ldots\ldots (110.11)$$

$$\Delta_3 = [(m_{21}m_{32} - m_{22}m_{31})\Delta p + (m_{12}m_{31} - m_{11}m_{32})\Delta p^a + (m_{11}m_{22} - m_{12}m_{21})\Delta p^c]/m \ldots\ldots\ldots\ldots\ldots\ldots\ldots\ldots\ldots\ldots\ldots\ldots (110.12)$$

$$\Phi[x] = \frac{K_o[xr]}{K_o[xR_w]} \ldots\ldots\ldots\ldots\ldots\ldots\ldots\ldots\ldots\ldots\ldots\ldots\ldots\ldots\ldots\ldots\ldots\ldots\ldots\ldots\ldots\ldots\ldots\ldots\ldots\ldots (110.13)$$

$$\Xi[x] = \frac{K_1[xr]}{(xrK_o[xR_w])} - \frac{R_wK_1[xR_w]}{(xr^2K_o[xR_w])} \ldots\ldots\ldots\ldots\ldots\ldots\ldots\ldots\ldots\ldots\ldots\ldots\ldots\ldots\ldots\ldots\ldots\ldots\ldots\ldots (110.14)$$

Where

$$m = m_{11}(m_{22}m_{33} - m_{23}m_{32}) - m_{12}(m_{21}m_{33} - m_{23}m_{31}) + m_{13}(m_{21}m_{32} - m_{22}m_{31}) \ldots\ldots\ldots\ldots\ldots\ldots\ldots\ldots\ldots\ldots\ldots\ldots\ldots\ldots\ldots\ldots (110.15)$$

$$\Delta p = p_{mud} + \Delta p_{mud-shale} - p_o \ldots\ldots\ldots\ldots\ldots\ldots\ldots\ldots\ldots\ldots\ldots\ldots\ldots\ldots\ldots\ldots\ldots\ldots\ldots\ldots\ldots\ldots\ldots\ldots (110.16)$$

$$\Delta p^a = \frac{RT}{V_o^f}(m_{mud}^s + \Delta m_{mud-shale}^a - m_o^a) \ldots\ldots\ldots\ldots\ldots\ldots\ldots\ldots\ldots\ldots\ldots\ldots\ldots\ldots\ldots\ldots\ldots\ldots\ldots\ldots\ldots\ldots\ldots\ldots (110.17)$$

$$\Delta p^c = \frac{RT}{V_o^f}(m_{mud}^s + \Delta m_{mud-shale}^c - m_o^c) \dots\dots\dots\dots\dots\dots\dots\dots\dots\dots\dots\dots\dots\dots\dots. (110.18)$$

$K_n = bessel\ function\ of\ second\ kind\ and\ order\ 'n'$

6.1.5: Mode 3- Far field stress deviator/ poroelastic deviatoric stress loading

Mode 3 is a deviatoric loading and since the loading is asymmetric, the solution includes a complete poroelastic coupling (Detournay et al., 1988). The boundary conditions near the wellbore are (Nguyen et al., 2008)

$$\sigma_{rr} = -\sigma_d \cos[2(\theta - \theta_r)] \dots\dots\dots\dots\dots\dots\dots\dots\dots\dots\dots\dots\dots\dots\dots\dots\dots\dots\dots\dots\dots\dots (111.1)$$

$$\sigma_{r\theta} = \sigma_d \sin[2(\theta - \theta_r)] \dots\dots\dots\dots\dots\dots\dots\dots\dots\dots\dots\dots\dots\dots\dots\dots\dots\dots\dots\dots\dots\dots.. (111.2)$$

$$p = p^a = p^c = 0 \dots\dots\dots\dots\dots\dots\dots\dots\dots\dots\dots\dots\dots\dots\dots\dots\dots\dots\dots\dots\dots\dots\dots\dots\dots\dots (111.3)$$

The solutions in Laplace transform space domain are

$$s\tilde{p}^{(3)} = \sigma_d \left\{ m_{11} D_1 K_2[\xi_1 r] + m_{12} D_2 K_2[\xi_2 r] + m_{13} D_3 K_2[\xi_3 r] + D_4 f_1 \left(\frac{R_w^2}{r^2} \right) \right\} cos[2(\theta - \theta_r)] \dots\dots\dots\dots\dots\dots\dots\dots\dots\dots\dots\dots\dots. (111.4)$$

$$s\tilde{p}^{a(3)} = \sigma_d \left\{ m_{21} D_1 K_2[\xi_1 r] + m_{22} D_2 K_2[\xi_2 r] + m_{23} D_3 K_2[\xi_3 r] + D_4 f_2 \left(\frac{R_w^2}{r^2} \right) \right\} cos[2(\theta - \theta_r)] \dots\dots\dots\dots\dots\dots\dots\dots\dots\dots\dots\dots\dots. (111.5)$$

$$s\tilde{p}^{c(3)} = \sigma_d \left\{ m_{31} D_1 K_2[\xi_1 r] + m_{32} D_2 K_2[\xi_2 r] + m_{33} D_3 K_2[\xi_3 r] + D_4 f_3 \left(\frac{R_w^2}{r^2} \right) \right\} cos[2(\theta - \theta_r)] \dots\dots\dots\dots\dots\dots\dots\dots\dots\dots\dots\dots\dots. (111.6)$$

$$s\widetilde{\sigma_{rr}}^{(3)} = -\sigma_d \left\{ 2\eta(m_{11}D_1\Theta[\xi_1] + m_{12}D_2\Theta[\xi_2] + m_{13}D_3\Theta[\xi_3]) \right.$$

$$\left. - 2G\left(h + \frac{\alpha}{\eta}\right) D_4\left(\frac{R_w^2}{r^2}\right) - D_5\left(\frac{R_w^4}{r^4}\right) \right\} cos[2(\theta - \theta_r)] \ldots\ldots\ldots\ldots\ldots (111.7)$$

$$s\widetilde{\sigma_{\theta\theta}}^{(3)} = \sigma_d \left\{ 2\eta(m_{11}D_1\Pi[\xi_1] + m_{12}D_2\Pi[\xi_2] + m_{13}D_3\Pi[\xi_3]) \right.$$

$$\left. - D_5\left(\frac{R_w^4}{r^4}\right) \right\} cos[2(\theta - \theta_r)] \ldots\ldots\ldots\ldots\ldots\ldots\ldots\ldots\ldots\ldots\ldots\ldots\ldots\ldots (111.8)$$

$$s\widetilde{\tau_{r\theta}}^{(3)} = -\sigma_d \left\{ 4\eta(m_{11}D_1\Omega[\xi_1] + m_{12}D_2\Omega[\xi_2] + m_{13}D_3\Omega[\xi_3]) - G\left(h + \frac{\alpha}{\eta}\right) D_4\left(\frac{R_w^2}{r^2}\right) \right.$$

$$\left. - D_5\left(\frac{R_w^4}{r^4}\right) \right\} sin[2(\theta - \theta_r)] \ldots\ldots\ldots\ldots\ldots\ldots\ldots\ldots\ldots\ldots\ldots\ldots\ldots\ldots (111.9)$$

Where

$$f_i = \alpha[Y]^{-1}\{1\ m_o^a\ m_o^c\}^T\ for\ i = 1, 2, 3 \ldots\ldots\ldots\ldots\ldots\ldots\ldots\ldots\ldots\ldots\ldots\ldots\ldots\ldots (111.10)$$

$$h = \frac{\eta f_1}{G} - 1 \ldots\ldots\ldots\ldots\ldots\ldots\ldots\ldots\ldots\ldots\ldots\ldots\ldots\ldots\ldots\ldots\ldots\ldots\ldots\ldots\ldots (111.11)$$

$$\begin{Bmatrix} D_1 \\ D_2 \\ D_3 \end{Bmatrix} = \frac{2}{G(h + \frac{\alpha}{\eta})} \begin{bmatrix} d_{11} & d_{12} & d_{13} \\ d_{21} & d_{22} & d_{23} \\ d_{31} & d_{32} & d_{33} \end{bmatrix}^{-1} . \begin{Bmatrix} f_1 \\ f_2 \\ f_3 \end{Bmatrix} \ldots\ldots\ldots\ldots\ldots\ldots\ldots\ldots\ldots\ldots\ldots\ldots (111.12)$$

$$d_{ij} = m_{ij}K_2[\xi_j R_w] - \frac{2\eta}{G\left(h + \frac{\alpha}{\eta}\right)} f_i \frac{K_1[\xi_j R_w]}{\xi_j R_w}\ for\ i, j = 1, 2, 3 \ldots\ldots\ldots\ldots\ldots\ldots (111.13)$$

$$D_4 = -\frac{2}{G\left(h + \frac{\alpha}{\eta}\right)} \{1 + \eta \sum_{i=1}^{3} [m_{1i}D_i \frac{K_1[\xi_i R_w]}{\xi_i R_w}]\} \ldots\ldots\ldots\ldots\ldots\ldots\ldots\ldots\ldots\ldots (111.14)$$

$$D_5 = 3\left\{1 + 2\eta \sum_{i=1}^{3} [m_{1i}D_i \left(\frac{K_1[\xi_i R_w]}{\xi_i R_w} + \frac{2K_2[\xi_i R_w]}{(\xi_i R_w)^2}\right]\right\} \ldots\ldots\ldots\ldots\ldots\ldots\ldots\ldots (111.15)$$

The functions Ω, Π, Θ are defined as

$$\Omega[x] = \frac{K_1[xr]}{(xr)} + \frac{3K_2[xr]}{(xr)^2} \dots \dots \dots \dots \dots \dots \dots \dots \dots \dots \dots \dots \dots \dots \dots \dots \dots \dots \dots \dots \dots \dots . (111.16)$$

$$\Theta[x] = \frac{K_1[xr]}{(xr)} + \frac{6K_2[xr]}{(xr)^2} \dots \dots \dots \dots \dots \dots \dots \dots \dots \dots \dots \dots \dots \dots \dots \dots \dots \dots \dots \dots \dots \dots . (111.17)$$

$$\Pi[x] = \Theta[x] + K_2[xr] \dots \dots \dots \dots \dots \dots \dots \dots \dots \dots \dots \dots \dots \dots \dots \dots \dots \dots \dots \dots \dots \dots \dots \dots (111.18)$$

6.2: Elastic Uniaxial stress problem

This loading yields a solution which is uniaxial and has constant vertical stress acting at every point of the field. It is visualized that the field is under a constant uniaxial stress without pore pressure. The solutions obtained are elastic and are time dependent.

The boundary conditions at the wellbore are

$$\sigma_{rr} = 0 \dots \dots \dots \dots \dots \dots \dots \dots \dots \dots \dots \dots \dots \dots \dots \dots \dots \dots \dots \dots \dots \dots \dots \dots \dots \dots \dots \dots \dots \dots \dots (112.1)$$

$$\tau_{r\theta} = \tau_{rz} = p = p^a = p^c = 0 \dots \dots \dots \dots \dots \dots \dots \dots \dots \dots \dots \dots \dots \dots \dots \dots \dots \dots \dots \dots \dots ... (112.2)$$

The far field boundary conditions

$$\sigma_{xx} = \sigma_{yy} = 0 \dots \dots \dots \dots \dots \dots \dots \dots \dots \dots \dots \dots \dots \dots \dots \dots \dots \dots \dots \dots \dots \dots \dots \dots \dots \dots \dots ... (112.3)$$

$$\sigma_{zz} = S_z - 2\nu\sigma_m - \alpha(1-2\nu)p_o \dots \dots \dots \dots \dots \dots \dots \dots \dots \dots \dots \dots \dots \dots \dots \dots \dots \dots \dots \dots (112.4)$$

$$\tau_{xy} = \tau_{xz} = p = p^a = p^c = 0 \dots \dots \dots \dots \dots \dots \dots \dots \dots \dots \dots \dots \dots \dots \dots \dots \dots \dots \dots \dots \dots \dots (112.5)$$

The solutions for the elastic uniaxial stress problem are

$$\sigma_{zz} = S_z - 2\nu\sigma_m - \alpha(1-2\nu)p_o \dots \dots \dots \dots \dots \dots \dots \dots \dots \dots \dots \dots \dots \dots \dots \dots \dots \dots \dots \dots (112.6)$$

6.3: Elastic anti- plane shear problem

Unlike the previous 2 problems, disturbance is introduced in elastic anti-plane shear problem due to a sudden change in shear stress from S_{xz} to 0 near the wellbore.

The boundary conditions at the wellbore are

$$\sigma_{rr} = \tau_{r\theta} = p = p^a = p^c = 0 \dots \dots \dots \dots \dots \dots \dots \dots \dots \dots \dots \dots \dots \dots \dots \dots \dots \dots \dots \dots \dots (113.1)$$

$$\tau_{rz} = \left(S_{xz}cos\theta + S_{yz}sin\theta\right)H(-t) \dots \dots \dots \dots \dots \dots \dots \dots \dots \dots \dots \dots \dots \dots \dots \dots \dots \dots . \dots (113.2)$$

The far field conditions are

$$\sigma_{xx} = \sigma_{yy} = \sigma_{zz} = \tau_{xy} = p = p^a = p^c = 0 \dots\dots\dots (113.3)$$

$$\tau_{yz} = S_{yz} \dots\dots\dots (113.4)$$

$$\tau_{xz} = S_{xz} \dots\dots\dots (113.5)$$

The solutions are elastic and listed below

$$\tau_{rz} = \left(S_{xz}cos\theta + S_{yz}sin\theta\right)\left(1 - \left(\frac{R_w^2}{r^2}\right)\right) \dots\dots\dots (113.6)$$

$$\tau_{\theta z} = -\left(S_{xz}sin\theta - S_{yz}cos\theta\right)\left(1 + \left(\frac{R_w^2}{r^2}\right)\right) \dots\dots\dots (113.7)$$

$$\sigma_{rr} = \sigma_{\theta\theta} = \sigma_{zz} = \tau_{r\theta} = p = p^a = p^c = 0 \dots\dots\dots (113.8)$$

6.4: Superposed solutions of the shale medium

The superposed solutions of $p, p^a, p^c, \sigma_{rr}, \tau_{r\theta}$ are obtained from equations 104 and $\tau_{rz}, \tau_{\theta z}$ are given by equations 113 while

$$\sigma_{\theta\theta} = \sigma_m - \sigma_d \cos\left(2(\theta - \theta_r)\right) + \sigma_{\theta\theta}^1 + \sigma_{\theta\theta}^2 + \sigma_{\theta\theta}^3 \dots\dots\dots (114.1)$$

$$\sigma_{zz} = S_z - 2\nu\sigma_m + \nu(\sigma_{rr} + \sigma_{\theta\theta}) + \alpha(1 - 2\nu)(p - p_o) \dots\dots\dots (114.2)$$

The inverse of the Laplace transform in the above solutions can be obtained using Stehfest's Algorithm presented in Appendix A.

Chapter 7: Numerical Modeling Results

7.1: MATLAB coding structure

The following flow chart shows the coding structure used to perform the analysis. The input parameters are those parameters which are obtained from the lab data after examining the cores. The data used in the simulations have been taken from various research papers on Pierre Shale and the references are tabulated below. The primary calculated parameters are those calculated by using the input parameters and from which the secondary parameters are also obtained.

If the secondary parameters calculated are zero (i.e., the wellbore is vertical) then the deviatoric stress loading is ignored and if the parameters are not zero, then the individual solutions of the deviatoric loading are calculated using equations 110 and 111. These solutions are combined with other individual solutions to get the superposed solutions of the model using equations 104, 113, 114.1 and 114.2.

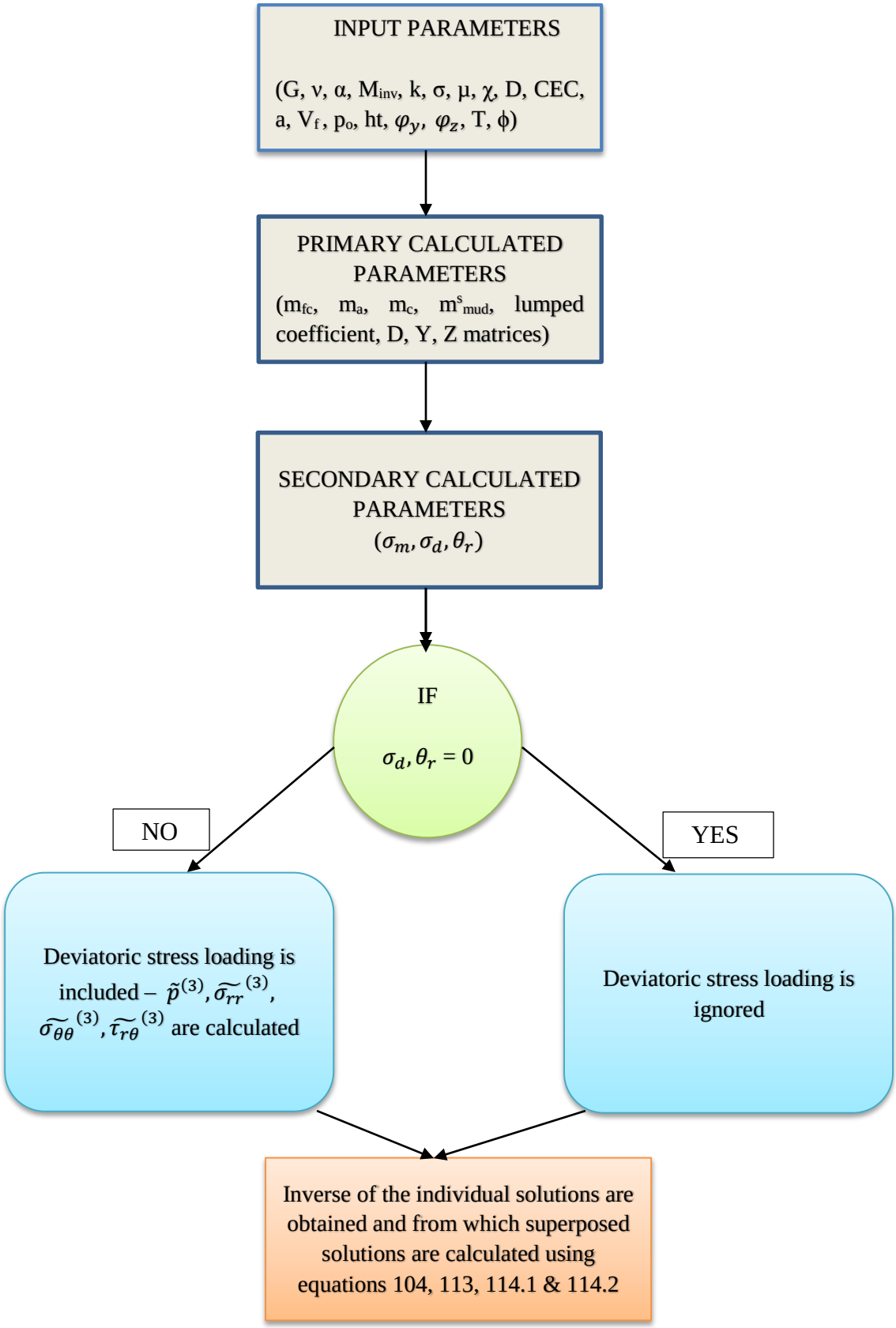

Figure 22: Flowchart of the MATLAB coding

7.2: Code Testing

7.2.1: Validation of results using analytical solutions of Nguyen et al., (2008)

The code generated to calculate the pore pressure distributions, radial and tangential stresses for Pierre Shale formations for the conditions of poroelastic medium and chemopotential medium is validated by testing the data of offshore Western Africa Shale used by Nguyen and Abousleiman (2008) and the results generated matches with the analytical solutions of Nguyen et al., (2008). Fractional differences in the results could be attributed to computer round off errors and physical modelling errors. The denominator in the formula for finding the coefficient used in the Stehfest's Laplace inverse algorithm is erroneous in case of Nguyen et al., (2008).

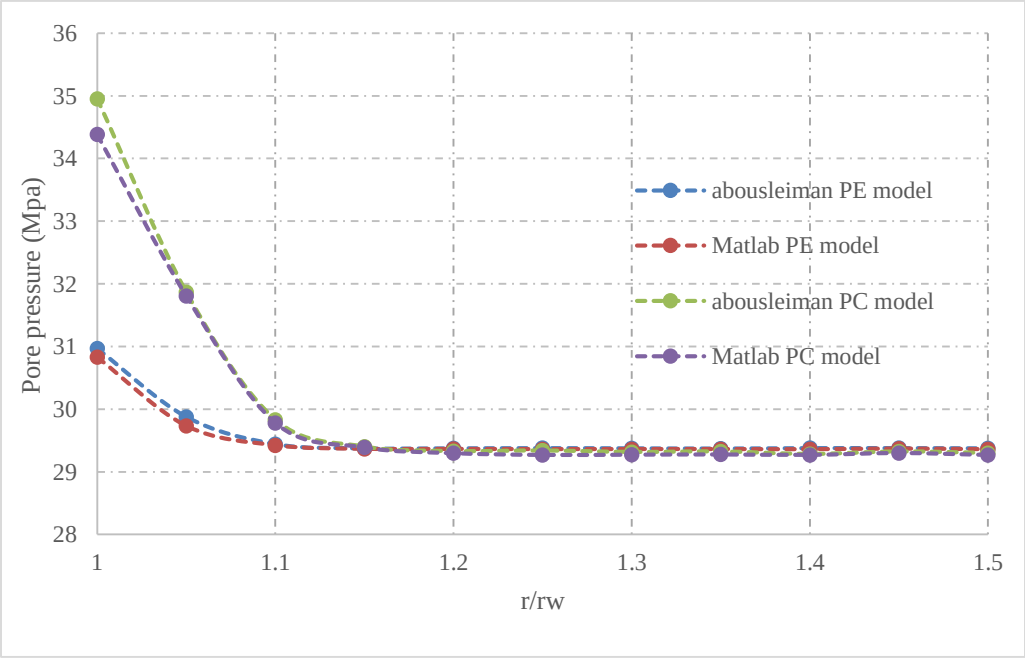

Figure 23: Pore pressure distributions near wellbore for high mud activity (Abousleiman et al & Matlab results)

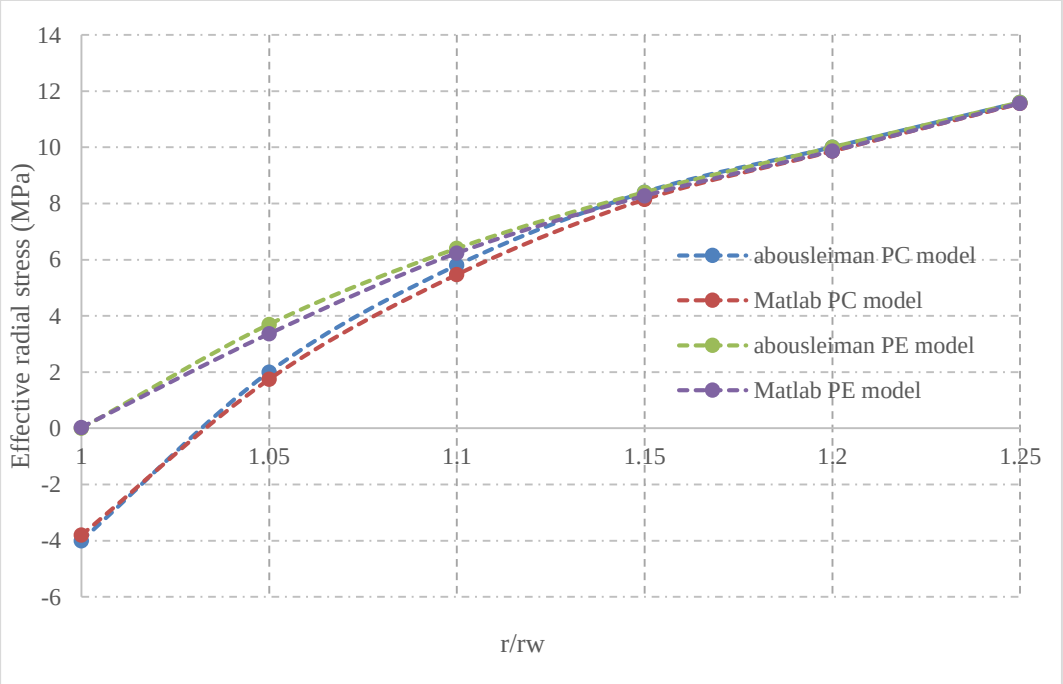

Figure 24: Effective radial stresses near wellbore for high mud activity (Abousleiman et al & Matlab results)

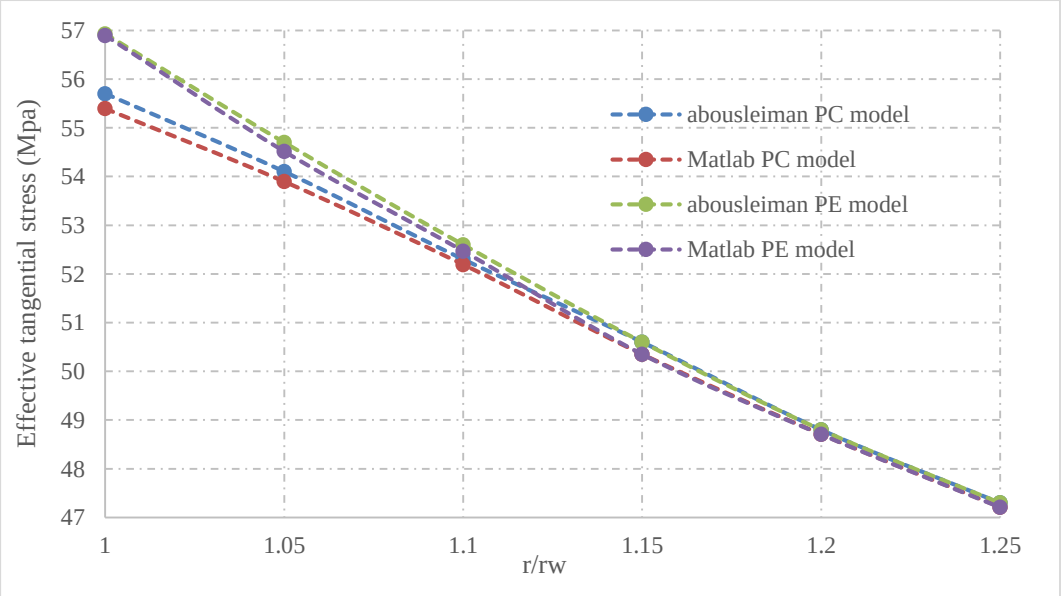

Figure 25: Effective tangential stresses near wellbore for high mud activity (Abousleiman et al & Matlab results)

Figures 23, 24 and 25 show the pore pressure, effective radial and effective tangential stress distributions near the wellbore for the Offshore Western Africa shales (data obtained from Nguyen et al., 2008) and compares the results generated using the MATLAB code with the results obtained by Nguyen et al., (2008) for the poroelastic and porochemoelastic models.

7.2.2: Validation of results using Jaeger's analytical solutions for 1-D consolidation of poroelastic medium

Jaeger et al., (2007) has developed an analytical solution for 1 dimensional consolidation of the poroelastic medium. 1 dimensional consolidation happens when a porous permeable column undergoes uniaxial strain in the vertical direction only. A constant load is applied at the top of the column, the fluid boundary pressure is set to zero gauge after the load is applied and displacement takes place only vertically.

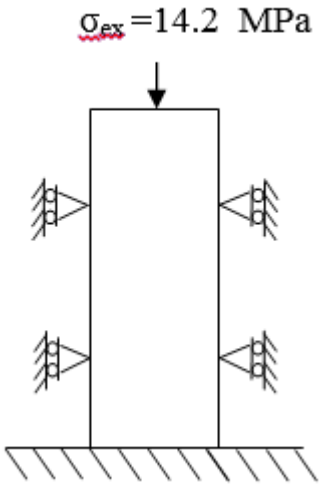

Figure 26: Problem Description

Jaeger's analytical solution for 1 dimensional consolidation gives a relationship between the displacement at the top of the column before and after the drained conditions with respect to dimensionless time.

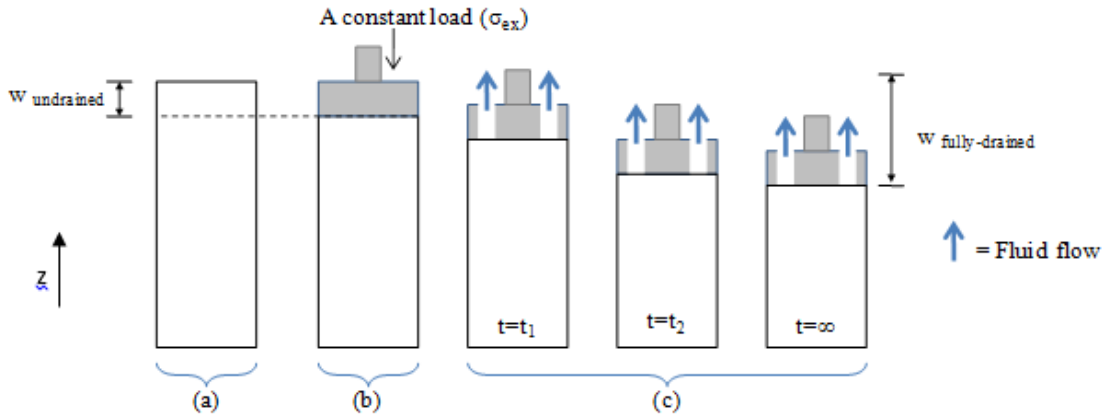

Figure 27: Column displacement for a 1-D consolidation problem; (a) The initial condition (undrained condition); (b) the column is subjected to a constant load, pressure is increased (undrained condition); (c) Fluid is drained from the column and pressure is decreased (drained condition) adapted from Charoenwongsa et al. (2010).

Equation describing the displacement of the column during different drainage conditions is given as:

$$w(z=0,t)=\frac{\sigma_{ex}h}{(\lambda+2G)}\left[1-\frac{\alpha_P^2 M}{(\lambda+2G+\alpha_P^2)}\sum_{n=1,3}^{\infty}\frac{8}{n^2\pi^2}exp\left(\frac{-n^2\pi^2 kt}{4\mu Sh^2}\right)\right] \ldots\ldots..(115)$$

Where

$$M = Biot'sModulus = \frac{1}{\phi c_t}\ (in\ Pa)$$

$$\sigma_{ex} = external\ load\ per\ unit\ area\ at\ the\ top\ of\ the\ column\ (Pa)$$

$$\alpha_P = Biot's\ constant\ (dimensionless)$$

$$\lambda = lame's\ constant\ (dimensionless)$$

$$S = \frac{1}{M} + \frac{\alpha_p^2}{(\lambda + 2G)} \; is\ storage\ coefficient\ (Pa^{-1})$$

A VBA code is used to generate the displacement Vs dimensionless time profiles for Berea Sand and Pierre Shale formations to validate the observations from the porochemopotential medium. The properties of Berea sand, the shale formation and pore fluid are listed in appendix B.

Figures 28 and 29 show that the matching between analytical solution and numerical solution is excellent. From figures 28 & 29 it is seen that the time taken for the column displacement when the fluid drainage begins is around 1000 (dimensionless time) for Berea sand (figure 28) and for Shale (figure 29) it is in the order of 10^{11} (dimensionless time). The reason for such significant difference in time is due to the permeability of the shale which is insignificant compared to the permeability of the Berea sand.

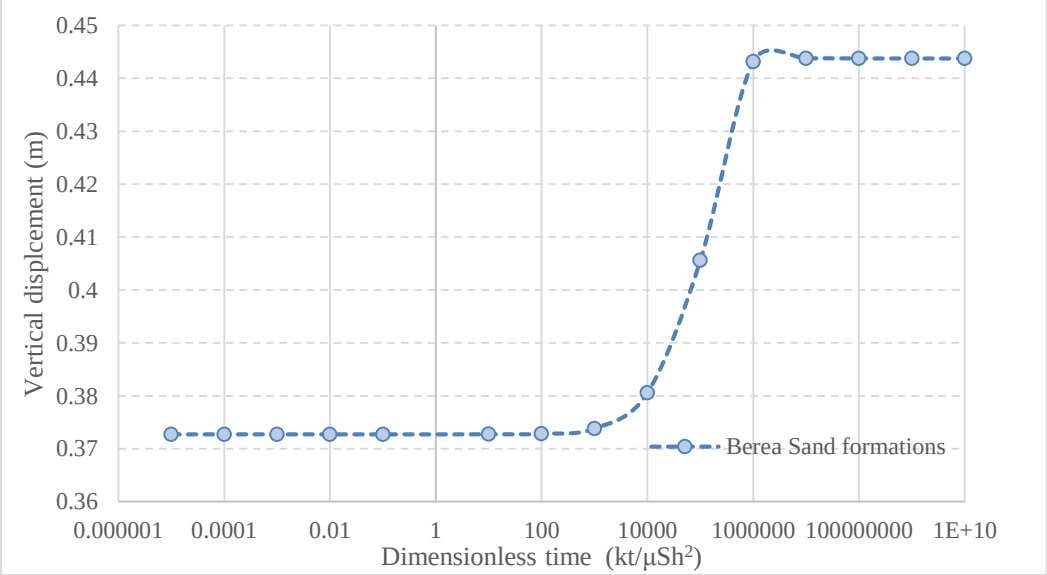

Figure 28: Displacement of the top of the column with dimensionless time for Berea Sand

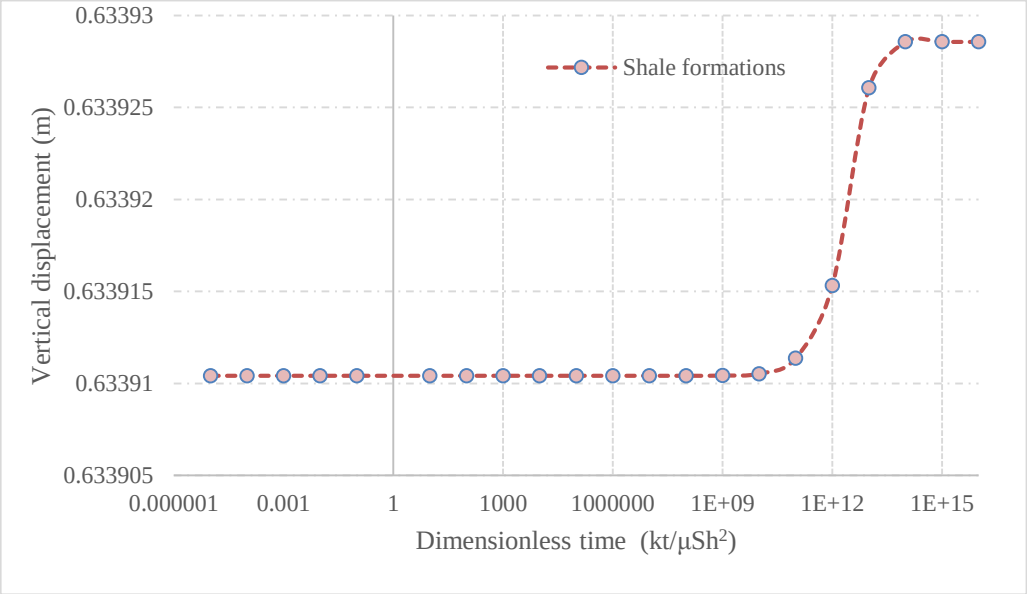

Figure 29: Displacement of the top of the column with dimensionless time for Shale formations

After testing the validity of numerical solution, the effect of permeabilities, porosities, bulk and shear modulus on the vertical displacement of the column with time for shale formations are studied.

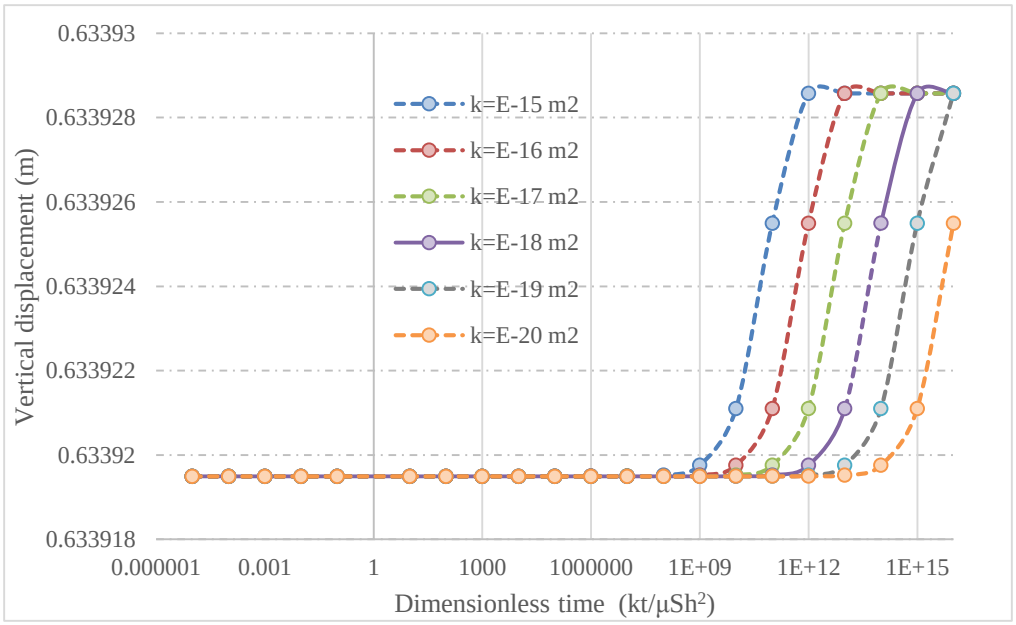

Figure 30: Displacement of the top of the column with dimensionless time for various permeabilities of Shale formation

Figure 30 shows vertical displacement as a function of dimensionless time for different permeabilities from 10^{-15} to 10^{-20} m^2. As permeability decreases the time taking for initiating drainage of the pore fluid increases. However the time interval is same because for low permeabilities decrease in pore pressure decreases the permeability further.

It is expected that the pore pressure decline for various permeabilities should give a plot where the decline is very gradual at relatively higher permeabilities unlike the significant drop for lower permeabilities. This happens because when rock is subjected to vertical loads, the pore throats reduce in size reducing the pore pressure which in turn reduces the absolute permeability of the rock more. This reduction in permeability is more for rocks with low permeability than with relatively higher permeability (Corelab, 1983).

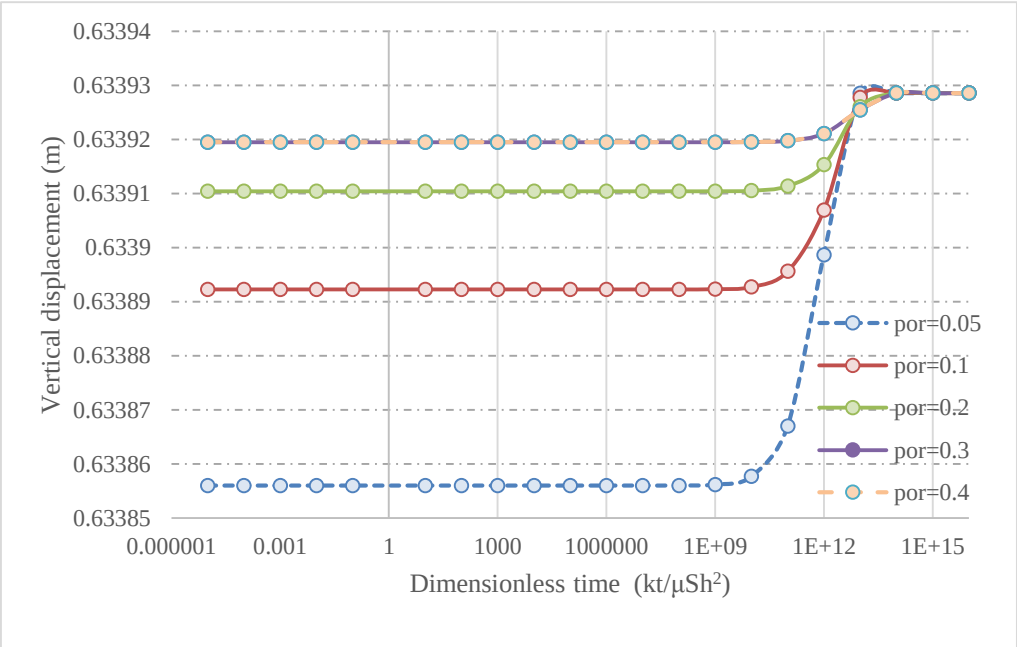

Figure 31: Displacement of the top of the column with dimensionless time for various porosities of Shale formation

Figure 31 shows the effect of porosity on vertical displacement. It is seen that as the porosity of the shale is increased, time taken to attain the final displacement for fully drained condition is decreasing because diffusion interferes the osmotic process. Hence a plot in which the pore pressure decline is significant for lower porosities while it is gradual for higher porosities is expected. The draining process is initiated faster in consolidated medium because of the excess capillary pressure acting in the smaller pores. Moreover, for the porosities above 30%, the curves overlap or the difference is insignificant as seen in figures 31.

This is because for higher porosities, the membrane efficiency is very less and most of the pore fluid (water) is lost along with the dominating process diffusion and has only little amount to be drained and the pore throats are also relatively bigger which eases the flow.

Similarly when shale formations with different bulk modulus and same hydrological properties were tested (figure 32), the displacement and the pore fluid draining process depends on the compressibility of the rock. As bulk modulus increases, the Poisson's ratio increases. A medium with higher Poisson's ratio is closer to have properties of incompressible medium and for the same dimensionless time displaces lesser than the medium with lower Poisson's ratio.

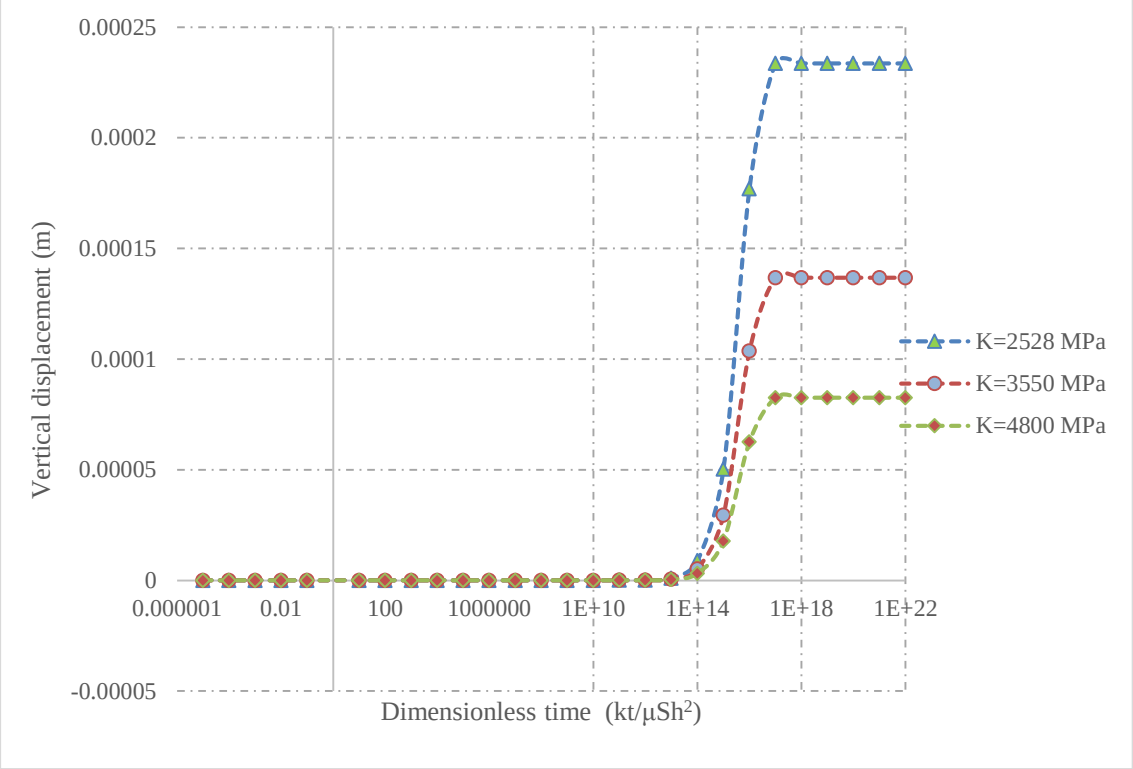

Figure 32: Displacement of the top of the column with dimensionless time for Shale formations of various Bulk modulus

In the following figure 33, the displacement at the top of the column with dimensionless time for shale formation with different shear modulus is plotted. As mentioned earlier, the displacement of the column and draining of pore fluid depends on the compressibility of the medium. As the shear modulus decreases, the Poisson's ratio increases. However in Pierre shales, the difference in ratio is less as shear modulus ranges is 400 – 1000 MPa. Hence a medium with lower shear modulus displaces little compared to medium with higher shear modulus for the same time interval.

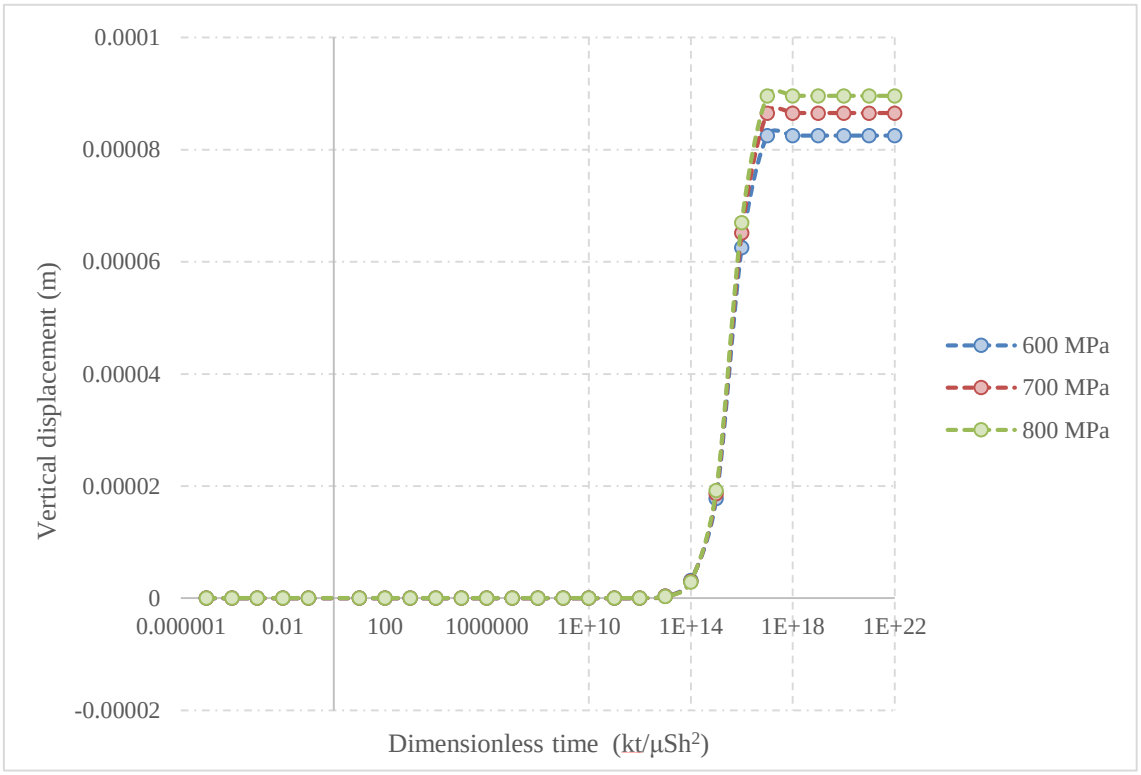

Figure 33: Displacement at the top of the column of Shales with varying Shear Modulus

7.3: Case study-Pierre Shale formations

The impact of hydraulic fluid and ion transfers on pore pressure and field stresses can be studied by considering an inclined wellbore such that it's angle of inclination is zero (simplified vertical wellbore)drilled in a Pierre Shale formation with hydrological and mechanical properties and also the corresponding drilling mud with fluid properties as listed in table 5. The wellbore has a radius of about 0.1 m and drilled to a depth of 2200 m. in the formation. The wellbore is filled with drilling mud which has NaCl and water as its major constituents. The drilling mud has 1.07 SG and exerts a pressure of 23.09 MPa. The initial pore pressure of the formation is 21.4 MPa. The response of the chemically active formation is studied with the chemo-potential model and is also compared with the response observed with the poroelastic model. The pore pressure values and effective stresses are calculated using equations 104.1, 104.3 and 114.1.

Table 5: Modeling parameters for an inclined wellbore

Parameters	Values	Units	References	Range
Shear Modulus	600	MPa	Brian Richards 1996	400-1000 MPa (Aminul et al., 2013)
Bulk modulus	4800	MPa	Brian Richards 1996	270 -12920 Mpa (Aminul et al 2013)
Poisson ratio	0.44	Dimensionless	Calculated	0.095-0.5 (Aminul et al 2013)
Pore pressure coefficient	0.9	Dimensionless	Ojala et al 2010	
Storage coefficient 1/M	1/10000	1/MPa		

Porosity	0.176	Dimensionless	Brian Richards 1996	5-30% (Leonard et al., 1980)
Grain density	2.37	g/cc	Fjaer 2008	2.2-2.5 g/cc
Permeability	6.00E-21	Sq m	Van Oort 1996	E-15 - E-20 sq m (C.E.Neuzil 1994)
Reflection coefficient	0.8	Dimensionless	Brian Richards 1996	
CEC	36	Meq/100grams	Salisbury et al 1991	
Water activity of pore fluid	0.96	Dimensionless	Brian Richards 1996	
Effective diffusion coefficient Na+	1.33E-10	Sq m /s	Yeung and Datla 1995	
Effective diffusion coefficient Cl-	2.032 E-10	Sq m /s	Yeung and Datla 1995	
Temperature	82	Deg celsius	Salisbury et al 1991	
Pore pressure	21.4	MPa	Salisbury et al 1991	
Depth	2200	m	Salisbury et al 1991	
Mud pressure	23.09	MPa	Calculated	
S_v	54	MPa	Salisbury et al 1991	
S_H , S_h	44	MPa	Salisbury et al 1991	
m^{fc}	0.0719	Dimensionless	Calculated using equation 90	
m^a	0.0052	Dimensionless	Calculated using equation 87	
m^c	0.0771	Dimensionless	Calculated using equation 88	

7.4: Simulation Results

7.4.1: When mud activity is greater than pore fluid water activity

Case is studied initially by considering the water activity of the mud to be greater than the activity of the pore fluid ($a^f_{mud} = 0.95$ & $a^f_o = 0.90$).

Table 6: Pore pressures of different models at various distances from wellbore for high mud activity

r/rw	Chemo-potential model	Poroelastic model
1	29.15527596	23.0804834
1.05	26.77902361	22.56434067
1.1	24.7850834	22.1315479
1.15	23.31868117	21.81372694
1.2	22.37656028	21.60998242
1.25	21.84457593	21.49525859
1.3	21.57888174	21.43815837
1.35	21.46170565	21.4130831
1.4	21.41689644	21.40354763
1.45	21.40285249	21.40058473
1.5	21.39989314	21.39997299
1.55	21.39998866	21.40000067

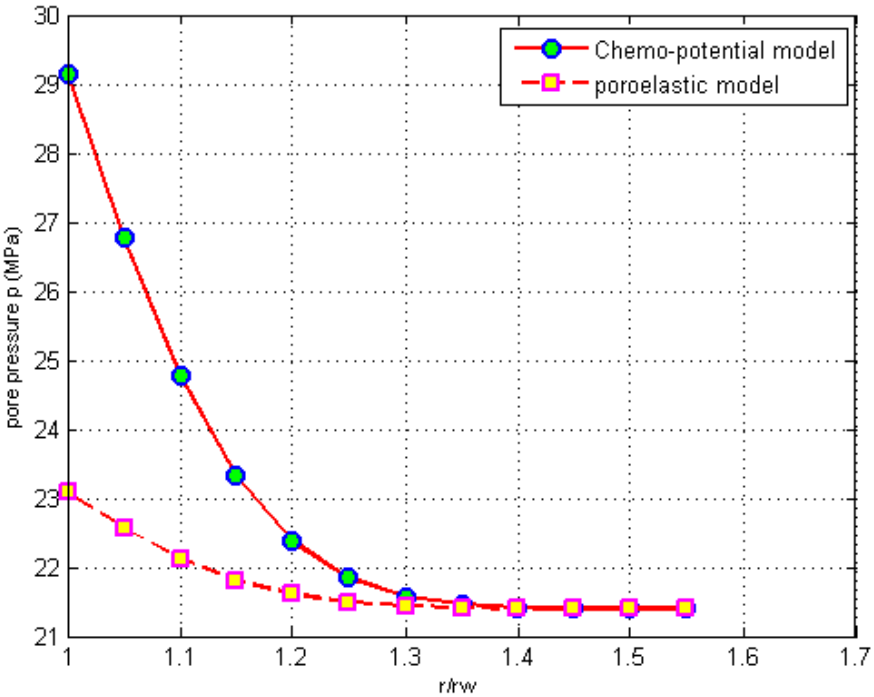

Figure 34: Pore Pressure distribution at time = 0.01 day (15 mins) for higher mud activity

Table 7: Effective Radial Stresses of different models at various distances from the wellbore for high mud activity

r/rw	Chemo-potential model	Poroelastic model
1	-6.062535963	0.012256601
1.05	-1.683937225	2.48484765
1.1	2.026703295	4.609318723
1.15	4.976571229	6.399913187
1.2	7.211205213	7.894160507
1.25	8.87825482	9.14646442
1.3	10.14776927	10.21182142
1.35	11.15802705	11.13493808
1.4	12.00143565	11.94791538
1.45	12.73272203	12.67260975
1.5	13.38235492	13.32397986
1.55	13.96736031	13.91275415

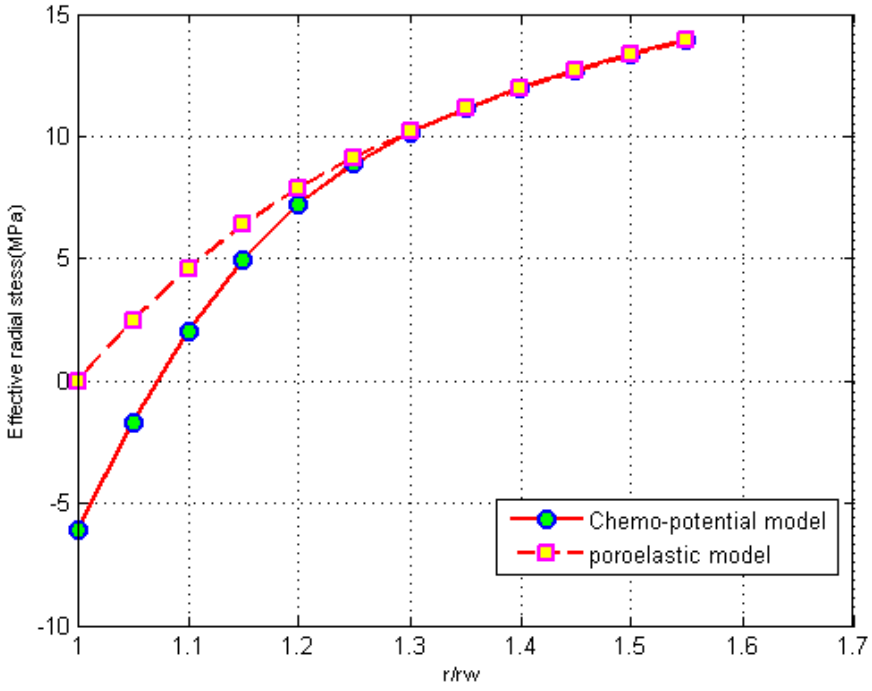

Figure 35: Effective radial stresses around the wellbore after time = 0.01 day (15 mins) for higher mud activity

Table 8: Effective Tangential stresses of different models for high mud activity

r/rw	Chemo-potential model	Poro-elastic model
1	37.2476444	42.15086983
1.05	37.16327313	40.61102243
1.1	37.05596742	39.26866972
1.15	36.7560978	38.05242313
1.2	36.22401086	36.92637127
1.25	35.51833297	35.88138971
1.3	34.72896588	34.91922096
1.35	33.93046203	34.0414189
1.4	33.16803007	33.24567355
1.45	32.46212312	32.52633357
1.5	31.8178382	31.87606895
1.55	31.23266019	31.28724465

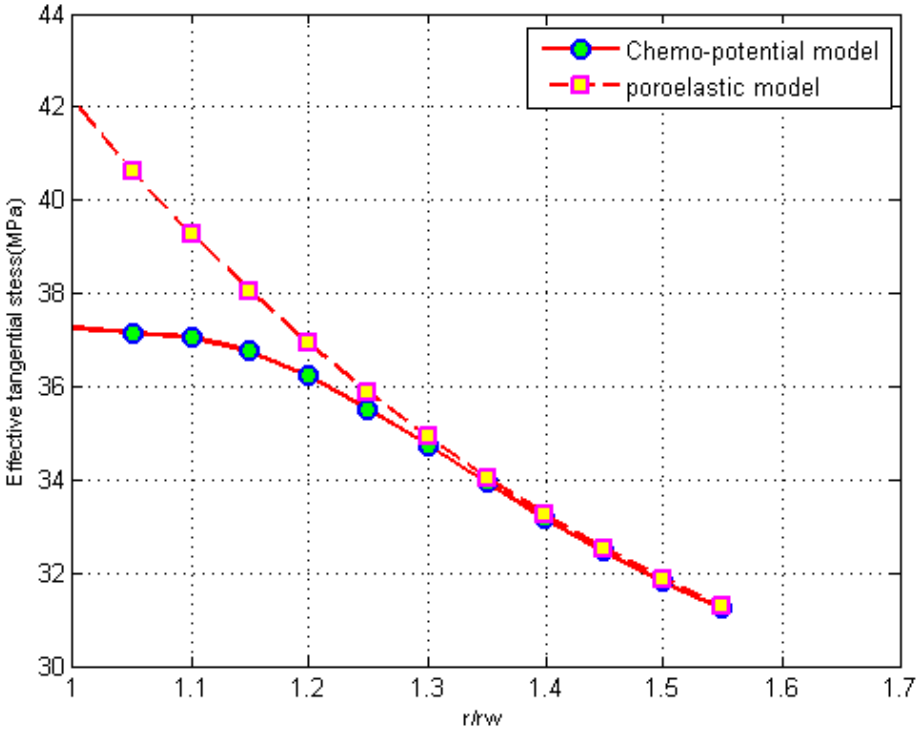

Figure 36: Effective tangential stresses around the wellbore when time = 0.01 day (15 mins) for higher mud activity

When the water activity in mud is higher than the water activity in the pore fluid, the salt concentration in mud is lower than the salt content in pore fluid. Hence the mud become less saline. The difference in the chemical potential of water on either side of the clay membrane develops a driving force causing water to flow from wellbore towards the formation.

However, in addition to chemical potential difference of water there exists concentration gradient of the chemical species. Hence the ions try to flow from higher saline fluid to fluid with less salinity. Based on the membrane efficiency and the surface charge the diffusion of ionic species is restricted and does not drag water against the osmotic process. As more pore fluid enters the shale, the pore pressure near the shale is very high compared to the other radial distances from the wellbore as seen in figure 34.

In figure 35, the corresponding effective radial stresses for chemo-potential model plunges to negative values near the wellbore region. The negative values correspond to tensile stresses. This is because of the additional pore pressure developed which is explained earlier. In this case the radial tensile stresses weaken the radial compressive stresses near the wellbore and causes fragmentation of the formation. Similarly in figure 36, the tensile tangential stresses weaken the compressive tangential stresses and causes the formation to spall.

7.4.2: When water activity of pore fluid is greater than the mud activity

Case is studied by considering the water activity of the mud to be lower than the activity of the pore fluid ($a_{mud}^{f} = 0.87$ & $a_{o}^{f} = 0.90$).

Table 9: Pore Pressure of different models for lower mud activity

r/rw	Chemo-potential model	Poro-elastic model
1	15.3440468	23.06123779
1.05	17.20024172	22.55359367
1.1	18.75764076	22.12728497
1.15	19.90276243	21.81325024
1.2	20.63824489	21.61099865
1.25	21.0533837	21.4964338
1.3	21.26062054	21.43899468
1.35	21.35196149	21.41354242
1.4	21.38686381	21.40374846
1.45	21.39778965	21.40064946
1.5	21.40008548	21.39998187
1.55	21.40000729	21.39999416

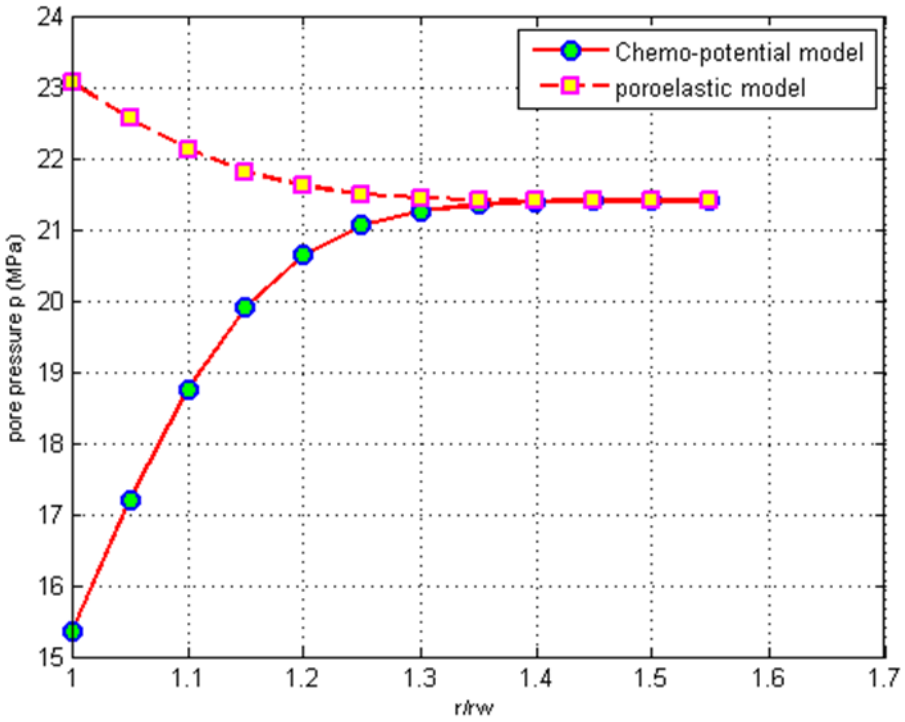

Figure 37: Pore Pressure distribution near wellbore for time = 0.01 day (15 mins) for lower mud activity

Table 10: Effective Radial stresses of different models for lower mud activity

r/rw	Chemo-potential model	Poro-elastic model
1	7.748693203	0.031502206
1.05	7.790510164	2.495461521
1.1	7.892961104	4.613398101
1.15	8.207038147	6.400204454
1.2	8.759530983	7.892977342
1.25	9.485193242	9.145144187
1.3	10.29186883	10.21085846
1.35	11.10488291	11.1343658
1.4	11.87958247	11.94761167
1.45	12.59609656	12.67244991
1.5	13.24975272	13.32388232
1.55	13.84333827	13.91267761

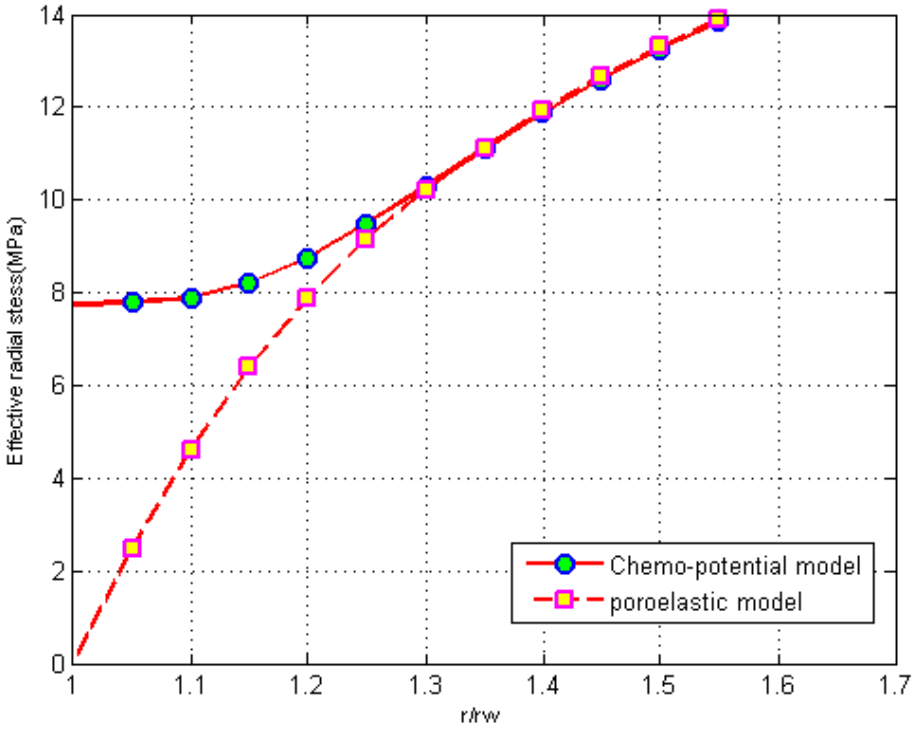

Figure 38: Effective radial stresses around the wellbore for time = 0.01 day (15 mins) for lower mud activity

Table 11: Effective Tangential stresses of different models for lower mud activity

r/rw	Chemo-potential model	Poro-elastic model
1	48.39527937	42.16640378
1.05	44.99905302	40.61982992
1.1	42.08215953	39.27229406
1.15	39.69868404	38.05299333
1.2	37.81706932	36.92571796
1.25	36.34119194	35.88058616
1.3	35.16000976	34.91867259
1.35	34.18192954	34.04116111
1.4	33.34415649	33.24561434
1.45	32.60789785	32.52637642
1.5	31.9500928	31.87615045
1.55	31.35664856	31.28733294

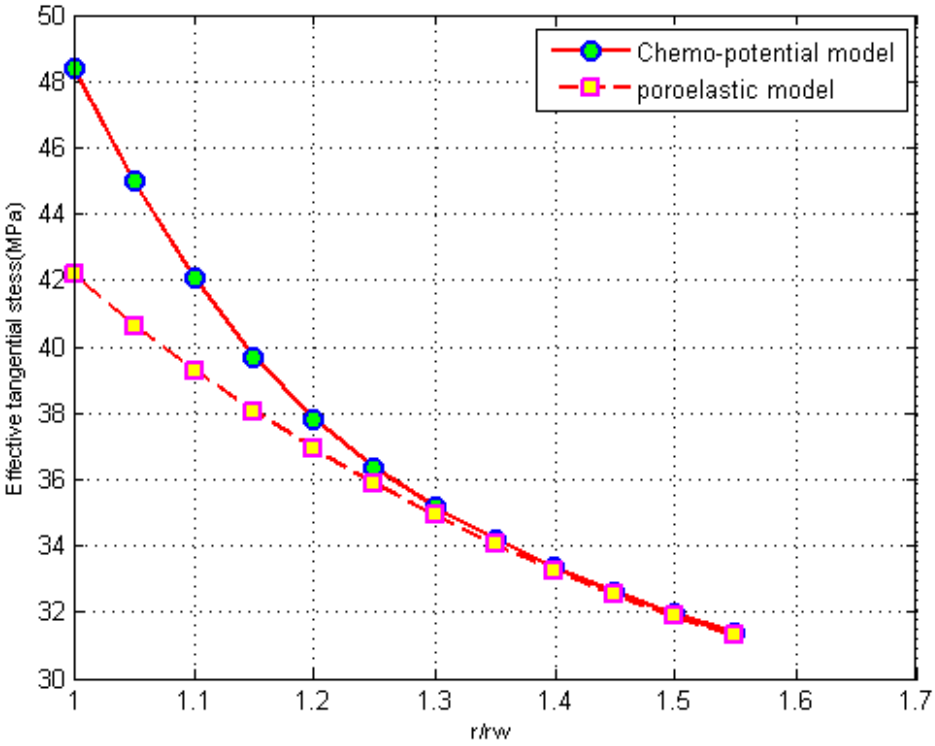

Figure 39: Effective tangential stresses around the wellbore when t = 0.01 day (15 mins) for lower mud activity

When the water activity in mud is lower than the activity of pore fluid then the salt content in the mud is greater than the salt concentration in the pore fluid. Hence in this case the drilling mud is more saline than the pore fluid. As a result, the water flows from the formation back into the wellbore and the chemical ions try to move towards the formation, the movement of which is restricted at the shale/ mud interface due to diffuse double layer and surface charges. The process of osmosis is not disturbed by diffusion of chemical species which generally drags away some water with it. Hence more water is removed from the formation at a distance very close to wellbore where the pore pressure drops low and increases gradually as the water removed from shale decreases with increase in the radial distance from the wellbore as shown in figure 37.

Figures 38 and 39 show the corresponding effective radial effective tangential stresses near the wellbore when mud activity is lower. The chemical osmosis of water has made the effective radial and tangential stresses more compressive than the poroelastic model. The opposing tensile and compressive stresses near the wellbore can cause formation fragmentation.

7.4.3: Time propagation of osmotic pore pressure generated

Figure 40 shows the changes in the pore pressure near the wellbore region for various time intervals such as 0.001 day, 0.01 day, 0.1 day and 1 day and for the case when mud activity is lower than the pore fluid activity. As the time elapses more water is being removed from shale such that even radial distances far from wellbore lose the water. Hence the pore pressure drops for a particular distance ratio when the time increases.

Table 12: Time propagation of the osmotic pressures generated

r/rw	t=0.001 day	t=0.01 day	t=0.1 day	t=1 day
1	15.34	15.34	15.34	15.34
1.05	19.98	17.20	16.03	15.64
1.1	21.29	18.76	16.69	15.93
1.15	21.40	19.90	17.29	16.20
1.2	21.40	20.64	17.85	16.46
1.25	21.40	21.05	18.37	16.71
1.3	21.40	21.26	18.83	16.95
1.35	21.40	21.35	19.25	17.18
1.4	21.40	21.39	19.61	17.39
1.45	21.40	21.40	19.93	17.60
1.5	21.40	21.40	20.20	17.80
1.55	21.40	21.40	20.44	17.99

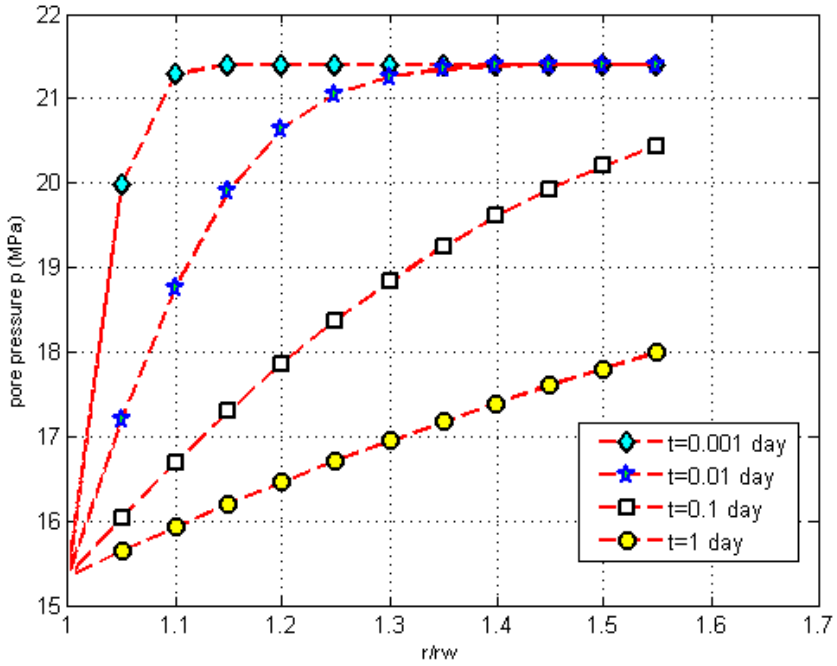

Figure 40: Time propagation of the osmotic pore pressure generated for lower mud activity

7.4.4: Effect of Mechanical Properties on Pore Pressures of Chemically Active Shale

Table 13: Pore pressure distributions for Chemically Active Shales for various Shear Modulus

r/rw	G=600 Mpa	G=700 Mpa	G=800 Mpa
1	29.155	29.157	29.158
1.05	26.779	26.795	26.809
1.1	24.785	24.809	24.831
1.15	23.319	23.343	23.366
1.2	22.377	22.396	22.415
1.25	21.845	21.858	21.870
1.3	21.579	21.586	21.593
1.35	21.462	21.465	21.469
1.4	21.417	21.418	21.420
1.45	21.403	21.403	21.404
1.5	21.400	21.400	21.400
1.55	21.400	21.400	21.400

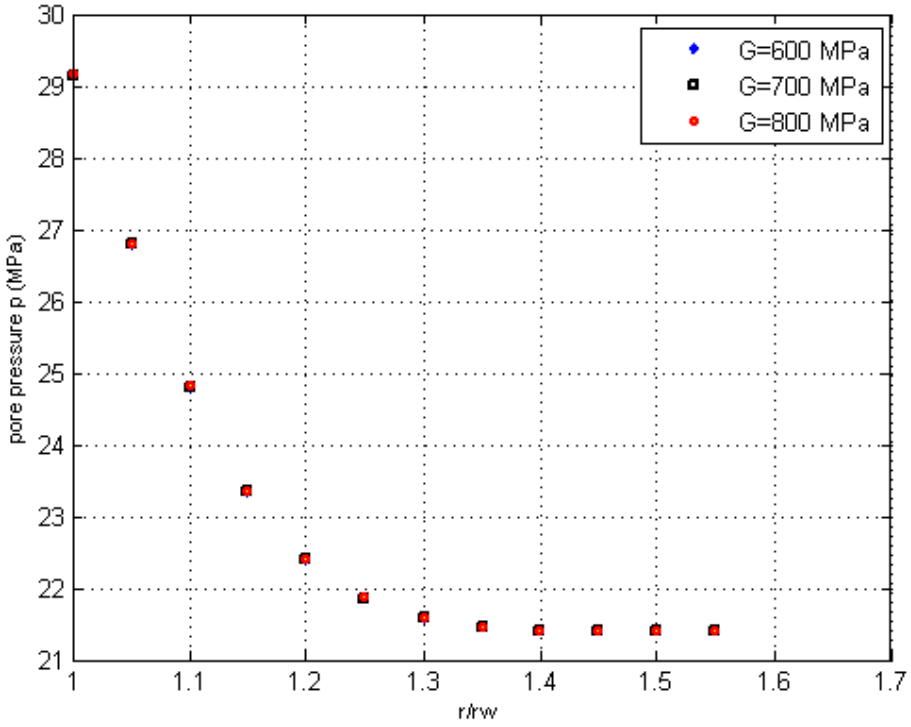

Figure 41: Pore pressure distribution for various Shear Modulus

Table 14: Pore Pressure distributions for Chemically Active Shales for various Bulk Modulus

r/rw	K=2528 Mpa	K=3550 Mpa	K=4800 Mpa
1	29.116	29.139	29.155
1.05	26.377	26.600	26.779
1.1	24.196	24.516	24.785
1.15	22.754	23.051	23.319
1.2	21.963	22.171	22.377
1.25	21.598	21.715	21.845
1.3	21.456	21.510	21.579
1.35	21.411	21.431	21.462
1.4	21.401	21.406	21.417
1.45	21.400	21.400	21.403
1.5	21.400	21.400	21.400
1.55	21.401	21.400	21.400

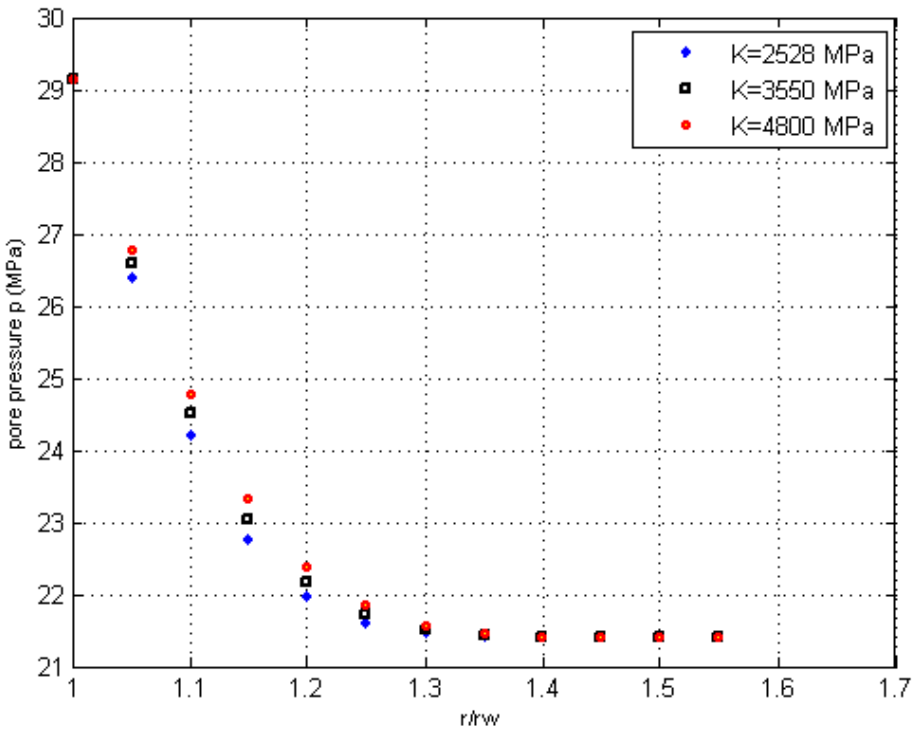

Figure 42: Pore Pressure distribution for various Bulk Modulus

Table 15: Pore Pressures for different Poisson's ratio

r/rw	ν = 0.2	ν = 0.3	ν = 0.4	ν = 0.5
1	29.01	29.06	29.12	29.21
1.05	25.58	25.91	26.45	27.59
1.1	23.19	23.58	24.29	26.13
1.15	21.99	22.25	22.84	24.86
1.2	21.54	21.67	22.02	23.83
1.25	21.42	21.46	21.63	23.03
1.3	21.40	21.41	21.47	22.45
1.35	21.40	21.40	21.42	22.05
1.4	21.40	21.40	21.40	21.78
1.45	21.40	21.40	21.40	21.61
1.5	21.40	21.40	21.40	21.51
1.55	21.40	21.40	21.40	21.45

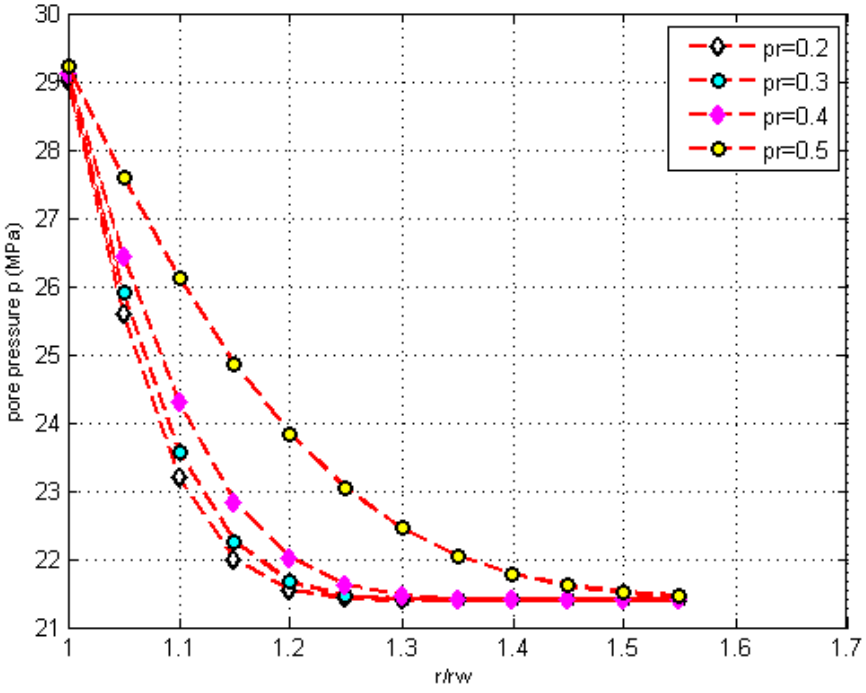

Figure 43: Effect of Poisson's ratio on Pore Pressure near the wellbore for high mud activity

Figures 41 and 42 show the pore pressure distributions near the wellbore region for the case of high mud activity and for varying shear modulus and bulk modulus respectively. For an increasing shear modulus the Poisson's ratio decreases and it increases with the increasing bulk modulus. For changes in the shear modulus, the reflecting variations in the Poisson's ratio is almost thrice the variations observed for the same changes in the bulk modulus.

Though the alterations in shear modulus and bulk modulus affected the near wellbore pore pressure distributions, the Poisson's ratio is found to have more direct and significant effect. In figure 43 it is observed that when the Poisson's ratio of Pierre Shale formation is 0.5 it becomes incompressible radially that it retains more water and tendency to allow volumetric changes is very less compared to medium with lower Poisson's ratio. Hence as the Poisson's ratio decreases, the pore pressure decreases faster for same distance from the wellbore when compared with incompressible shale formation. The differences in the pore pressure distribution at a particular distance from the wellbore is insignificant for lower Poisson's ratios when compared with the ratio of 0.5.

7.4.5: Effect of Petrophysical and Surface Charge Properties on Pore Pressure distribution near wellbore region

The plots are applicable only for NaCl pore fluid of concentration 0-3 M /liter. Figures 44 and 45 show that the reflection coefficient or the membrane efficiency of Pierre shale increases with increasing surface charges or Cation Exchange Capacity and also with decreasing porosity. This is because when the surface charges increases, the net

negative potential increases causing the clay membrane to exclude the anions more effectively. Similarly when the porosity decreases, the shale compacts and the diffuse double layers overlap and deflect the anions.

Table 16: Relation between membrane efficiency and CEC for porosity range 0 - 40%

CEC	φ = 0.0001	φ = 0.1	φ = 0.2	φ = 0.3
20	1	0.9591	0.90894	0.86256
40	1	0.97015	0.91578	0.86442
60	1	0.97775	0.92597	0.87032
80	1	0.98254	0.93588	0.87856
100	1	0.98572	0.94431	0.88764

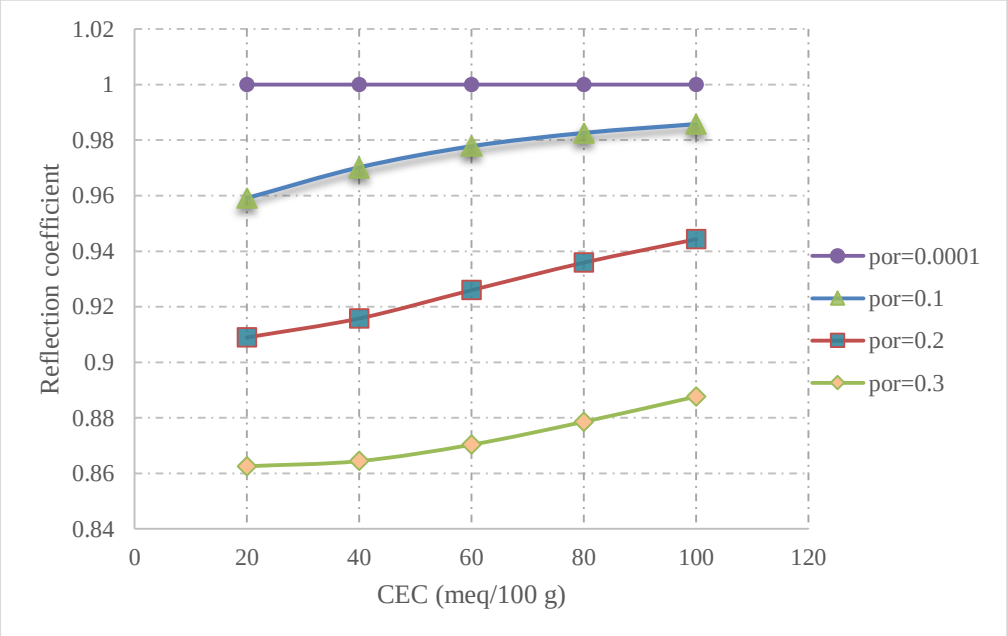

Figure 44: Variation of membrane efficiency with Cation Exchange Capacity for porosity range of 0-30%

Table 17: Relation between membrane efficiency and CEC for porosity range 40 - 60%

CEC	φ = 0.4	φ = 0.5	φ = 0.6
20	0.59079	0.49145	0.39271
40	0.58802	0.48643	0.38725
60	0.5915	0.48503	0.38372
80	0.60032	0.48712	0.38212
100	0.61313	0.49239	0.38242

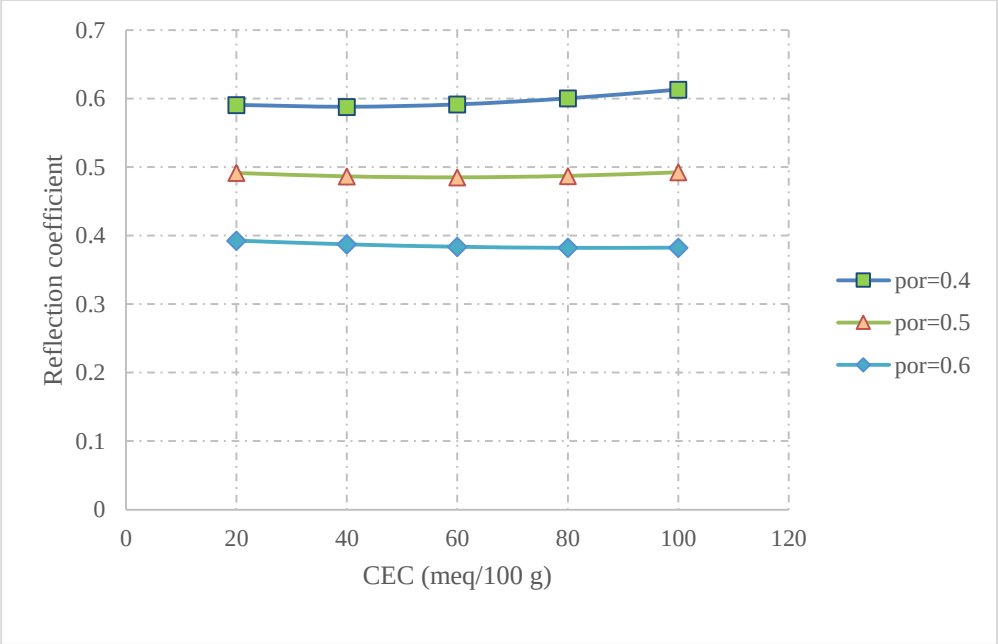

Figure 45: Variation of membrane efficiency with Cation Exchange Capacity for porosity range of 40 - 60%

From figures 44 and 45, it is observed that for Pierre Shale formations with same Cation Exchange Capacity and having porosities in the range 0-30%, a difference in porosity of 0.1 gives a difference in membrane efficiency which is half of the difference observed if the porosities are in the range of 40-60%.

Similarly the changes in membrane efficiency for a Pierre Shale formation with porosity in the range 0-30% are significantly observed for varying Cation Exchange Capacity unlike the clay membrane with the porosity in the range 40-60% for which the change in the reflection coefficient is insignificant. The reasons for the observed facts are attributed to the concept of double layer overlap and increase in net negative potential for low porosity and high CEC respectively.

When the porosity of the Pierre Shale formations are very less in the orders of < 0.1 the membrane efficiency or the reflection coefficient of the membrane is very high. So the ion exclusion behavior is more effective and deflects the diffusion of ions through it. Hence the pressure build up within the pores of formation is relatively higher compared to pore pressures developed for increasing porosities at the same distance ratio from the wellbore due to interference of osmosis by diffusion. This result is a consequence of the concept explained using figures 44 and 45.

Table 18: Pore Pressure distributions for Pierre Shale formations of different porosities and constant CEC = 36 meq/ 100 g

r/rw	ϕ = 0.1	ϕ = 0.2	ϕ = 0.3	ϕ = 0.4	ϕ = 0.5	ϕ = 0.6
1	38.36	27.82	24.96	23.91	23.47	23.26
1.05	33.22	25.85	23.87	23.14	22.83	22.69
1.1	28.89	24.20	22.95	22.49	22.30	22.21
1.15	25.69	22.98	22.28	22.02	21.91	21.86
1.2	23.61	22.21	21.84	21.71	21.66	21.63
1.25	22.42	21.77	21.60	21.54	21.52	21.50
1.3	21.82	21.55	21.48	21.46	21.45	21.44
1.35	21.55	21.45	21.43	21.42	21.42	21.41
1.4	21.44	21.41	21.41	21.41	21.40	21.40
1.45	21.41	21.40	21.40	21.40	21.40	21.40
1.5	21.40	21.40	21.40	21.40	21.40	21.40
1.55	21.40	21.40	21.40	21.40	21.40	21.40

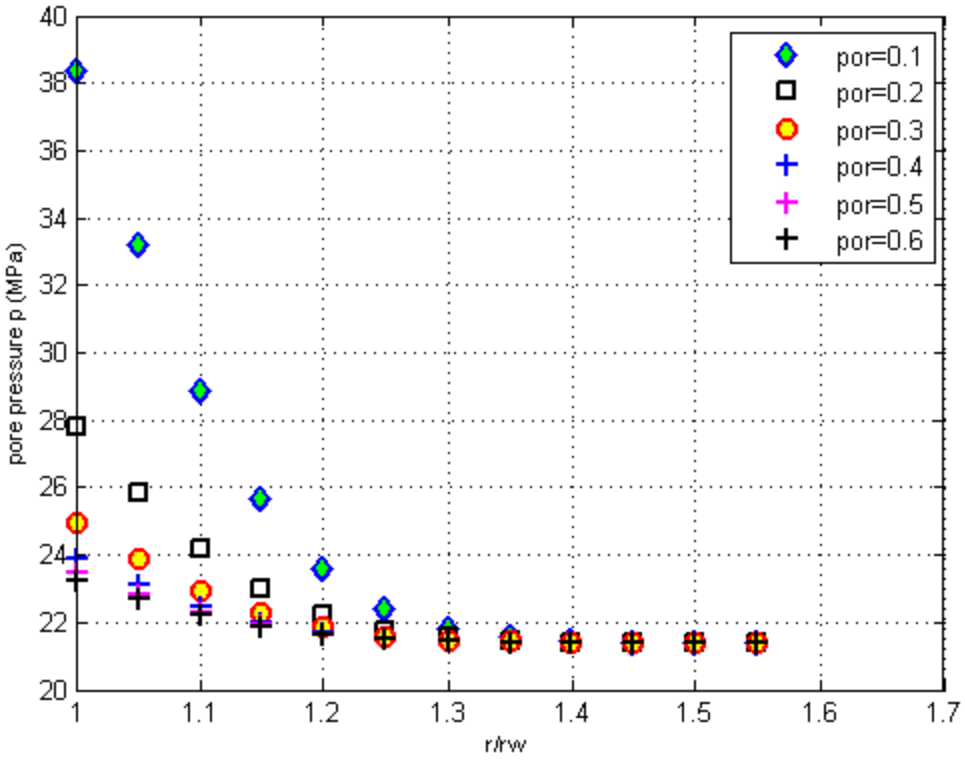

Figure 46: Pore Pressure distribution near wellbore region for various porosities and CEC = 36 meq/ 100 g (higher mud activity)

When the Pierre Shale formations have a surface charge or Cation Exchange Capacity in the orders of higher magnitude ≥ 40 meq/ 100 g, the membrane efficiency or the reflection coefficient of the Pierre Shale formation is very high restricting the ion movement through it, a result observed in figures 44 and 45. Hence more pressure is developed and this pressure build up is relatively higher than the pore pressure generated for Pierre Shale formation with lower CEC or surface charges at the same distance ratio.

Table 19: Pore pressure distributions for Pierre Shale formations with different surface charges and constant porosity of 0.176

r/rw	CEC= 10	CEC= 20	CEC= 30	CEC=40	CEC=50
1	23.7	25.4	27.6	30.2	33.0
1.05	23.0	24.1	25.7	27.5	29.5
1.1	22.4	23.1	24.1	25.3	26.5
1.15	22.0	22.4	22.9	23.6	24.3
1.2	21.7	21.9	22.2	22.5	22.9
1.25	21.5	21.6	21.8	21.9	22.1
1.3	21.5	21.5	21.5	21.6	21.7
1.35	21.4	21.4	21.4	21.5	21.5
1.4	21.4	21.4	21.4	21.4	21.4
1.45	21.4	21.4	21.4	21.4	21.4
1.5	21.4	21.4	21.4	21.4	21.4
1.55	21.4	21.4	21.4	21.4	21.4

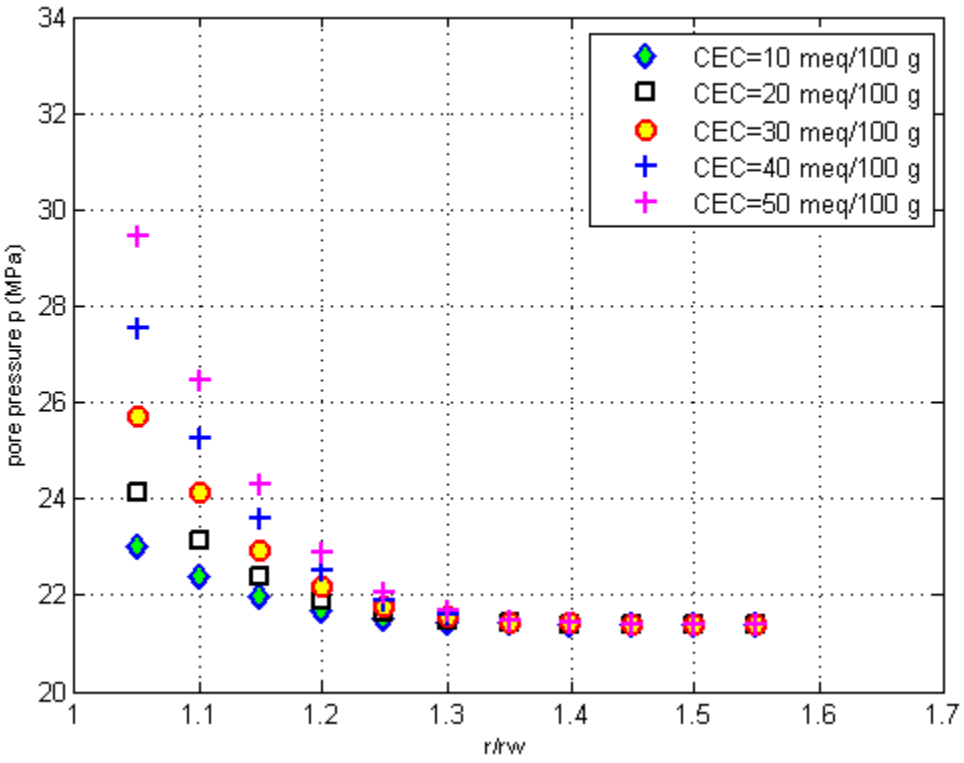

Figure 47: Pore Pressure distributions near wellbore region for various CECs and porosity = 0.176 (higher mud activity)

Table 20: Pore pressure distributions for Pierre Shale formations with various permeabilities (in m^2)

r/rw	k=0.6E-15	k=0.6E-16	k=0.6E-17	k=0.6E-18	k=0.6E-19	k=0.6E-20
1	29.16	29.16	29.16	29.16	29.16	29.16
1.05	29.06	29.02	28.95	28.77	28.27	26.78
1.1	28.97	28.90	28.75	28.41	27.44	24.79
1.15	28.88	28.77	28.56	28.06	26.66	23.32
1.2	28.80	28.66	28.38	27.72	25.94	22.38
1.25	28.72	28.55	28.21	27.41	25.28	21.84
1.3	28.64	28.44	28.05	27.10	24.69	21.58
1.35	28.56	28.34	27.89	26.81	24.16	21.46
1.4	28.49	28.24	27.73	26.53	23.69	21.42
1.45	28.42	28.14	27.58	26.27	23.28	21.40
1.5	28.36	28.05	27.44	26.01	22.93	21.40
1.55	28.29	27.96	27.30	25.77	22.63	21.40

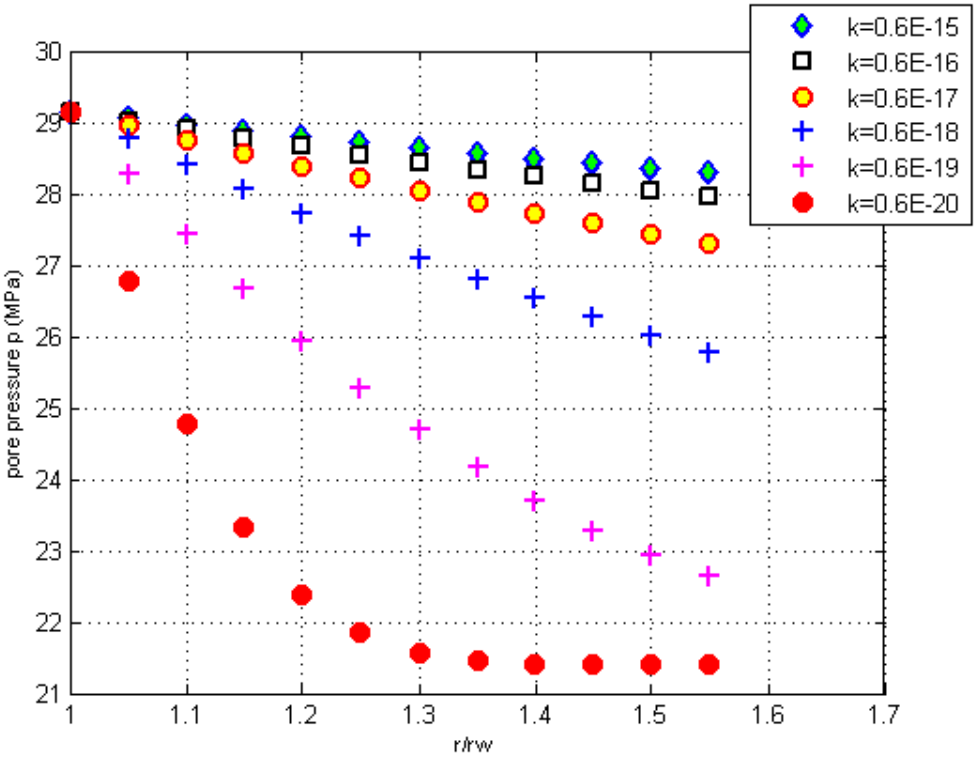

Figure 48: Pore pressure distributions for Pierre Shale formations with various permeabilities

From figure 48, it is observed that the pore pressure decline is linear in case of relatively higher permeabilities while it is very gradual in less permeable formations. This is because when water enters the formation due to difference in the water activity of the solutions, water penetrates more into formations which are more permeable. Hence at a particular distance ratio from the wellbore, more permeable formations have higher pore pressure. As permeability falls below E^{-17} m^2 the differences in the pore pressure is significant.

The reduction in permeability due to drop in pore pressure is significant for formations of low permeability compared to formations of relatively higher permeability (Katz and Lee., 1990).

Chapter 8: Conclusions

8.1: Conclusions from the above study on Pierre Shale formations

1. The poroelastic model used in modeling the pore pressure distributions in many commercial software gives underestimated/ overestimated values as it considers only the fluid movement due to hydraulic pressure difference unlike the Chemo-potential model which includes the fluid and ion movement due to coupled driving forces.
2. The unexpected surge or drop in pore pressures near the wellbore region causes wellbore instability.
3. The important compositional properties of the pore fluid and drilling mud which can affect the pore pressure distributions are water activity and the salt concentration and CEC based on types of clays in case of shales.
4. Based on the differences in the water activity of the pore fluid and drilling mud, the water moves from fluid with higher water content to a fluid with lower water content. This could lead to increased water saturation in the shales thereby weakening the formation if shale has low water activity. Similarly when shale has higher water activity and loses higher percentage of water such that it gets dehydrated, then fractures develop and lead to wellbore collapse.
5. When water moves from mud to formation, the pore pressure near the wellbore surges due to excess water that enters and the pore pressure declines further based on the distance ratio that water entered has propagated. Similarly when the water moves from formation to mud, the formation pressure is very low near

the wellbore compared to the poroelastic model and increases gradually. This is because as the radial distance increases, the amount of water lost by the formation to mud decreases.

6. When the water moves in one direction, the flow is opposed by the flow of ions due to differences in the concentration of the solutes in the solutions. Hence diffusion of chemical species takes place in direction opposing the osmosis. Based on the dominating phenomena, the flow changes. If diffusion is much greater than osmotic pressure then water is dragged along in diffusional process. The dominancy of the diffusion depends on CEC, porosity, membrane efficiency and permeability.
7. The effective radial and tangential stresses become less compressive when water flows from the mud to the formation as it exerts more tensile stresses which can cause rock failure and lead to wellbore collapse. Similarly when the water flows from formation to mud, the shale gains strength by loss of water as it becomes more compressive than the stresses calculated by the poroelastic model.
8. The important mechanical parameter affecting the pore pressure distributions is Poisson's ratio. Changes in the shear modulus has greater impact on Poisson's ratio than the bulk modulus of same changes. Values of Poisson's ratio closer to 0.5 makes the formation incompressible and the decline in the pore pressure is very slow compared to formations with lower Poisson's ratio (< 0.3).
9. Formations with lower porosities and higher Cation Exchange Capacity have higher membrane efficiency, and the pore pressures vary significantly from the

values calculated with poroelastic model based on the direction of the water flow.

10. When the porosity of the formation is in range of 0-30% the changes in membrane efficiency for changes in CEC are significant compared to a formation with porosity in the range 40-60%.
11. The changes in the membrane efficiency for change in porosity for a formation with porosity in range 0-30% and with particular CEC is half the changes observed for the same change in porosity for a formation with porosity in range 40-60% and with the same CEC.
12. The pore pressure decline is very sharp and linear for formations of higher permeability compared to formations of lower permeability. It is observed that the time taken by more permeable formations to lose water and attain constant pore pressure is higher when compared with formations of low permeability. This is because formations with high permeability allows water to penetrate more and cover larger distance ratios when compared with less permeable formations for the same time interval. Hence the pore pressure at a particular distance is higher for more permeable formations and it takes more time to lose the water gained. So the plot looks linear with fewer points.
13. The pore pressure drop near the wellbore region is significant for formations with lower permeability compared to relatively high permeable formations. This is because the lower permeability formations undergo significant reduction in permeability for changes in pore pressure unlike the formations with higher

permeability for the same pore pressure changes which is in accordance with conclusions of Katz and Lee (1990).

8.2: Limitations of the model

1. The model has uncoupled the chemical reactions that take place inside the formation from the ion diffusions based on the Curie Prigogine Principle which is valid only for isotropic medium. Hence the model cannot be used for an anisotropic medium.
2. The model is based on the assumption that the porous medium behaves completely elastic.
3. This model does not include the impact of thermal effects on pore pressure distributions.

8.3: Recommendation

Based on the above study, it is recommended that the condition of maintaining low water activity in drilling mud is optimal with minimal increase in the diffusion osmosis and drilling fluid viscosity, as the strength of shale formation can be increased by back flow of water from formation to wellbore which prevents wellbore instability and also helps to control the rock failure due to effective tensile stresses compared to the condition of higher water activity in the mud.

References

1. “Methylene Blue Test for Drill Solids and Commercial Bentonites.” Section 12 in: API Recommended Practices 13I: Laboratory Testing of Drilling Fluids, 7th ed. And ISO 10416:2002; American Petroleum Institute (February 2004), 34-38.
2. Abass, H., Shebatalhamd, A., Khan, M., Al-Shobaili, Y., Ansari, A., Ali, S., & Mehta, S. (2006, January 1). Wellbore Instability of Shale Formation; Zuluf Field, Saudi Arabia. Society of Petroleum Engineers. doi:10.2118/106345-MS
3. Al-Bazali, Talal M., et al. "Factors controlling the membrane efficiency of shales when interacting with water-based and oil-based muds." International Oil & Gas Conference and Exhibition in China. Society of Petroleum Engineers, 2006.
4. Alshawabkeh, Akram N., and Ray Mark Bricka. "Basics and applications of electrokinetic remediation." ENVIRONMENTAL SCIENCE AND POLLUTION CONTROL SERIES (2000): 95-112.
5. B. Ratner, A. Hoffman, F. Schoen, and J. Lemons: Biomaterials Science, 2nd edition (San Diego: Elsevier Academic Press. 2004). 30.
6. Bardon, Ch. "Recommandations pour la détermination expérimentale de la capacité d'échange de cations des milieux argileux." Oil & Gas Science and Technology 38.5 (1983): 621-626.
7. Bennett, Richard H., William R. Bryant, and Matthew H. Hulbert, eds. Microstructure of fine-grained sediments: From mud to shale. Springer, 1991.
8. Biot, Maurice A. (1941) "General theory of three-dimensional consolidation." Journal of applied physics 12.2: 155-164.

9. Bresler, Eshel. "Anion exclusion and coupling effects in nonsteady transport through unsaturated soils: I. Theory." Soil Science Society of America Journal 37.5 (1973): 663-669.
10. Carter, J. P., and J. R. Booker. "Elastic consolidation around a deep circular tunnel." International journal of Solids and Structures 18.12 (1982): 1059-1074.
11. Casagrande, Leo. "Electro-Osmosis in Soils*." Geotechnique 1.3 (1949): 159-177.
12. Casagrande, Leo. "Stabilization of soils by means of electro-osmosis: State of the art." Journal of the Boston Society of Civil Engineers 69.2 (1983): 255-302.
13. Charoenwongsa, S., et al. "A fully-coupled geomechanics and flow model for hydraulic fracturing and reservoir engineering applications." Canadian Unconventional Resources and International Petroleum Conference. Society of Petroleum Engineers, 2010.
14. Chenevert, M. E. "Shale control with balanced-activity oil-continuous muds." Journal of Petroleum technology 22.10 (1970): 1-309.
15. Chenevert, M. E., and J. E. Strassner. "Temperature effects on water activities of argillaceous shales and oil mud systems." Fifteenth Oil and Gas Conference. 1975.
16. Composition and Properties of the Pierre Shale and Equivalent Rocks, Northern Great Plains Region: Mineralogical and Chemical Study, Including Trace Elements, of Marine and Nonmarine Rocks of Late Cretaceous Age. US Government Printing Office, 1980.

17. Corapcioglu, M. Yavuz. "Formulation of electro-chemico-osmotic processes in soils." Transport in porous media 6.4 (1991): 435-444.
18. Crank, J. "The Mathematics of Diffusion, 347." (1956).
19. Darley, Henry CH, and George Robert Gray. Composition and properties of drilling and completion fluids. Gulf Professional Publishing, 1988.
20. Datla, S., and A. T. Yeung. "Subsurface migration of contaminants under the coupled influences of hydraulic, electrical and chemical gradients." Proc. 8th International Conference of the International Association for Computer Methods and Advances in Geomechanics, Morgantown, WV. Vol. 2. 1994.
21. De Sitter, L. U. "Diagenesis of oil-field brines." AAPG Bulletin 31.11 (1947): 2030-2040.
22. Deem, J. A. (1973). Lange's Handbook of Chemistry.
23. Detournay, E., and AH-D. Cheng. "Poroelastic response of a borehole in a non-hydrostatic stress field." International Journal of Rock Mechanics and Mining Sciences & Geomechanics Abstracts. Vol. 25. No. 3. Pergamon, 1988.
24. Esrig, Melvin I. "Pore pressures, consolidation, and electrokinetics." Am Soc Civil Engr J Soil Mech (1968).
25. Fitts, Donald D. Nonequilibrium thermodynamics: a phenomenological theory of irreversible processes in fluid systems. New York: McGraw-Hill, 1962.
26. Fjaer, Erling, et al. Petroleum related rock mechanics. Vol. 53. Elsevier, 2008.
27. Fonseca, C. F., and M. E. Chenevert. "The effect of total stress and temperature on the water activity of shales." International Journal of Rock Mechanics and Mining Sciences and Geomechanics Abstracts. Vol. 35. No. 4. Elsevier, 1996.

28. Freeze, R. A., and J. A. Cherry. "1979, Groundwater. Englewood Cliffs, New Jersey: Prentice-Hall."
29. Ghassemi, A., Q. Tao, and A. Diek. "Influence of coupled chemo-poro-thermoelastic processes on pore pressure and stress distributions around a wellbore in swelling shale." Journal of petroleum science and Engineering 67.1 (2009): 57-64.
30. Gillham, R. W., et al. "Diffusion of nonreactive and reactive solutes through fine-grained barrier materials." Canadian Geotechnical Journal 21.3 (1984): 541-550.
31. Gillham, ROBERT W., and JOHN A. Cherry. "Contaminant migration in saturated unconsolidated geologic deposits." Spec. Pap. Geol. Soc. Am 189 (1982): 31-62.
32. Gray, Donald H. "Coupled flow phenomena in clay-water systems." (1966).
33. Helset, H. M., et al. "Improved Pore Pressure Prediction from Seismic Data." 72nd EAGE Conference & Exhibition. 2010.
34. Hendershot, William H., and Martin Duquette. "A simple barium chloride method for determining cation exchange capacity and exchangeable cations." Soil Science Society of America Journal 50.3 (1986): 605-608.
35. http://koll1.chem.u-szeged.hu/colloids/staff/zoli/Pharmacy/Lecture%208.pdf
36. http://www.capp.ca/canadaIndustry/naturalGas/ShaleGas/Pages/default.aspx
37. http://www.engineering.ucsb.edu/~hpscicom/projects/stress/introge.pdf
38. http://www.intmath.com/laplace-transformation/1a-unit-step-functions-definition.php

39. http://www.theory.physics.manchester.ac.uk/~xian/thermal/chap1.pdf
40. Islam, Md Aminul, and Paal Skalle. "An Experimental Investigation of Shale Mechanical Properties Through Drained and Undrained Test Mechanisms." Rock Mechanics and Rock Engineering 46.6 (2013): 1391-1413.
41. Jaeger, John Conrad, Neville GW Cook, and Robert Zimmerman. Fundamentals of rock mechanics. John Wiley & Sons, 2009.
42. Johnson, C. R. "Positive definite matrices." American Mathematical Monthly (1970): 259-264.
43. Katz, Donald La Verne, and Robert L. Lee. Natural gas engineering: production and storage. New York: McGraw-Hill, 1990.
44. Katzir-Katchalsky, Aharon, and Peter F. Curran. "Nonequilibrium thermodynamics in biophysics." (1965).
45. Keijzer, Th JS, and J. P. G. Loch. "Chemical osmosis in compacted dredging sludge." Soil Science Society of America Journal 65.4 (2001): 1045-1055.
46. Lai, W. M., and V. C. Mow. "Transport of multi-electrolytes in charged hydrated biological soft tissues." Transport in Porous Media 34.1-3 (1999): 143-157.
47. Marine, I. Wendell, and Steven J. Fritz. "Osmotic model to explain anomalous hydraulic heads." Water Resources Research 17.1 (1981): 73-82.
48. McKay, Larry, John A. Cherry, and Robert W. Gillham. "Field experiments in a fractured clay till: 1. Hydraulic conductivity and fracture aperture." Water Resources Research 29.4 (1993): 1149-1162.

49. McLean, M. R., and M. A. Addis. "Wellbore stability analysis: a review of current methods of analysis and their field application." SPE/IADC Drilling Conference. Society of Petroleum Engineers, 1990.
50. Meier, Lorenz P., and Guenter Kahr. "Determination of the cation exchange capacity (CEC) of clay minerals using the complexes of copper (II) ion with triethylenetetramine and tetraethylenepentamine." Clays and Clay Minerals 47.3 (1999): 386-388.
51. Mitchell, J. K. "Fundamentals of soil behavior, 1976."
52. Mitchell, James K., and Albert T. Yeung. "Electro-kinetic flow barriers in compacted clay." Transportation Research Record 1288 (1990).
53. Neuzil, C. E. "How permeable are clays and shales?." Water resources research 30.2 (1994): 145-150.
54. Neuzil, C. E. "Osmotic generation of 'anomalous' fluid pressures in geological environments." Nature 403.6766 (2000): 182-184.
55. Nguyen, Vinh X., and Youname N. Abousleiman. "Incorporating electrokinetic effects in the porochemoelastic inclined wellbore formulation and solution." Anais da Academia Brasileira de Ciências 82.1 (2010): 195-222.
56. Nguyen, Vinh X., Younane N. Abousleiman, and Terry Hemphill. "Geomechanical Coupled Poromechanics Solutions While Drilling in Naturally Fractured Shale Formations With Field Case Applications." SPE Annual Technical Conference and Exhibition. Society of Petroleum Engineers, 2009.
57. Olsen, Harold W. "Simultaneous fluxes of liquid and charge in saturated kaolinite." Soil Science Society of America Journal 33.3 (1969): 338-344.

58. Olsen, Harold W., Elliot N. Yearsley, and Karl R. Nelson. "Chemico-osmosis versus diffusion-osmosis." Transportation Research Record 1288 (1990).
59. Onsager, Lars. "Reciprocal relations in irreversible processes. I." Physical Review 37.4 (1931): 405.
60. Onsager, Lars. "Reciprocal relations in irreversible processes. II." Physical Review 38.12 (1931): 2265.
61. Osuji, Collins Emenike, Martin E. Chenevert, and Mukul Mani Sharma. "Effect of porosity and permeability on the membrane efficiency of shales." SPE Annual Technical Conference and Exhibition. Society of Petroleum Engineers, 2008.
62. Overbeek, J. Th. "The Donnan equilibrium." Progress in biophysics and biophysical chemistry 6 (1956): 57.
63. Passey, Quinn R., et al. "From oil-prone source rock to gas-producing shale reservoir–geologic and petrophysical characterization of unconventional shale-gas reservoirs." Beijing, China, June 8 (2010).
64. petrowiki.spe.org/borehole-instability
65. REUSS. Mem. de la Sot. Imper. des Naturalistes de Moscou, 1908, 2, 327.
66. Revil, A., and M. Pessel. "Electroosmotic flow and the validity of the classical Darcy equation in silty shales." Geophysical research letters 29.9 (2002): 14-1.
67. Roshan, Hamid, and Sheik S. Rahman. "Analysis of stress and pore pressure in naturally fractured shale formations: a finite element based chemo-thermo-poroplastic model." SPE Eastern Regional Meeting. Society of Petroleum Engineers, 2010.

68. Sachs, Jeffrey R., and A. J. Grodzinsky. "An electromechanically coupled poroelastic médium driven by an applied electric-current-surface détection of bulk material properties." Physicochemical Hydrodynamics 11.4 (1989): 585-614.
69. Salisbury, D. P., G. G. Ramos, and B. S. Wilton. "Wellbore instability of shales using a downhole simulation test cell." The 32nd US Symposium on Rock Mechanics (USRMS). American Rock Mechanics Association, 1991.
70. Schultz, Leonard G. "Mixed-layer clay in the Pierre Shale and equivalent rocks, northern Great Plains region." Geological Survey Professional Paper. Vol. 1064. US Government Printing Office, 1978.
71. Simpson, J. P., and H. L. Dearing. "Diffusion Osmosis-An unrecognized cause of shale instability." IADC/SPE Drilling Conference. Society of Petroleum Engineers, 2000.
72. Snoeyink, Vernon L., and David Jenkins. Water chemistry. John Wiley, 1980.
73. Stehfest, Harald. "Algorithm 368: Numerical inversion of Laplace transforms [D5]." Communications of the ACM 13.1 (1970): 47-49.
74. Stephens, M., S. Gomez, and M. Churran. "Laboratory Methods to Assess Shale Reactivity with Drilling Fluids." AADE2009-NTCE-11-04, AADE National Technical Conference and Exhibition, New Orlands, March 31-April 2, 2009.
75. Sumner, M. E., et al. "Cation exchange capacity and exchange coefficients." Methods of soil analysis. Part 3-chemical methods. (1996): 1201-1229.
76. Tan, Chee P., and Brian G. Richards. "Modelling of time-dependent pore pressure change in shales due to chemical potential difference." 2nd North

American Rock Mechanics Symposium. American Rock Mechanics Association, 1996.

77. Terzaghi, Karl. "Principles of soil mechanics, IV—Settlement and consolidation of clay." Eng. News Rec 95.3 (1925): 874-878.
78. Van Meerveld, J., et al. "Analytical solution of compression, free swelling and electrical loading of saturated charged porous media." Transport in porous media 50.1-2 (2003): 111-126.
79. Van Olphen, Hendrik. "Introduction to clay colloid chemistry." (1963).
80. Van Oort, E., et al. "Transport in shales and the design of improved water-based shale drilling fluids." SPE Drilling & Completion 11.03 (1996): 137-146.
81. Whitworth, T. M., and S. J. Fritz. "Electrolyte-induced solute permeability effects in compacted smectite membranes." Applied Geochemistry 9.5 (1994): 533-546.
82. Winston, Paul W., and Donald H. Bates. "Saturated solutions for the control of humidity in biological research." Ecology (1960): 232-237.
83. www.eia.gov
84. www.geology.com/rocks/shale
85. www.spe.org/dl/docs/2012/osisanya
86. Yeung, A. T., and J. K. Mitchell. "Coupled fluid, electrical and chemical flows in soil." Geotechnique 43.1 (1993): 121-134.
87. Yeung, Albert T., and Subbaraju Datla. "Fundamental formulation of electrokinetic extraction of contaminants from soil." Canadian geotechnical journal 32.4 (1995): 569-583.

88. Yeung, Albert Tak-Chung. Electro-kinetic barrier to contaminant transport through compacted clay. Diss. University of California, Berkeley, 1990.
89. Young, Allen, and Philip F. Low. "Osmosis in Argillaceous Rocks: GEOLOGICAL NOTES." AAPG Bulletin 49.7 (1965): 1004-1007.

Appendix A: Laplace Inversion-Stehfest's Algorithm

This section presents the Stehfest's method for numerical inversion of the Laplace transform of form $\tilde{f}[s]$ of the function $f_{num}[t]$ at any time 't'. The formula for the inversion is as following

$$f_{num}(t) = \frac{ln2}{t}\sum_{i=1}^{N} G_i \tilde{f}(i * \frac{ln2}{t}) \dots\dots\dots\dots\dots\dots\dots\dots\dots\dots\dots\dots\dots\dots\dots\dots\dots\dots\dots\dots\dots\dots\dots\dots\dots\dots (A1)$$

Where

$$N = Stehfest\ number\ and\ has\ to\ be\ even\ integer\ between\ 2\ and\ 20$$

The coefficient G_i is given by

$$G_i = (-1)^{i+\frac{N}{2}} \sum_{k=(i+1)/2}^{\min(i,\frac{N}{2})} \frac{k^{\frac{N}{2}}(2k)!}{\left(\frac{N}{2}-k\right)!\, k!\, (k-1)!\, (i-k)!\, (2k-i)!} \dots\dots\dots\dots\dots\dots\dots\dots\dots (A2)$$

Appendix B: Properties of the Berea Sand and Shale gas formations used for validation of results

Table 21: Properties of Berea sand used for results validation (Chareonwongsak, S., et al. 2010)

Rock Properties	Values	Units
Porosity (ϕ)	0.19	
Permeability (k)	0.00000000000010	m^2
Rock Compressibility (C_ϕ)	4.40E-10	Pa^{-1}
Fluid Properties		
Density (ρ)	1000	Kg/m^3
Viscosity (μ)	0.0008900000000	Pa.s
Fluid compressibility (C_f)	0.0000000006000	Pa^{-1}
	1.04E-09	
Mechanical Properties		
Biot's coefficient (α_P)	0.8	
Bulk modulus (K)	8000000000	Pa
Shear modulus (G)	6000000000	Pa
Lame's constant (λ)	4000000000	Pa
Poisson's ratio (ν)	0.20	Pa
Biot modulus (M)	5060728745	Pa
External stress (σ_{ex})	14200000	Pa
Reservoir dimensions		
Height (H)	500	m
Incremental pressure P_o	2988215.49	Pa
Storage coefficient S	0.00000000024	Pa^{-1}

Table 22: Properties of Shale gas formations used for results validation (data from table 5)

Rock Properties	Values	Units
Porosity (ϕ)	0.173	
Permeability (k)	0.00000000000000000001	m^2
Rock Compressibility (C_ϕ)	3.00E-06	Pa^{-1}
Fluid Properties		
Density (ρ)	1000	Kg/m^3
Viscosity (μ)	0.0008900000000	Pa.s
Fluid compressibility (C_f)	0.0000000006000	Pa^{-1}
	3.00E-06	Pa^{-1}
Mechanical Properties		
Biot's coefficient (α_P)	0.9	
Bulk modulus (K)	4800000000	Pa
Shear modulus (G)	600000000	Pa
Lame's constant (λ)	4400000000	Pa
Poisson's ratio (ν)	0.44	Pa
Biot modulus (M)	1926397	Pa
External stress (σ_{ex})	14200000	Pa
Reservoir dimensions		
Height (H)	500	m
Incremental pressure P_o	4395.09	Pa
Storage coefficient S	0.00000051925	Pa^{-1}